Università degli Studi di Verona
Graduate School of Translational Biomedicine

MUSCLE MECHANICAL WORK IN WALKER-ASSISTED LOCOMOTION: INSTRUMENTATION AND MODELLING FOR AN INTEGRATED GAIT ANALYSIS IN CEREBRAL PALSY

Candidate: Davide Conte

Supervisors:

Prof. Carlo Capelli, Università degli Studi di Verona

Dr. Nicola Petrone, Università degli Studi di Padova

Dedicated to

my grandmother Pina and my grandfathers Mario and Lino

my uncle Gianni

"A child's education starts with a well-estabilished knowledge (e.g. 2 x 2 = 4) and fairly tales. The fairly tales always end happly. When a student enters a college, the same principle pertains: the student studies well-estabilished knowledge. Fairly tales for students also exist: they are called "problems"in the textbooks. Textbook problems contain all the necessary information and are always solvable. Science is different. Many problems cannot be solved bacause the necessary information is not available; some problems are not solvable at all. Still, it is important to understand the problem and the difficulties associated with its solution."

(Vladimir Zatsiorsky, *"Kinetics of Human Motion", Chap. 6*)

Muscle mechanical work in walker-assisted locomotion: Instrumentation and modelling for an integrated gait analysis in cerebral palsy

A dissertation presented by **Davide Conte**
to the Graduate School of Translational Biomedicine for the degree of
Doctor of Philosophy in Physical Exercise and Human Movement Sciences

University of Verona, Italy, 22^{nd} of June 2012

Abstract

The estimation of muscle mechanical work can be useful to assess movement efficiency, but it is still a challenging task in biomechanics. Different methods to estimate muscle work during walking have been presented in the literature and, although attempts have been made to investigate differences among them, all methods are still used in research and clinical applications. A deeper understanding of theoretical differences and analogies would allow to know what is exactly computed by each method and help to make a more appropriate use of this information. To this purpose, a 16 segments full-body 3D model was validated and used to collect kinematic and kinetic data from healthy children and cerebral palsy (CP) children walking at self-selected speed. Two instrumented handles fixable on the frame of posterior paediatric walkers were also developed, to measure upper limb kinetics in subjects with more severe walking impairements. Whole-body muscle mechanical power curves and work values, either *positive*, *negative* or *net*, during normal gait and during walker locomotion were obtained, demonstrating that all methods are equivalent when energy transfers between segments are allowed. With no transfers allowed, methods differ among each other, with differences depending on the movements and the methods considered. Apart from some critical issues evidenced and discussed, the analysis of whole-body muscle mechanical power curves and work estimates can provide valuable information on the overall locomotion function, highlighting propulsive deficits, gait asymmetries, movement inefficiencies associated to reduced energy recuperation.

Declaration

The work presented in this thesis is based on research carried out at:

- the Biomechanics Laboratory, University of Verona, Italy
- the Machine Design Laboratory, University of Padova, Italy
- the Oxford Gait Laboratory, Nuffield Orthopaedic Centre, Oxford, UK
- the Gait Analysis Laboratory, San Bassiano Hospital, Bassano del Grappa, Italy

No part of this thesis has been submitted elsewhere for any other degree or qualification and it is all my own work unless referenced to the contrary in the text.

My visit at the University of Oxford and at the Oxford Gait Lab was supported through the grant *Cooperint 2010* by the University of Verona. Instrumented handles have been realized with the financial support of Fondazione Cariverona and tested on walkers kindly provided by Fumagalli srl (Como, Italy).

Contacts: davideconte.bioeng@gmail.com.

Acknowledgements

Many people really helped me during the time I spent in Verona, Padova, Oxford and Bassano developing this thesis, through discussions, suggestions and analysis of unexpected problems!

I would especially like to thank my supervisors, Carlo Capelli and Nicola Petrone, who continuously supported me, providing precious hints and adjustments.

I am very grateful to the people with whom I shared part of my time and my research, learning always something new: Francesco Baldan, Mario Saraceni, Giuseppe Marcolin, Luca Modenese, Fausto Panizzolo at the University of Padova;
Emma Hawke, Valeria Marconi, Gabriela Fischer, Niek van Ulzen, Matteo Bertucco, Fabio Pizzolato, Paola Zamparo, Luca Ardigò at the University of Verona;
Mauro Recalcati, Francesca Pinto, Mirco Bendinelli, Alessandro Cosentino at the Don Calabria rehabilitation center in Verona;
Diego Pigatto, Alessandro Ceccato, Cristina Smiderle at the San Bassiano hospital in Bassano del Grappa;
Julie Stebbins, Joanne Bates, Amy Zavatsky at the Oxford Gait Laboratory and the University of Oxford.

For suggestions and support related to instrumentation and devices, I would like to recognize the help of Andrea Cazzaniga, Daniela Vorazzo, Gabriele Paolini, Michele Caramella, Andrea Menegolo.

Many thanks go to all the children who participated in the study and their parents for their patience!

My gratitude to my wife Patrizia and my family is unmeasurable.

Contents

Abstract vi

Declaration vii

Acknowledgements viii

1 Introduction 1

1.1 A little bit of mechanics... 7

1.2 Muscle mechanical work 10

1.2.1 Joint power analysis 11

1.2.2 External/Internal power analysis 12

1.2.3 Segmental power analysis 15

1.3 A comparison of the different approaches 17

1.3.1 Effects of external energy sources 18

1.3.2 Summation and integration of the power components 20

1.3.3 Further elements of discussion 21

2 Materials and Methods 23

2.1 Human movement analysis 23

2.2 Instrumentation and models 24

2.3 Data acquisition 25

2.3.1 Laboratory setup 25

2.3.2 Subjects 25

2.3.3 Data acquisition protocol 26

2.4 Data processing 28
2.5 Statistical analysis 29
2.6 Muscle mechanical work computation 30
2.6.1 Computing power components 31
2.6.2 Summation and integration of power components 34
2.6.3 Normalization of muscle work 35

3 Instrumented Handles **37**
3.1 Strain gauge measurement 37
3.2 Measuring system design 39
3.3 Handles design: FEM analysis 40
3.4 Handles realization and instrumentation 51
3.5 Handles static calibration setup 52
3.6 Handles static calibration results 56
3.6.1 Handle A 57
3.6.2 Handle B 59
3.7 Handle protection and signal amplification 64
3.8 Connection with the motion-capture system 68
3.9 Handles dynamic calibration 70
3.10 First tests on walkers 72

4 Full-body model **75**
4.1 The Upper-Body 75
4.1.1 Segments definitions 77
4.2 The Lower Body 79
4.2.1 Segments definitions 80
4.3 Inertial properties of the model 82
4.4 Body centre of mass 83
4.5 Model implementation in Vicon BodyBuilder 86
4.6 Full-body model validation 89
4.7 UL model test with walker 101

4.7.1 Test results 102
4.7.2 Discussion of test results 106

5 Results **107**
5.1 Analysis of joints and segments powers 108
5.2 Whole-body power during normal gait 113
5.3 Muscle mechanical work during normal gait 118
5.4 Muscle power and work during simulated walker-assisted gait 121
5.5 Muscle work during impaired gait 125
5.6 Gait/walker, healthy/CP comparisons 130

6 Discussion **133**

7 Conclusions **141**

Appendix **145**

A Basic and auxiliary results **145**
A.1 All trials data, healthy children 145
A.1.1 Normal gait 145
A.1.2 Walker-assisted gait 148
A.2 Details on statistics 151
A.3 All trials data, CP children 154

References **166**

Chapter 1

Introduction

Human movement and locomotion have been studied since antiquity in art, medicine (Aristotle, IV century BC), and sport.

In both the last two cases, the aim is the same: trying to bring the subject studied to the best performance he/she can achieve. A professional runner or a child affected by cerebral palsy or an hemiplegic post-stroke patient are all looking for a common aim: walk (or run) more efficiently, that is equivalent to move with the need of less metabolic energy. The problem is: how can we assess how efficient is a certain movement? And, if we could quantify walking efficiency, how can we use this information?

Figure 1.1 gives an example of the energetic relationships involved in human movement. Our body can be represented as a multi-linked system of rigid (or, better, supposed to be rigid) segments connected by joints with certain degrees of freedom actuated by motors called "muscles". A motor can supply motive power at the expense of energy and with a loss of part of the original energy (entropy) during the process. Energy supplied to the muscles can be provided by several sources. In sub-maximal exercises, like walking, the metabolic energy source is oxygen.

Muscles then perform work by exerting a certain force while changing their length (shortening or lengthening): this *linear* work is translated into *rotational* work at the level of the body joint (or joints) spanned by those muscles, to produce the desired movement.

Work, measured as the mechanical effect of muscle action, is different from *energy expenditure*, the energy needed to perform that action. Muscles spend energy not only for

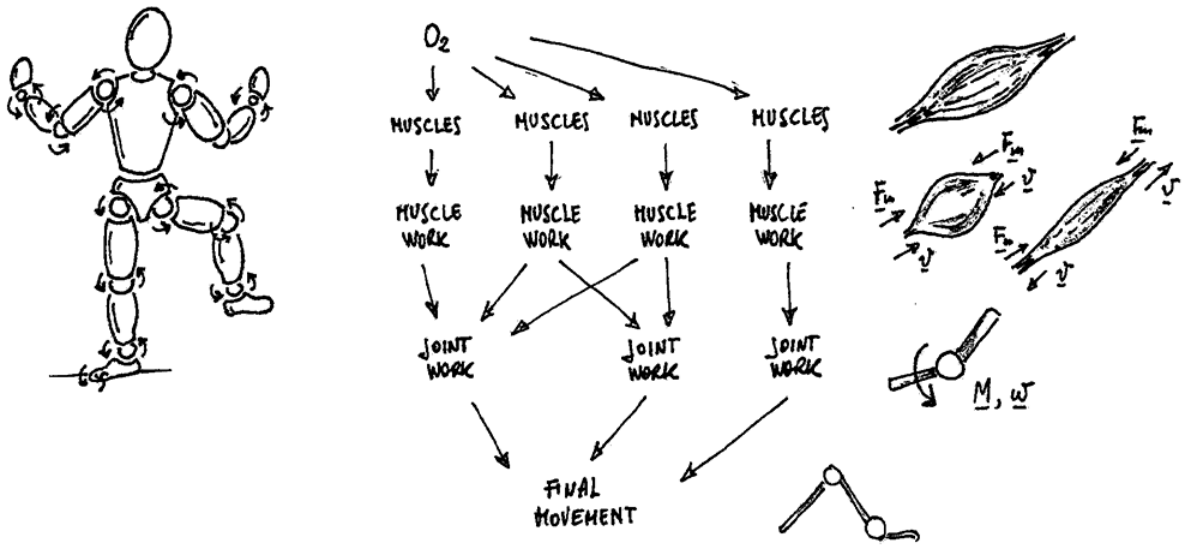

Figure 1.1: Relationship between metabolic energy, muscles activity (concentric/eccentric) and final output in terms of joint work and body movement.

work production but also for force generation. Therefore, if in classical mechanics *energy* represents the capacity to *do work*, in biomechanics energy has to be seen as the capacity to do work and to exert muscle force whether or not there is a displacement involved (Zatsiorsky, 2002).

In classical mechanics the work of a force can be *positive* or *negative*, producing an increase or a decrease in the mechanical energy of the body which is subjected to that force. But, if the force is generated by a muscle, energy is needed to perform both types of work, although the amount of the cost might be physiologically different in the two situations (Zatsiorsky, 2002).

The distinction is evident if we analize a cyclic movement, as a gait cycle or climbing and descending stairs. With the classical definition, the overall value of work associated with that movement will be equal to zero, because positive and negative fractions of work will cancel out each other. However, it is evident that metabolic energy is needed by the muscles to perform both parts of the movement.

There is therefore the need do take these differences into account and define a proper terminology for each computed quantity.

We will use the term *work* to address the general definition of work from classical

mechanics, the product of force by displacement.

When discussing muscle action, we will use the term *metabolic energy expenditure* for the metabolic energy used by the muscles to perform a certain movement, and the terms *mechanical energy expenditure* or *muscle mechanical work* to define the estimated magnitude of work done by the muscles which involves metabolic energy to be performed (e.g. positive and/or negative work).

If the system studied is not a single joint or a single body segment, but the whole body, the analysis then involves many muscles, interacting each other, and each one exerting its own force, while producing negative, positive or null work, absorbing metabolic energy or accumulating a certain amount of elastic energy at the level of muscle-tendon structures. Contemporaneous contractions of antagonist muscles further complicate the real situation.

Answering to our original question on *how efficient is a certain movement?* is then becoming rather complicated.

It is possible, in certain conditions and for certain movements, to estimate the *metabolic* energy expenditure by measuring the overall amount of metabolic energy (i.e. the *fuel*) spent by the body. On the other side, we can try to estimate the *mechanical* energy expenditure by measuring the final mechanical output of the movement in terms of *work*.

Sometimes the two different measures, the *mechanical* and the *metabolic* one, can be put together to evaluate the *mechanical efficiency* of a movement, given by the ratio between mechanical energy expenditure and metabolic energy expenditure (Cavagna, 1988; Winter, 1979, 2005):

$$\rho = \frac{W_{mech}}{E_{metab}} \tag{1.1}$$

However, it is clear that the muscle mechanical work estimated will give a measure of muscle work, as a net output effect in terms of joints and segments movement, and not a measure of the "real"action performed by the muscles. This problem has no solution unless we could measure every single muscle's force and length variation during time, a task which is impossible to achieve in living humans.

The problem can be overcome by using dynamic models of the human body. More specifically, by using models that describe structure and behaviour of the human musculoskeletal system (Delp et al., 2007).

With the help of the model, measures of the kinematics and kinetics of the real subject can be used to predict, by looking "directly"inside the body, the behaviour of the muscles and therefore get closer to the "true"muscle mechanical work (Zajac et al., 2002, 2003; Neptune et al., 2004a,b; Seth and Pandy, 2007; Neptune et al., 2008, 2009a; Sasaki et al., 2009).

Indeed, to get realistic and useful outcomes from this approach, further competences inside the research/clinical team are needed, together with the need to define subject specific adjustments of the model, critical assumptions about optimization of muscle activation and so on...

We believe that, although being aware of the limitations of this approach, the "indirect"estimation of muscle work can still provide some useful information on the energy expenditure associated with a particular movement. However, despite its relative simplicity with respect to an approach based on musculo-skeletal models, estimation of energy expenditure in terms of muscle work computation is not that easy!

Mechanical energy and work definitions in terms of mechanical laws are clear, but terminology related to the study of muscle mechanical energy expenditure in biomechanics is not always so clear, and the same expression might sometimes be found cited by different authors with a slightly different meaning. For example, there is still confusion related to the meaning assigned to the expressions *muscle work*, *muscle energy expenditure*, *external* and *internal* muscle work...

Different approaches to estimate muscle mechanical work during walking and running have been presented in the literature, creating a warm debate on which one is the most correct (see, for example, (Thys et al., 1996; Zatsiorsky, 1997; Thys et al., 1997; Zatsiorsky, 1998)), with a few attempts to investigate differences either theoretically or practically (Aleshinsky, 1986a,b; Purkiss and Robertson, 2003; van de Walle et al., 2012).

Approaches differ from each other in defining equations and instrumentation needed to acquire necessary data.

Up to now, despite the discussions and a few attempts to provide rigorous mathematical demonstrations, different models are still used in this field of research and in clinical

evaluations, utilized, in the latter case, mostly for studing walking efficiency in impaired gait, for example in cerebral palsy.

The term cerebral palsy (CP) indicates a group of movement disorders produced by brain damages during early stages of development (Miller, 2005). Physical rehabilitation of CP children is a task that involves several factors: Neurological impairments, spasticity, muscle weakness, skeletal deformities. Identification and correction of these factors are the aims of the rehabilitation process. However, a subject-specific analysis of the neuro-muscular system is extremely complex. Efficacy of the rehabilitation process depends on the ability to correctly identify and measure the factors to be corrected and, therefore, to organize the adequate therapy (Gage et al., 2009).

Technology has provided clinical gait analysis with instruments to measure kinematics and kinetics of human gait (joint angles, moments, forces, powers) together with electrical activity of the muscles (Perry, 2005; Robertson et al., 2004; Kirtley, 2006; Richards, 2008).

Besides these joint-by-joint (or segment-by-segment) measures, it is also useful to analyse the overall locomotion function by sinthetic variables as the *body centre-of-mass* or by assessing locomotion *efficiency* by measuring the amount of energy involved with the execution of a certain movement, and it has been demonstrated that CP children have increased oxygen consumption and increased muscle co-contraction during walking (Detrembleur et al., 2000; Bennett et al., 2005; Hsue et al., 2009a,b; Unnithan et al., 1996; Frost et al., 1997; Unnithan et al., 1999; Damiano et al., 2000; Detrembleur et al., 2003; Schepens et al., 2001, 2004; van den Hecke et al., 2007; Marconi et al., 2009; van de Walle et al., 2010, 2012).

There is still the need, however, to improve methodological aspects regarding muscle work computation and muscle co-contraction quantification.

When the locomotion function is seriously impaired by causes related to insufficient muscle force of the lower limbs, or by instability of the equilibrium, the use of walking aids is needed. If there is enough force that can be provided by the upper limbs, locomotion is still possible using crutches or walkers (Fig. 1.2).

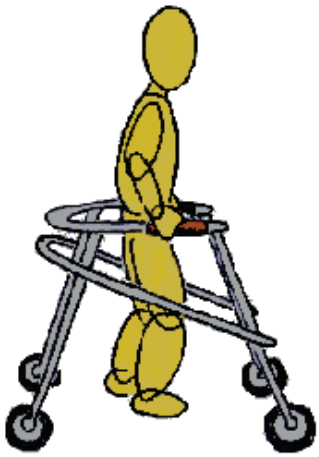

Figure 1.2: Paediatric posterior walker

In this case the interaction of the body with the external world depends not only on the feet contacting the ground, but also on the hands loading the walking device, resulting in an increased energy expenditure at the level of the upper limbs and trunk muscles.

Walking aids instrumented with force sensors have been used to evaluate the loads at the upper limb joints during locomotion. Shoulder joint forces were evaluated in people with incomplete spinal chord injury (SCI) during ambulation with crutches or with a walker (Haubert et al., 2006). Instrumented walkers and load cells, applied to walkers or crutches, were used to study upper limbs kinetics during assisted locomotion in children and adults (Bachschmidt et al., 2001; Strifling et al., 2008; Konop et al., 2009a,b; Slavens et al., 2010, 2011).

This project will focus on studying the energetics of human locomotion in healthy children and CP children, paying attention to the issues regarding the computation of muscle mechanical work. The use of an instrumented walker will permit to extend this analysis also to children who need to use a posterior walker to move.
Given the premises above, the aims of this research are therefore to:

1. Provide a review of the methods used to compute muscle mechanical work
2. Discuss and investigate open issues related to muscle mechanical work estimation
3. Experimentally develop and evaluate models for clinical application of this measure,

particularly to estimate muscle mechanical work during normal gait and during walker-assisted locomotion

4. Test the models in a clinical environment on children with cerebral palsy.

The text is organized as follows: the second part of this Introduction will focus on the theoretical basis of muscle mechanical work computation. Then, chapter 2 will provide an overview of the experimental protocols, instruments, data processing methods and characteristics of the recruited subjects. Chapters 3 and 4 will describe in more detail the instruments and the biomechanical models specifically developed for this study. Finally, chapters 5, 6 and 7 will illustrate and critically analize the results of the work.

1.1 A little bit of mechanics...

If we consider a dimensionless point with mass m, which, during a time interval dt is displaced by a quantity $d\mathbf{r}$ by the action of a force $\mathbf{F}$, then we can define the *work done by the force* $\mathbf{F}$ as:

$$dW = \mathbf{F} \cdot d\mathbf{r} \tag{1.2}$$

For a displacement from position P_1 to position P_2, the total work done is obtained via the integration:

$$W \,|_{P_1}^{P_2} = \int_{P_1}^{P_2} \mathbf{F} \cdot d\mathbf{r} \tag{1.3}$$

Power is the time rate of doing work:

$$P = \frac{dW}{dt} = \mathbf{F} \cdot d\mathbf{v} \tag{1.4}$$

where $\mathbf{v}$ represents the velocity vector of the point of application of the force. Displacement is measured in meters (m), force in newton (N), work in joule ($N \cdot m = J$), power in watt ($J/s = W$).

No work is done if the force and displacement vectors are mutually perpendicular or if the displacement is null.

Extending the analysis to a system of particles forming a rigid body rotating around an

axis z, the component of *rotational* work done on the body by the action of an external moment $\mathbf{M}$ is:

$$dW \;=\; M_z d\theta \tag{1.5}$$

where $\mathbf{M}_z$ is the axial component along z of the external moment and $d\theta$ is the infinitesimal angular displacement of the rigid body. In general, $\mathbf{M}$ might change with the variation of the angle θ. A moment is measured in $N \cdot m$.

In terms of *rotational* power:

$$P \;=\; \frac{dW}{dt} \;=\; M_z \frac{d\theta}{dt} \;=\; M_z \omega \tag{1.6}$$

with $\omega = \dfrac{d\theta}{dt}$ (in $rad \cdot s^{-1}$).

Therefore, the total work done by a set of forces acting on a rigid body, for an infinitesimal displacement, is:

$$dW \;=\; \mathbf{F} \cdot d\mathbf{r} + \mathbf{M} \cdot d\boldsymbol{\theta} \tag{1.7}$$

where $\mathbf{F}$ and $\mathbf{M}$ represent the external resultant force and moment, $d\mathbf{r}$ is the infinitesimal translation of the body center of mass and $d\boldsymbol{\theta}$ is the infinitesimal rotation of the body around its centre of mass.

We define *positive* work the work done by a force acting along the same direction of the displacement vector, while we define *negative* work the work done by a force acting in the opposite direction. The same applies to the moment action: rotational work is *positive* when moment action boosts the rotation of the body and *negative* otherwise (producing in the first case an increase in the magnitude of rotational velocity ω and a decrease in the second case).

A rigid body can be represented as a system of n material points with masses m_i whose reciprocal distances do not change. It is known from the fundamental laws of mechanics (Alonso and Finn, 1969) that, for a system of points subjected to internal (generated by interactions among points) and external (generated by interactions of the system with the surrounding environment) forces, the change in the total kinetic energy of the system, K, from the time instants t_0 and t_1, equals the sum of the work done by the external forces, W_{ext}, and by the internal forces, W_{int}:

$$\Delta K \;=\; K_1 - K_0 \;=\; W_{ext} + W_{int} \tag{1.8}$$

with $K = \sum_{i=1}^{n} \frac{1}{2} m_i v_i^2$.

For a rigid body, in planar motion, internal forces contributions cancel each other out, then $W_{int} = 0$, and kinetic energy can be defined as:

$$K = \frac{1}{2} m v_{COM}^2 + \frac{1}{2} I \omega^2 \tag{1.9}$$

with v_{COM} being the linear velocity of the centre of mass of the body (in m/s), I the *moment of inertia* of the body around an axis passing by its centre of mass (in $Kg \cdot m^2$), and ω the angular velocity around the same axis. If the motion is not planar and the body is simultaneously rotating around more axes, all the associated rotational energy components have to be considered in the analysis with their different moments of inertia, and the equation becomes:

$$K = \frac{1}{2} m \mathbf{v}^T \mathbf{v} + \frac{1}{2} \boldsymbol{\omega}^T \mathbf{I} \boldsymbol{\omega} \tag{1.10}$$

with $\mathbf{I}$ being the *tensor of inertia*.

Since the change in kinetic energy of the body depends only on the resultant vector of the external forces, it is necessary to point out that the summation of all the work fractions done by the individual forces on the body might differ from the work done by the resultant force (Zatsiorsky, 2002).

If the change in kinetic energy from the time instants t_0 and t_1 depends only by the work of *conservative* forces ($\mathbf{F}_c$), as *gravity* or *elastic forces*, the overall *mechanical energy* of the body will not change, since the definition of mechanical energy as:

$$E = K_0 + U_0 = K_1 + U_1 \tag{1.11}$$

with U called *potential energy*, energy associated to the work of a conservative force.

Forces (and moments) are *conservative* when the work done on a body, while moving it from one point in space to another, is independent of the path followed. In a body subjected only to conservative forces, the sum of the potential and kinetic energy components is constant.

Non-conservative forces ($\mathbf{F}_{nc}$) are instead affected by the path followed when the body is moved, as happens with friction forces and hydrodynamic resistance. Also the action

of the muscles has the characteristics of non-conservative force. Muscle-tendon structures can be considered as conservative elastic forces as far as they can act as ideal springs, allowing the recovery of elastic energy.

If non-conservative forces are also acting on the body, mechanical energy is then computed as:

$$E = K_0 + U_0 + W_{nc} = K_1 + U_1 \tag{1.12}$$

Where W_{nc} is the work done by non-conservative forces, that can be estimated from the variation of mechanical energy of the body: $W_{nc} = E_1 - E_0 = \Delta E$.

To study human motion, we have to extend these thoughts to a system composed by several rigid bodies linked together.

1.2 Muscle mechanical work

Despite clear definitions in terms of mechanical laws, terminology related to the study of mechanical work in biomechanics can be somewhat confusing. It is the case, for examples, of some terms like *external* and *internal* work that we will use extensively in this work, and that need, therefore, to be given a unique definition, or, at least, to be clarified with respect to the meaning that each author gives to the different terms (Cavagna and Kaneko, 1977; Winter, 1979; Zatsiorsky, 2002; Robertson et al., 2004).

Muscles are capable of two functions (Zajac et al., 2002): generate or absorb power via concentric or eccentric contractions, and redistribute energy between segments.

When body muscles do work, some of the energy expended can be used to move body segments and some can be used to do work on the external environment: the first component is sometimes referred to as *internal energy*, the second one as *external energy* (Winter, 1979; Robertson et al., 2004).

In the literature there exist three main methods that have been used to estimate muscle mechanical work: (a) the *Joint powers* approach, (b) the *External/Internal powers* approach and (c) the *Segmental powers* approach. In this section a short description of the three different methods is provided. Then, in section 1.3 a critical comparison beween the methods will be delineated.

1.2.1 Joint power analysis

The amount of power exerted by a muscle can be calculated by multiplying the muscle force by the shortening/lengthening velocity:

$$P = \mathbf{F} \cdot \mathbf{v} \tag{1.13}$$

If the muscle is acting with an isometric contraction, the power is zero.

Instead of looking at the single isolated muscle, we can refer its activity to the joint it is spanning. In joint terms, the amount of power can be computed from the product of the joint moment vector by the angular velocity vector of the joint:

$$P = \mathbf{M} \cdot \boldsymbol{\omega}_{joint} \tag{1.14}$$

with $\boldsymbol{\omega}_{joint} = \boldsymbol{\omega}_{proximal} - \boldsymbol{\omega}_{distal}$. If we write the previous equation in the form:

$$P = \mathbf{M} \cdot \boldsymbol{\omega}_{proximal} - \mathbf{M} \cdot \boldsymbol{\omega}_{distal} \tag{1.15}$$

we can observe that the power flowing through the muscle has two components, one related to the power delivered to, or subtracted from, the proximal segment and the other one delivered to, or subtracted from, the distal segment. These are defined as the *active power* flows to the segments, because they depend directly from the muscle attached to the segments connected to the observed joint (Kirtley, 2006). When $M\boldsymbol{\omega}_{proximal} = M\boldsymbol{\omega}_{distal}$ the muscle is contracting isometrically.

Power can also be transferred directly from one segment to another through the joint. This quantity is defined as *passive power* (Kirtley, 2006), and is calculated as:

$$P_{passive} = \mathbf{F}_{joint} \cdot \mathbf{v}_{joint} \tag{1.16}$$

which is different from the quantity expressed by eq. 1.13.

Even if it is defined as *passive*, $\mathbf{F}_{joint}$ can be dependent on the level of muscles activity around the joint (Zatsiorsky, 2002). Since at every joint the reactions from the proximal and distal segments are equal but opposite in sign, joint forces redistribute mechanical energy among body segments without changing the total mechanical energy of the whole human body (Robertson et al., 2004).

Mechanical energy expenditure (muscle work) for the whole body can be estimated summing up all the *active powers* acting on all the $N-1$ body joints, as defined in (Aleshinsky, 1986a,b):

$$W_m = \int_{T1}^{T2} \sum_{i=1}^{N-1} |\mathbf{M}_{i,i+1} (\boldsymbol{\omega}_{i+1} - \boldsymbol{\omega}_i)| \, dt \tag{1.17}$$

Taking the absolute value of each joint moment contribution means that all power contributions, negative and positive, are summed up together without any energy intercompensation among them. Net joint moments are computed via the *inverse dynamics* approach (Winter, 2005; Zatsiorsky, 2002; Robertson et al., 2004; Richards, 2008).

Although described in literature as the most accurate and mechanically correct way to *indirectly* estimate muscle mechanical work, results given by this method are influenced by the accuracy of the inverse dynamics process which affects the precision of joint moment computation, as will be discussed in more detail in chapter 4.

1.2.2 External/Internal power analysis

The *External/Internal powers* method is used to estimate muscle mechanical work from the computation and summation of two quantities, the so-called *external* work and *internal* work (Cavagna and Kaneko, 1977; Willems et al., 1995; Minetti et al., 1995).

The *external* work, W_{ext}, is related to the changes of mechanical energy of the the body centre of mass (COM, or BCOM) measured in the global reference system, while the *internal* work, W_{int}, is here associated with the changes in mechanical energy of the body segments, measuring their relative motion with respect to the COM.

External work is defined in (Cavagna, 1975) from the assumption that the resultant of the external forces acting on a body produces a change in the mechanical energy of the centre of mass of the body. This sentence is physically not fully correct: As described in section 1.1 the resultant of the external forces acting on a body, conservative or not, produces a change in the *kinetic* energy of the body. The change in mechanical energy depends only on that set of external forces which are non-conservative. During ground walking, two external forces are active on the human body: Gravity and the resultant of the ground reaction forces (GRF). The latter depends on the former, plus the effect of

muscles activity. The definition in (Cavagna, 1975) still works because the net external force acting on the COM is measured as:

$$\mathbf{R}_{ext} = \mathbf{GRF} + m\mathbf{g} \tag{1.18}$$

Since the change in potential energy is equal and opposite to the work done by the conservative forces (m**g**), and the quantity m**g** appears also inside the **GRF** term, then the work done by the muscles (non-conservative forces) against the force plate and gravity appears when $\mathbf{R}_{ext}$ is not zero, and is correctly measured as the variation of mechanical energy (in the hypothesis that air friction is negligible). [1]

By measuring the change in the mechanical energy of the COM, the *external* power done by the muscles can be estimated from:

$$P_{ext} = \frac{dW_{ext}}{dt} = \frac{dE_{mecc}}{dt} = \frac{dU}{dt} + \frac{dK_{COM}}{dt} \tag{1.19}$$

With $U = mgh$ being the potential energy of the COM (with m = mass, g = gravity acceleration, h = height of the COM from a reference point), $K_{COM} = \frac{1}{2}mv_{COM}^2$ its kinetic energy.

An advantage of *external* power computation is its relative simplicity of measurement. It can be estimated integrating the measured ground reaction forces, minus body weight and scaled by the body mass, and knowing the velocity of the COM at the beginning of the movement, without the need of any other kinematic and anthropometric data. In

[1] The definition of work done by external forces on a body is:

$\mathbf{R}_{ext}\, d\mathbf{r} = dK$

$(\mathbf{F}_{nc} + \mathbf{F}_c)\, d\mathbf{r} = dK$

$\mathbf{F}_{nc}\, d\mathbf{r} = dK + dU = dE$

Following Cavagna's definition:

$\mathbf{R}_{ext}\, d\mathbf{r} = dE = dK + dU$

$(\mathbf{GRF} - m\mathbf{g})\, d\mathbf{r} = dK + dU$

$\mathbf{GRF}\, d\mathbf{r} = dK + dU - dU$

$(\mathbf{F}_{nc} + m\mathbf{g})\, d\mathbf{r} = dK$

$\mathbf{F}_{nc}\, d\mathbf{r} = dK + dU = dE$

(Cavagna, 1975) external forces were measured at the interface between the body and the ground via force plates that were, for this reason, called "ergometers".

However, if needed, COM movement can also be computed from kinematics (Eames et al., 1999; Rabuffetti and Baroni, 1999; Gard et al., 2004).

Considering König theorem for kinetic energy (Mazzoldi et al., 2006), the kinetic energy of a system made by N points can be divided into two components:

$$\begin{aligned} K &= \sum_{i}^{N} \frac{1}{2} m_i v_i^2 \\ &= K_{COM} + K_{i,COM} \\ &= \frac{1}{2} M v_{COM}^2 + \sum_{i}^{N} \frac{1}{2} m_i \|v_i - v_{COM}\|^2 \end{aligned} \tag{1.20}$$

with K_{COM} being the kinetic energy of the COM measured in the global reference system and $K_{i,COM}$ being the kinetic energy of the body points measured in the COM reference system. Therefore, the term K_{COM} is associated with external work computation, while $K_{i,COM}$ is used to compute the kinetic energy of the points measuring their translational velocity relative to the centre of mass.

If the body is composed by N rigid segments, the second term of the previous equation is associated to the power produced by the muscles to change the kinetic energy of the segments relatively to the centre of mass of the body:

$$\begin{aligned} P_{int} &= \frac{d}{dt} K_{i,COM} + \frac{d}{dt} K_{rot} \\ &= \sum_{i=1}^{N} \frac{1}{2} \left(\frac{d}{dt} \left[m_i \|v_{COM} - v_i\|^2 \right] + \frac{d}{dt} \left[\boldsymbol{\omega}_i^T \mathbf{I}_i \boldsymbol{\omega}_i \right] \right) \end{aligned} \tag{1.21}$$

Total muscle mechanical work computation with this approach is generally obtained by summation of all the positive increments of mechanical energy, P_{ext}^{+} and P_{int}^{+}, happened during the movement to be analized:

$$W_{tot} = \int_{T1}^{T2} P_{ext}^{+} + P_{int}^{+} \, dt \tag{1.22}$$

Limitations of the approach and possible fractions of work incorrectly measured due to wrong evaluation of energy transfers were discussed in (Willems et al., 1995; Minetti et al., 1995) as a reply to (Aleshinsky, 1986a,b,c,d,e).

The choice to consider only the production of positive power does not take into account metabolic energy necessary for negative work production by the muscles.

Despite the limitations that can arise related to the estimation of the total muscle mechanical work with this approach, the method is still valuable when applied to simplified models of walking, where the focus is to study the movement and the energy of the centre of mass as a global representation of the whole body behaviour, as in the *inverted pendulum model* (Cavagna et al., 1976, 1977; Cavagna, 1988; Kuo, 2007; Gordon et al., 2009).

However, in the original definition only the resultant ground reaction force applied to the centre of mass was considered (a method called later as *combined limbs* method), leading to reciprocal cancellation of simultaneous positive and negative work fractions produced by the two separate legs during the double support phase, as shown in (Donelan et al., 2002). Therefore, only if external work on the COM is computed separately from the two ground reaction forces associated to the two legs (*combined limbs* method) then the different simultaneous work components can be measured.

If external work is computed evaluating COM motion from kinematic data, only the net external work can be estimated.

1.2.3 Segmental power analysis

In the *Segmental powers* method the muscle mechanical work required to move the body segments is estimated by measuring the changes in the mechanical energy of the body segments.

Potential and kinetic energy components of all the separate segments, measured in the global reference frame at each instant of time, are calculated and then the absolute values of energy variations are summed together (Winter, 1979).
The mechanical energy of the i-th segment at any instant of time is:

$$E_i = m_i g h_i + \frac{1}{2} m_i v_i^2 + \frac{1}{2} \boldsymbol{\omega}_i^T \mathbf{I}_i \boldsymbol{\omega}_i \tag{1.23}$$

The summation of all the segmental energy variations to compute the total mechanical work can be done in different ways (Pierrynowski et al., 1980) by:

(1) Accounting for energy transfer within (w) and between (b) segments:

$$Wwb = \int_{T1}^{T2} |\sum_{i=1}^{N} \frac{d}{dt} E_i| dt \tag{1.24}$$

(2) Accounting for energy transfer within (w) but not between segments:

$$Ww = \int_{T1}^{T2} \sum_{i=1}^{N} |\frac{d}{dt} E_i| dt \tag{1.25}$$

Equations 1.24 and 1.25 differ in the different possibilities of energy intercompensation allowed inside the system. In the first equation all possible energy transfers are admitted, and therefore the mechanical energy expenditure computed would be lower than in the second equation, where reciprocal energy cancellations between segments is prevented. In some investigations a compromise between the two equations has been attempted, allowing energy transfers between some segments (e.g. segments belonging to the same limb) but not between others (e.g between limbs and trunk). A deep investigation on the different combinations of energy transfers and on the possibile elastic energy recuperation during running at different speeds was done by Williams and Cavanagh in (Williams and Cavanagh, 1983), where they concluded that a dramatically wide range of values for mechanical power can be obtained for running, depending upon the particular assumptions made and computational procedures employed.

Muscle mechanical work necessary to change the mechanical energy of the body segments as computed in equations 1.24 and 1.25 was defined in (Winter, 1979) as *internal*, but note that this definition is different from the *internal* work definition given in section 1.2.2. A difference that has never been clearly pointed out in the literature. In (Winter, 1979) the author defined *external* work as the additional work performed by the muscles during (possible) interaction of the body with external forces like a weight to lift, a load to push or pull, or an ergometer load. Gravity, acting directly on all the single body segments as a conservative force, is included in the mechanical energy expression and therefore muscle work done against gravity is already taken into account in the *internal* work component.

Therefore, in Winter's definition, the overall work done by the muscles, in the hypothesis that external work is related only to external forces originated by muscles activity

(e.g. by pulling a load, and not by being lifted by an elevator) is computed considering:

$$W_{muscles} = W_{ext} + W_{int} \tag{1.26}$$

1.3 A comparison of the different approaches

For every body segment i we can write an *energy balance equation*:

$$\mathbf{F}_{-i} \cdot \mathbf{v}_{-i} - \mathbf{F}_{+i} \cdot \mathbf{v}_{+i} + \mathbf{M}_{-i}\boldsymbol{\omega}_{-i} - \mathbf{M}_{+i}\boldsymbol{\omega}_{+i} = \frac{d}{dt} m_i g h_i + \frac{d}{dt}\frac{1}{2} m_i v_i^2 + \frac{d}{dt}\frac{1}{2}\boldsymbol{\omega}_i^T \mathbf{I}_i \boldsymbol{\omega}_i \tag{1.27}$$

where we used the simplifications: $-i = i-1, i$ referring to power exchanges with the previous/proximal segment, and $+i = i, i+1$ referring to power exchanges with the following/distal segment.

Following (Aleshinsky, 1986a) we can define forces and moments acting on a body segment as *sources of mechanical energy*. Through this equation, the work done by the non-conservative *sources* of mechanical energy (joint moments and forces) acting on a segment are related to the change in the *potential* and *kinetic* energy components of that segment, if the segment is supposed to be rigid (Zatsiorsky, 2002; Aleshinsky, 1986a). Considering a system composed by N segments, the rate of change of the total mechanical energy of the body is:

$$\frac{dE}{dt} = \sum_{i=1}^{N} \frac{dE_i}{dt} = \sum_{i=1}^{N} (\mathbf{F}_{i,i-1} \cdot \mathbf{v}_{i,i-1} - \mathbf{F}_{i,i+1} \cdot \mathbf{v}_{i,i+1} + \mathbf{M}_{i,i-1}\boldsymbol{\omega}_{i,i-1} - \mathbf{M}_{i,i+1}\boldsymbol{\omega}_{i,i+1}) \tag{1.28}$$

Considering segments O and N as the terminal links, and remembering that powers of joint forces, being *internal* forces to the system, cancel out each other, the equation can be expanded and simplified:

$$\frac{dE}{dt} = \mathbf{F}_O \cdot \mathbf{v}_O - \mathbf{F}_N \cdot \mathbf{v}_N + \mathbf{M}_O\boldsymbol{\omega}_1 - \mathbf{M}_N\boldsymbol{\omega}_N + \sum_{i=1}^{N-1} \mathbf{M}_{i,i+1} (\boldsymbol{\omega}_{i+1} - \boldsymbol{\omega}_i) \tag{1.29}$$

This equation describes the rate of change of the total mechanical energy of the system as a function of the external energy sources and as a function of the internal (muscular) sources.

If there are no external energy sources, the energy change depends only on internal muscle action:

$$\frac{dE}{dt} = \sum_{i=1}^{N-1} \mathbf{M}_{i,i+1} \left(\boldsymbol{\omega}_{i+1} - \boldsymbol{\omega}_i \right) \tag{1.30}$$

Theoretical differences among the Aleshinsky's *Joint powers* method and the *Segmental powers* method used to compute whole body muscle work, in the end, depend on which member of equation 1.27 is used.
If there are no absolute values symbols embracing any of the quantities involved, their computed values should be equivalent (Cappozzo et al., 1976). Moreover, they should also be equivalent to the *External/Internal powers* method in the original Cavagna's definition, since the equality is guaranteed by the König theorem.

Therefore, two critical points have to be considered when comparing the three methods: (1) Effects of external energy sources and (2) Summation and integration of the power components.

1.3.1 Effects of external energy sources

In the *Segmental powers* method, action of external forces need to be added considering the particular situation that is being examined, since there might be forces that act on the system changing segments energy with no muscle work, or, on the other side, there might be forces that act on the system with little change in segments energy but large work done by the muscles.

As already pointed out in section 1.2.3, the *internal* work, as defined in (Winter, 1979; Pierrynowski et al., 1980), is related to the total work necessary to change the kinetic and the potential energy of the body segments, measured in the global reference frame. The author defined *external* work as the additional work performed by the muscles during (possible) interaction of the body with external forces like a weight to lift, a load to push or pull, or an ergometer load.

The *internal* work, as intended in (Cavagna and Kaneko, 1977; Willems et al., 1995; Minetti et al., 1995), is instead the work necessary to change only the kinetic energy of the

body segments measured with respect to the body center of mass. The potential energy changes of the body segments are included in the *external* work component. Reciprocal movements of different segments with variations of potential energy opposite in sign, therefore, cancel out each other without any possibility to be separately measured.

In the following, we will use the terms *internal* and *external* work referred to the second method, while *internal* work as defined in (Winter, 1979) will be referred to simply as *(total) segmental* work, remembering, however, that during walker locomotion there is a fraction of work done by the body on the handles of the device that has to be added separately to the segmental work to give the final whole-body muscle (*segmental*) mechanical work.

In the *Joint powers* method, the action of external forces (other than gravity) is considered in terms of forces and moments applied to the terminal link(s) of the system. Therefore, their effects on the joint activity is already taken into account as part of the inverse dynamics computations, and the total muscle work produced to move body segments and to do work against external forces is computed using eq.1.30.

Our discussion was restricted on the investigation of muscle mechanical work during walking and walking with walking aids. A similar analysis can be done when studying running movements. But with complex movements that involve the body interacting with external work in a more complex way, a careful analysis of the problem has to be done. In the *External/Internal powers* method this issue appears more critical, since action of external forces is considered only in terms of changes in energy of the centre of mass!

As a general example, let us imagine a subject standing on an elevator: His total mechanical energy is changing (in terms of potential energy plus, if the elevator is also accelerating, kinetic energy). In this case there has been no muscle action involved. But if we consider a subject pedaling on a cyclo-ergometer with the same frequency against different external loads, we have to include in the computation not only the mechanical energy changes of the segments, which will be always the same in all the conditions, but also the power exchanged by the body with the external forces and moments transmitted by the saddle and the pedals. A similar example could be a man placed horizontally (no

need to include gravity in the problem) who extends symmetrically his legs and his arms acting against two compressing loads (like two ideal springs). There would be almost no COM displacement and very little variation in kinetic energy of the body segments...

If a subject is walking with the use of a walker, of with the use of crutches, there might be a certain amount of work performed by the muscles while interacting with the device which needs to be taken into account.

1.3.2 Summation and integration of the power components

Ideally, from the definitions of power and work seen earlier in this chapter, the computation of mechanical work over a time interval $[T_1, T_2]$ comes straightforwardly from integration of eq.1.29.
However, this point is the most critical for the estimation of *muscle* mechanical work. With a simple integration we obtain:

$$\Delta E\,|_{T1}^{T2} = \int_{T1}^{T2} \{\mathbf{F}_O \cdot \mathbf{v}_O - \mathbf{F}_N \cdot \mathbf{v}_N + \sum_{i=1}^{N-1} \mathbf{M}_{i,i+1}\,(\boldsymbol{\omega}_{i+1} - \boldsymbol{\omega}_i) + \mathbf{M}_O \cdot \boldsymbol{\omega}_1 - \mathbf{M}_N \cdot \boldsymbol{\omega}_N\}\,dt \quad (1.31)$$

The result is the same if we consider the second term of eq.1.27 for integration:

$$\Delta E\,|_{T1}^{T2} = \int_{T1}^{T2} \sum_{i}^{N} \{\frac{d}{dt} m_i g h_i + \frac{d}{dt}\frac{1}{2} m_i v_i^2 + \frac{d}{dt}\frac{1}{2} \boldsymbol{\omega}_i^T \mathbf{I}_i \boldsymbol{\omega}_i\}\,dt \quad (1.32)$$

We can define the quantity calculated with equations 1.31 and 1.32 as *net* muscle mechanical work, which, for cyclic movements, gives $\Delta E = W = 0$ since positive and negative work contributions would be equal in magnitude but opposite in sign.

To overcome the problem of *zero-work* computation, some authors consider only muscle energy expenditure coming from positive power production (Cavagna and Kaneko, 1977; Willems et al., 1995), while others use definitions that take into account both negative and positive power quantities, introducing summation and integration of the absolute values of the different power components, as described in the previous sections (Aleshinsky, 1986b; Winter, 1979; Pierrynowski et al., 1980).

Aleshinsky suggests that the energy expenditure (EE) of external and internal (muscle)

sources in the system has to be computed as:

$$EE = \int_{T1}^{T2} \{|\mathbf{F}_O \cdot \mathbf{v}_O| + |-\mathbf{F}_N \cdot \mathbf{v}_N| + \sum_{i=1}^{N-1} |\mathbf{M}_{i,i+1} (\boldsymbol{\omega}_{i+1} - \boldsymbol{\omega}_i)| + |\mathbf{M}_O \cdot \boldsymbol{\omega}_1| + |-\mathbf{M}_N \cdot \boldsymbol{\omega}_N|\} dt \tag{1.33}$$

In this case the equivalence between equations 1.31 and 1.32 is lost.

Therefore, if we wanted to study the energy necessary to perform a movement that involves several body segments, we could approach the problem from either the first or the second term in eq.1.27, summing up joint powers from all body joints or summing up the mechanical energy variations of all the body segments, keeping in mind, however, that results will be theoretically equivalent only summing up terms without the introduction of absolute values among the integrands.

To avoid the problem of *zero-work* values and, at the same time, maintain the equivalence among the different methods, we can introduce absolute values symbols just before the final integration of the *whole-body* power curves of time, that is, after all the joint-by-joint or the segment-by-segment summations. Physiologically, this operation is equivalent to allow, at every time instant, all the possible energy transfers between segments, but without allowing any recuperation of this energy over time.
It is doubtful if the results obtained in this way (as, of course, in all the other possible formulations) are then able to reflect the metabolic energy needed by the muscles to perform the movement investigated, but answering this question is out of the scope of this work. It is undoubtful, instead, that none of the methods, with or without any absolute values, is capable of quantifying the energy associated with isometric force production by the muscles.

1.3.3 Further elements of discussion

In (Aleshinsky, 1986a,b,c,d,e) the author claims that his formulation of the joint powers approach gives the closest estimation of muscle mechanical work which can give evidence of the muscles energy expenditure. His formulation is rigorous and physically correct, and, by looking at the *net* muscle action at joint level instead of measuring its final effect on the segments, probably allows to analyse power production closer to the real power

sources.

However, a couple of flaws can be found, in his attempt to analise critically the other two approaches, originated by a misinterpretation of the definitions of external work given in their publications respectively by G. Cavagna and D. Winter.

In (Aleshinsky, 1986b), page 299, eq. 34, the author arrives at the conclusion that, considering an ideal situation with a person moving as an inverted pendulum with a foot contacting the ground, Cavagna's definition of total work as summation of the internal and external work components would give a value different from zero. But a careful examination of eq. 34 shows that all terms inside the integral signs will cancel out each other with final null result (since the ground reaction force acting on an inverted pendulum produces no net work on the center of mass!).

In (Aleshinsky, 1986d), at page 308, the author discusses the calculation of muscle mechanical work with the segmental method when allowing for energy transfer between segments (W_{wb}, see eq.1.24 described previously here). He criticises that with this approach "(...) *intercompensation of the external and internal sources is admitted that physically makes no sense at all*". However, in the original definition given in (Winter, 1979), it is not clearly defined if work done by external sources is taken into account separately, or if it is included within the summation of segments energies.

The *joint powers* approach, based on inverse dynamics computations, has the advantage to provide an unambiguous representation of the external and internal forces and moments involved.

Chapter 2

Materials and Methods

This chapter contains a description of instruments, data acquisition protocols, implementation of models for data processing. Further details on instruments and biomechanical models specifically designed and developed during this work will be given in the following chapters, 3 and 4.

2.1 Human movement analysis

Technology has provided movement analysis with instruments to investigate the characteristics of the human movement and, focusing on clinical applications, of the human gait (Perry, 2005; Kirtley, 2006; Richards, 2008). Traditionally, during a gait examination the lower limbs joint angles, moments and powers are investigated in the three anatomical planes during a *gait cycle*, which is defined as the time period from a heel strike of a foot on the ground to the following heel strike of the same foot. Pelvis and trunk movements can also be computed.

The analysis can also be extended to the upper-limbs and whole body movements, with aims not only related with rehabilitation purposes, but also to sport performance and ergonomics.

Kinematics of the human body is commonly measured via optoelectronic systems which register the three-dimensional movement of reflective markers placed on the subject's anatomical landmarks. A biomechanical model is then built to compute internal

joint centers and measure the movement of the body segments (Cappozzo et al., 2005; Chiari et al., 2005; Leardini et al., 2005; Della Croce et al., 2005). Dynamic interaction of the body with the external world is measured by force plates placed at the ground level and, eventually, by other load cells, that provide the input forces and moments for the inverse dynamics computations used to estimate loads acting at the body joints. Estimation of the inertial properties of the subject are needed at this stage, to link kinematic and kinetic information. Surface or fine-wire electromyography provides information on the muscle activity, allowing a deeper segment-by-segment analysis of the possibile control strategies or alterations of the locomotion function (Winter, 2005; Zatsiorsky, 2002; Robertson et al., 2004; Richards, 2008; Merletti, 2000).

2.2 Instrumentation and models

In order to estimate the whole body muscle mechanical work during normal walking and walker-assisted locomotion, a full-body 3-dimensional kinematic and kinetic model was needed to compute kinetic and potential energy of body segments, whole body centre of mass, joint moments and angles. Details on the model are described in chapter 4.

Kinematic data were measured by reconstructing the spatial 3-dimensional position of reflecting spherical markers via optoelectronic motion capture systems equipped with infrared light emitters and high-resolution digital cameras. Dinamic interaction of the feet with the ground was measured via force plates.

Hands interaction with the walker frame needs to be measured via load cells. We designed two instrumented handles to be placed on the walker to measure 6 degrees of freedom loads applied by the hands of the subject. Details on handles design, construction and calibration are described in chapter 3.

2.3 Data acquisition

2.3.1 Laboratory setup

Data on healthy children and one cerebral palsy child, MM, were all acquired at the Biomechanics Laboratory at the University of Verona, Italy, equipped with a 8 cameras Vicon system (Vicon, Oxford, UK) a 90x90 cm AMTI (Advanced Mechanical Technology, Inc., Watertown, USA) and a 60x40 cm Kistler (Kistler Instruments corp, Amherst, NY, USA) force plates.

All the other cerebral palsy children were acquired at the Gait Analysis Laboratory at San Bassiano Hospital, Bassano del Grappa, Italy, equipped with a 6+2 cameras Vicon system and two 60x40 cm AMTI force plates.

Preliminary data on upper limbs with instrumented handles applied to an adult anterior walker were acquired at the Oxford Gait Laboratory, Nuffield Orthopaedic Centre, Oxford, UK, equipped with a 12 cameras Vicon system and three 60x40 cm AMTI forceplates.

Instrumented handles were connected to the different Vicon systems during the acquisition sessions.

For the tests on healthy and CP children, handles were applied to a posterior walker with wheels (Crocodile walker model, R82, Gedved, Denmark), available in two sizes depending on the subjects height.

2.3.2 Subjects

This section contains anthropometric characteristics of the healthy and the cerebral palsy (CP) subjects involved in the study.

Healthy children group

Data from 10 subjects between 6 and 13 years old (mean age 9.8 y $\pm$ 2.7, mean height 1.36 m $\pm$ 0.17, mean weight 33.9 Kg $\pm$ 11) were acquired during ground level walking at self-selected speed and during walker locomotion at self-selected speed.

Age difference is quite large, however, in (Stansfield et al., 2001) it was shown that speed is more determinant than age on kinematic and kinetic changes observed in growing children.

Table 2.1: Characteristics of the healthy group subjects. Age is relative to data acquisition date. Styloid height is the measure of the height of the right ulnar styloid from the ground with the subject in a neutral position. Body mass in expressed in *Kg*, all length measures are in *mm*.

Subject	**VT**	**IC**	**EC**	**MS**	**GZ**	**FF**	**GV**	**FC**	**LC**	**PT**
Sex	f	m	m	m	m	m	f	f	m	m
Age (y)	13	13	8	9	10	9	12	10	6	6
Bodymass	34.7	48.7	31.4	25.4	29.8	42.6	52.5	32.3	21.2	20.2
Height	1580	1550	1320	1300	1335	1371	1570	1360	1120	1120
Styloid height	780	760	610	585	625	630	780	660	520	510
R leg length	850	830	650	645	695	700	900	715	615	530
L leg length	840	830	650	640	690	700	900	715	615	530
R knee width	93	102	91	82	86	102	107	87	77	74
L knee width	93	102	91	82	86	101	107	85	77	74
R ankle width	61	70	64	54	54	63	64	56	50	52
L ankle width	61	70	64	54	55	64	65	55	50	52
Walker size	larger	larger	smaller	smaller	smaller	larger	larger	larger	smaller	smaller

Cerebral palsy children group

Data from five CP children with age between 6 and 12 were acquired in their usual walking condition, either with or without walking aid; one subject only was analyzed in both conditions. No mean values on the group were computed, since each subject was considered as a single case-study. Subjects were asked to walk at their self-selected speed, wearing their orthopaedic shoes and ankle-foot orthosis, if that was their normal walking condition (see table for details).

2.3.3 Data acquisition protocol

Video data were acquired at 100 Hz.

Ground Reaction Forces (GRFs) were recorded using two adjacent floor-mounted force-plates, while Handle Reaction Forces (HRFs) and Moments (HRMs) were recorded using the two instrumented handles.

Force plate and handles data were acquired at 1000 Hz, since some surface electromyographic data (which need a sampling frequency of 1 kHz) were collected synchronously during the trials.

Table 2.2: Characteristics of the CP group subjects. Age is relative to data acquisition date. Styloid height is the measure of the height of the right ulnar styloid from the ground with the subject in a possible neutral position. Body mass in expressed in *Kg*, all length measures are in *mm*.

Subject	**MM**	**AV**	**IA**	**FM**	**PA**
Diagnosis	diplegia	emiplegia (L)	tetraplegia	diplegia	diplegia
Sex	m	m	m	m	m
Age (y)	6	8	12	7	9
Bodymass	20.0	23.8	32.6	21.9	33.1
Height	1180	1230	1420	1120	1265
Styloid height	–	–	680	510	630
R leg length	570	620	710	540	670
L leg length	560	615	710	540	670
R knee width	73	80	85	65	90
L knee width	72	80	85	65	90
R ankle width	49	55	55	75	65
L ankle width	46	55	55	75	65
Trial	gait	gait	walker	walker	both
Condition	AFOs and shoes	barefoot	AFOs and shoes	AFOs and shoes	shoes
Walker size			larger	smaller	smaller

Walker wheels were isolated from the ground via two 6 meters long rails which supported the wheels avoiding contact with the forceplates.

Healthy subjects

With the healthy subjects, data were acquired, in the same day, during normal walking and during locomotion with a posterior walker.

Handles were placed at the height of the right ulnar styloid (approximately 45% of subjects' height) taking into account the height of the rails.

Subjects were asked to walk using the walker in order to reduce the loads on the lower limbs. Mean loads exerted on the walker during the trial, compared to the subject's body weight, were later computed from the collected data.

CP subjects

With the CP subjects, data were acquired either during normal walking or during locomotion with a posterior walker. For one subject, AP, data were collected in both conditions, since the subject was able to walk short distances without the walker.
GRFs were recorded whenever possible. Despite the use of rails, it has been very hard to get proper feet position over the forceplates, due to irregular step length, scissoring leg movements, easy fatigability of the subjects.
Handles were placed either at the height of the ulnar styloid, or at the habitual height of their walker handles, if they came to the laboratory with that.
A security brake was activated on the two posterior wheels of the walker to prevent backward movement and help, if needed, the possibility to act on the walker handles to generate forward propulsion together with forward support.

2.4 Data processing

Healthy subjects

Three trials with *clean* double support over the two forceplates could be selected for all the 10 subjects but one, for whom it was possibile to select only two trials, during normal walking and when using the walker. A right and left gait cycles were selected from each trial, correspondent to the subject placing the right foot on a plate and the left foot on the other one.

CP subjects trials

All possible trials with *clean* double support over the two forceplates were selected. For those subjects for whom good GRF data were not available in at least one trial, kinematic data from a right and left gait cycles were in any case selected from three trials.

Processing

All selected trials were processed in Vicon Nexus 1.5 (Vicon Motion Systems, Oxford, UK).

A biomechanical model was developed and applied to the data using Vicon BodyBuilder software (see section 4.5) to obtain joint centers trajectories, joint angles, moments and powers, segments COMs and whole-body COM.

Kinematic data were filtered before (Vicon Woltring filtering routine, $MSE = 5$ option, to provide the necessary smoothing to compute velocities and accelerations) and after (Vicon Woltring filtering routine, GCV option, to filter noise introduced by kinetic data and to fill gaps introduced by Vicon BodyBuilder computations) inverse dynamics computations. Digital filtering of raw force plate data before inverse dynamics was not available in Vicon Nexus version 1.5.

Trials data were exported in .C3D format (http://www.c3d.org/). A library of functions written in MATLAB 7 (The MathWorks, Natick, Massachussets, USA) was developed to import and process the data in order to compute whole-body muscle mechanical work and generate final plots.

Since ground reaction force data were available from two force plates only, bilateral lower limbs kinetics was not available during both double support phases in none of the gait cycles selected. To solve the problem we selected, for the following processing, the gait cycle on the side whose foot hit the first of the two force plates. Then, in the hypothesis that the subject was walking with constant speed and constant kinematics/kinetics, we extracted the contralateral lower limb kinetic data (ankle, knee and hip joints forces, moments and powers) during all the ground contact phase (stance) and, after interpolation of the signals to fit exactly the pasting region, we pasted them over correspondent signals during the stance phase in the previous gait cycle. Time duration of the two stance segments was compared for all the collected trials, to check if there were differences too large to accept the hypothesis of constant kinetics between adjacent gait cycles. Measured differences were all below 10 samples (0.1 s).

2.5 Statistical analysis

Statistical analysis was performed with SPSS (version 16.0, SPSS Inc.) on healthy children data only.

Statistical comparison of the results obtained for the healthy children during normal gait and walker with the different methods was performed on the parameters *Wpositive* (W+) and *Wabsolute-net*, (Wabsnet).

Intra-subject mean values were used for the comparisons, since we had two good trials instead of three for one subject, in both gait and walker conditions.

Evaluations were made by using analysis of variance for repeated measures. Differences between methods were investigated by pairwise post hoc comparisons (Bonferroni correction).

Walking speed was not considered here as an effect to be taken into consideration, since all trials were performed at the subject's own self selected speed and the interest here was a comparison of the different methods used to estimate muscle work, which get applied to the same original kinematic data.

Further details and results on the statistical analysis are provided in appendix A.

2.6 Muscle mechanical work computation

For all healthy subjects, muscle mechanical work was computed during normal gait and walker locomotion following the three different methods described in chapter 1. For CP subjects, the method applied was dependent on walking conditions and availability of data acquired.

Differently from other authors who investigated this topic, we did not apply straightforwardly each methods as it was originally defined in the literature. In order to better highlight and understand the differences connected with the founding equations, once computed the basic power components as a function of time (joint powers, segment powers or external plus internal powers), we applied the same criteria to all the three methods to sum together all the components and integrate along the gait cycle.

2.6.1 Computing power components

For the *Joint powers* method, rotational joint powers were computed for all the body joints as

$$P_j(t) = \mathbf{M}_j \cdot \boldsymbol{\omega}_j \tag{2.1}$$

via inverse dynamics implemented in Vicon BodyBuilder (see chapter 4 for more details). For the *Segmental powers* method, powers were computed as the rate of change of segments mechanical energy

$$P_s(t) = dE_s(t)/dt \tag{2.2}$$

with the mechanical energy of each segment $E(t)$ computed from kinematic data and the use of anthropometric tables (section 4.3) to estimate the inertial parameters and the center of mass of the segments, following eq.1.23. The external powers done by the hands on the walker handles were included as additional power contribution terms:

$$P_{Hr}(t) = -\mathbf{HRF}_r(t) \cdot \mathbf{v}_{right-handle}(t) \tag{2.3}$$

$$P_{Hl}(t) = -\mathbf{HRF}_l(t) \cdot \mathbf{v}_{left-handle}(t) \tag{2.4}$$

With **HRF** being the Handle Reaction Force, and **v** being the velocity vector of the handle centre, for the right and left sides.
For a complete analysis of the hand/handle interaction, frictional forces $\mathbf{F}_{fr}$ and handle acceleration should be taken into consideration:

$$\mathbf{F}_{hand} + \mathbf{HRF} + \mathbf{F}_{fr} = m_W \mathbf{a}_H \tag{2.5}$$

With $\mathbf{F}_{hand}$ the force applied by the hand on the handle, **HRF** the handle reaction, m_W the walker mass and $\mathbf{a}_H$ the acceleration of the handle, which can be different from zero even at constant walking speed, since the gait cycle consists of different phases. However, in this analysis we supposed the term $m_W \mathbf{a}_H$ to be minimal and that frictional forces are negligible, defining $\mathbf{F}_{hand} = -\mathbf{HRF}$.
For the *External/Internal* powers method, the *external* component was computed in two different ways, using both the *combined limbs* and the *individual limbs* methods described in section 1.2.2. With the combined limbs method, we estimated the power associated to

the COM from kinematics as:

$$P_{COM}(t) = dE_{COM}(t)/dt \tag{2.6}$$

while with the individual limbs method we computed the external mechanical power separately generated by each one of the two legs:

$$P_{COM}(t) = \mathbf{grf}_{right}(t) \cdot \mathbf{v}_{COM}(t) + \mathbf{grf}_{left}(t) \cdot \mathbf{v}_{COM}(t) \tag{2.7}$$

following the same method outlined in (Donelan et al., 2002). The two methods were applied only to gait trials of the healthy subjects group, to highlight the numerical differences between the two. To apply the *individual limbs* method also to the walker trials, upper limbs contributions should be taken into account.
Internal powers were estimated following eq.1.21, and therefore using the same data used for the segmental powers computations, with the difference that translational velocity of the segments was here expressed in the body COM reference system.

As we discussed in section 1.3, the *Joint powers* and the *Segmental powers* methods are equivalent until we do not introduce any absolute value among the power terms to be summed together (see eq.1.27). The *External/Internal powers* method differs from the *Segmental* one due to the fact that the center of mass is an overall syntheses of the contemporaneous positive and negative work performed by muscles at the different limbs, but if the summation of all the power components is done without absolute values, the final net result should be equivalent to the previous two.

Therefore, depending on the different methods we can use to sum together the power values between the different segments and to integrate power curves during time, we will obtain different values for the muscle mechanical work (Fig.2.1). Since it appeared interesting, and innovative, to discuss the different results obtainable with the different summation/integration methods with all the three power approaches, we defined five whole-body power components to be computed and compared. With $f_i(t) = P_i(t)$ for the $n-1$ joint power components and $f_i(t) = dE_i(t)/dt$ for the n segmental power components, we have:

$$F^+(t) = \sum_i f_i^+(t) = \sum_i (f_i(t) > 0) \tag{2.8}$$

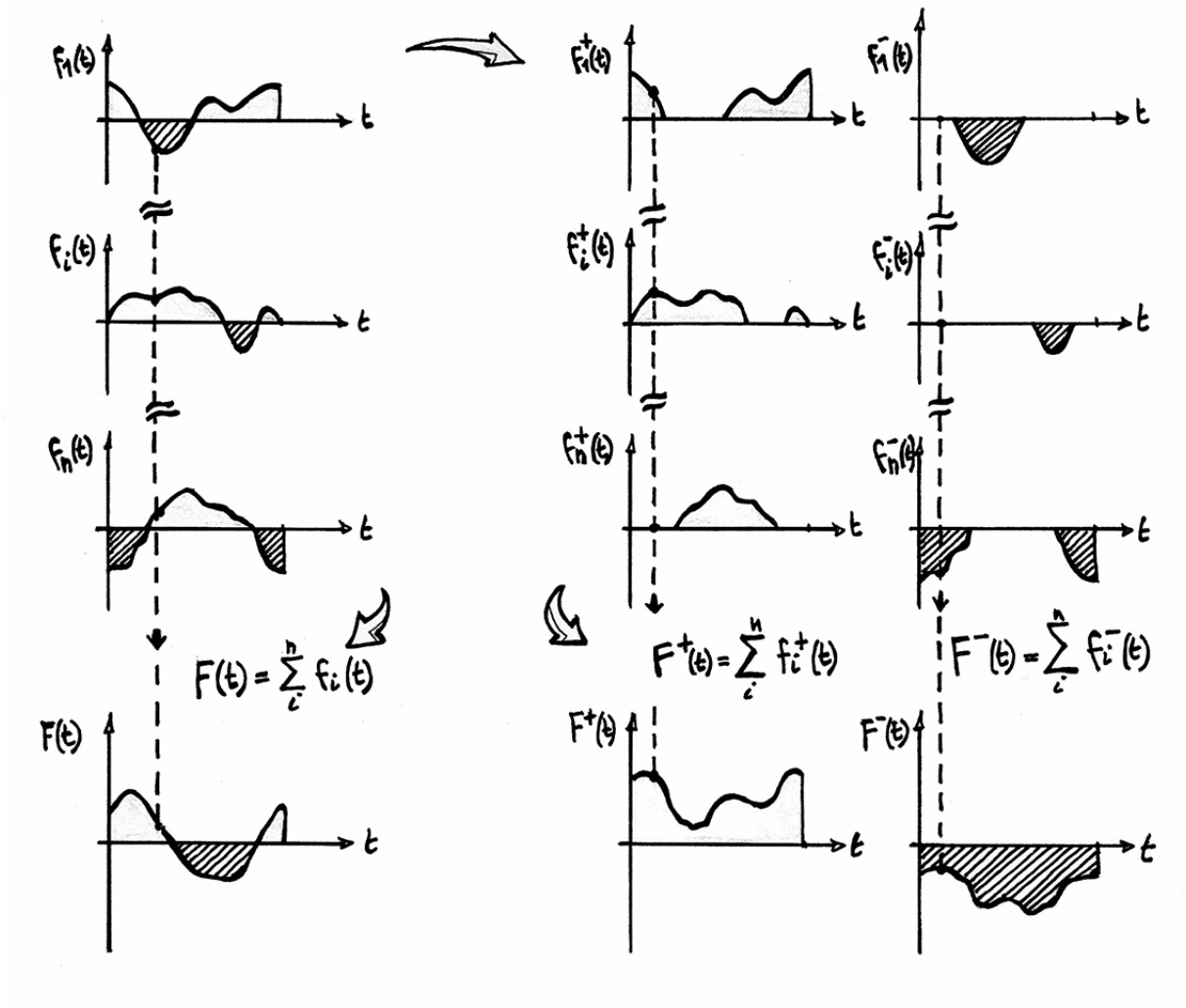

Figure 2.1: Different ways of summation of the joint or segmental power components during a gait cycle. See text for symbols explanation.

$$F^-(t) = \sum_i f_i^-(t) = \sum_i (f_i(t) < 0) \tag{2.9}$$

$$F(t) = F^+(t) + F^-(t) = \sum_i f_i(t) \tag{2.10}$$

With the *External/Internal* powers method, the equations above were separately applied to the COM *external* power curve and to the segments *internal* power curves. In the literature energy expenditure has mostly been studied in terms of work (i.e. energy expended for a unit of locomotion as a step, a stride, 1 meter). However, it seems also interesting to have the possibility to investigate the total body power curve variations

during gait **before** integration, because this information could provide useful insights on global production, absorption and recuperation of energy during the gait cycle phases.

2.6.2 Summation and integration of power components

Depending on the way we integrate the F elements above, different values can be obtained for the estimated muscle mechanical work:

$$\begin{aligned} Wtot^{+} &= Total\ \textbf{positive}\ muscle\ mechanical\ work \\ &= \int F^{+}(t)dt \end{aligned} \tag{2.11}$$

$$\begin{aligned} Wtot^{-} &= Total\ \textbf{negative}\ muscle\ mechanical\ work \\ &= \int F^{-}(t)dt \end{aligned} \tag{2.12}$$

$$\begin{aligned} W_{net} &= Total\ \textbf{net}\ muscle\ mechanical\ work \\ &= \int F^{+}(t) + F^{-}(t)dt \ = \ \int \sum_{i} f_i(t)dt \end{aligned} \tag{2.13}$$

$$\begin{aligned} |Wtot| &= Total\ \textbf{absolute}\ muscle\ mechanical\ work \\ &= \int |F^{+}(t)| + |F^{-}(t)|dt \ = \ \int \sum_{i} |f_i(t)|dt \end{aligned} \tag{2.14}$$

$$\begin{aligned} W_{absnet} &= Total\ \textbf{absolute/net}\ muscle\ mechanical\ work \\ &= \int |F^{+}(t) + F^{-}(t)|dt \ = \ \int |F(t)|dt \ = \ \int |\sum_{i} f_i(t)|dt \end{aligned} \tag{2.15}$$

Every value has a different biomechanical meaning, because computing an absolute value before or after a summation prevents or allows energy transfers beween segments. The *net* work value considers every power component with its sign, allowing all possibile energy transfers, and it is therefore expected to give the lower values of muscle mechanical work. The *absolute* (| |) work value considers all positive and negative power contributions separately, to sum together their absolute values in the end. The *absolute/net* (*absnet*) work value is a sort of combination of the previous two, because contemporaneous positive and negative power values from different joints/segments are allowed to cancel out each

other, while the resultant whole-body power curve during the gait cycle is integrated considering the absolute values of the positive and negative powers.

2.6.3 Normalization of muscle work

Power values were computed by normalizing with respect to the body mass of the subject, (W/Kg). Since the age of the subjects ranges from 6 to 13 years old, in order to reduce effects related to body size and walking speed, the total work (J/Kg) produced during a gait cycle, from heel strike to the ipsilateral heel strike, was normalized by the ratio between stride length (m) and subject's height (m), which is, in the end, equivalent to compute the work (J/Kg) necessary to walk a distance equivalent to the subject's height:

$$Normalized\,W = \frac{W_{STRIDE}(J)}{Bodymass(Kg)} / \left(\frac{L_{STRIDE}(m)}{Height(m)} \right) \tag{2.16}$$

To keep in mind the different contributions to the normalized value, we will associate to the muscle mechanical work the units $(J * m)/(Kg * m)$.

Height was chosen as a length normalization parameter instead of leg length to have a single parameter to normalize both work measures and upper and lower limb joint moments.

An alternative normalization measure could have been used, based on the dimensionless walking speed $v*$ provided by the *Froude number* (Hof, 1996; Zatsiorsky, 2002; Schwartz et al., 2008):

$$v* = v/\sqrt{gL_{leg}} \tag{2.17}$$

with v being the walking speed in m/s, g gravity acceleration, L_{leg} the leg length, in meters. This last choice, very useful for walking speed normalization, seemed less intuitive for the interpretation of the muscle work values. Anyway, values expressed with different normalization approaches can be easily converted and compared if the anthropometric parameter used is known.

Chapter 3

Instrumented Handles

By using anterior and posterior walkers instrumented with load cells (AMTI MCW-6-500, Watertown, MA, USA) Harris and co-workers characterized upper limbs kinetics during locomotion in children with Cerebral Palsy (CP) (Konop et al., 2009a,b).

Starting from their pioneering work, we developed two instrumented handles with a different design, based on strain gauges, that can be easily and quickly adapted to a wider range of different walkers, to measure bilateral three-dimensional forces and moments applied by the subject while walking with his/her own walker, thus allowing data more representative of typical walking to be collected.

This instrumentation needs to be lightweight and compact in size, in order to minimise interference with the normal use of the walker. It also needs to be easily fixed to the walker frame, whilst strong enough to avoid any undesirable dislocation when loaded in particular conditions by larger subjects.

This chapter describes the design of the instrumented handles and their connection with the motion capture framework, in order to collect synchronized data.

3.1 Strain gauge measurement

Many publications and technical notes on strain gauges measurement are freely available in the scientific and technical literature, for example (Audenino et al., 1997; Dally and Riley, 2005). We will describe here just a few concepts and definitions useful to understand

the following sections.

Strain (ε) is the amount of linear deformation of a body due to an applied force, measured in terms of a relative change in length:

$$\varepsilon = \frac{\Delta L}{L} \tag{3.1}$$

Since forces can be tensile or compressive, strain can be positive or negative. Normally, the amount of meaured strain is very small, and therefore it is common to express it as $\mu\varepsilon$.

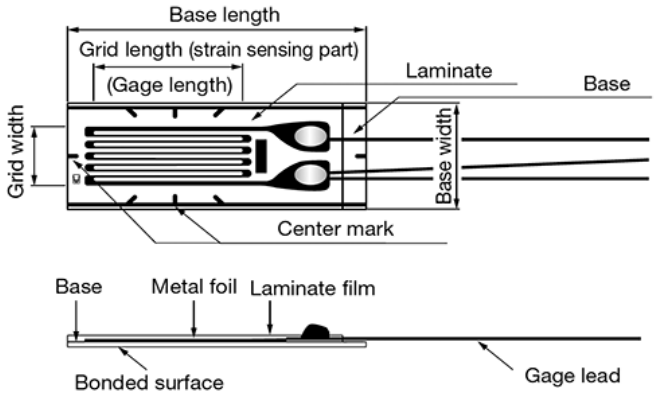

Figure 3.1: A foil strain gauge has a metal foil photo-etched in a grid pattern over a thin electric insulator base, with gauge soldering leads attached (adapted from Kyowa Corp. strain gauge technical manuals, available online at www.kyowa-ei.co.jp.

Strain can be measured via a *strain gauge* (or *gage*), a sensor commonly based on a very fine wire, or on a very thin metallic foil, arranged in a grid pattern with anisotropic configuration (Fig. 3.1). The strain gauge is bonded to the measuring body with a dedicated adhesive. Strain occurring on the measuring site is transferred to the strain sensing element via the gauge base, causing the electrical resistance ρ of the grid material to change proportionally to the amount of strain. By using a configuration of sensor elements in a Wheatstone bridge (Fig.3.3), the change in resistance is converted into a voltage change which can be amplified and measured.

3.2 Measuring system design

Signals provided by the strain gauges included in the instrumented handle need to be synchronized to video and other analog data acquired via the motion capture system. Since the Vicon MX system is equipped with an Analog-to-Digital conversion module which is used to acquire data from force plates and surface electromyographic systems, we aimed at integrate our instrumented handles in the Vicon processing system, in order to be able to acquire, visualize and process data straightforwardly with Vicon Nexus and Vicon BodyBuilder software (Fig. 3.2).

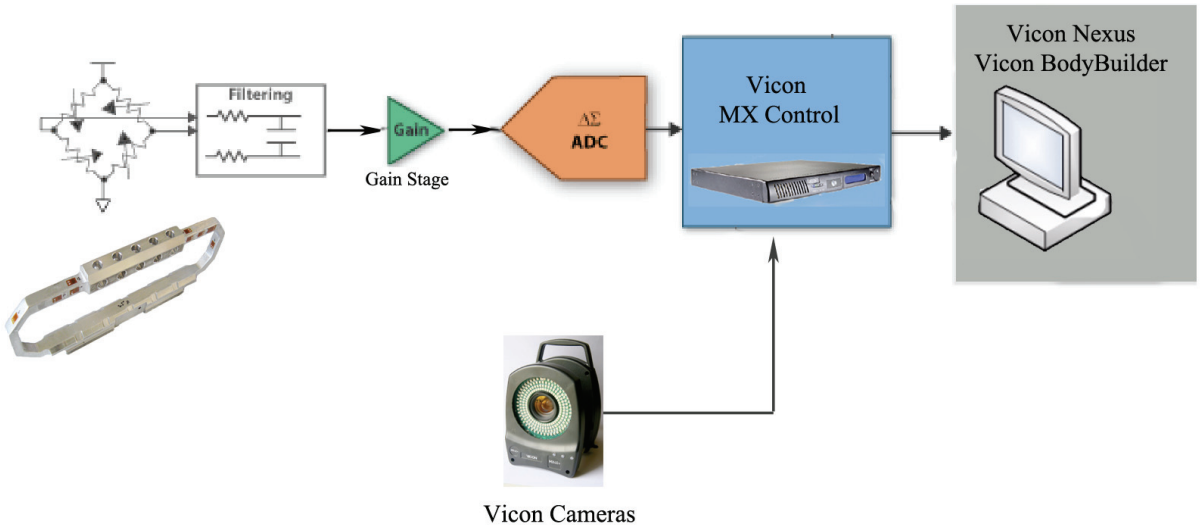

Figure 3.2: Measuring system: signals from instrumented handles are immediately filtered and amplified before sending them as inputs to the Vicon AD converter.

3.3 Handles design: FEM analysis

(This part would have never been realized without the seminal hints by Nicola Petrone and the precious help of Francesco Baldan and Mario Saraceni, Dep. of Mechanical Engineering, University of Padova). The couple of handles realized have the function to measure all the load components (forces and moments) transmitted to the walker frame by the user.

The whole handle was designed as a load cell consisting in an octagonal shaped 7075 T6 aluminium alloy structure fixable to the tubes that form the handles of walkers with different sizes by means of metal bands. Besides the traditional use of the octagonal cell to measure vertical and horizontal forces, we used other parts of the structure to host the strain gauges dedicated to the measure of the additional load components.

Preliminary analysis of the load cell behaviour under simulated working conditions was performed via Finite Element (FEM) Analysis.

For all the analysis, the reference system used is a right-handed XYZ orthogonal axes system, with the X axis pointing forward towards the walking direction and the Y axis pointing vertically (see Fig. 3.4).

The following table summarizes the configurations used to measure all the load components. All the six degree-of-freedom loads are measured by full strain gauge Wheatstone bridges organized and positioned as shown in table 3.1 and in the figures 3.3 and 3.4.

Table 3.1: Labelling number of the strain gauges and relative position in the Wheatstone bridge.

Component	**I**	**II**	**III**	**IV**
Fy	1	2	3	4
Fx	5	6	7	8
Fz	9	10	11	12
Mz	13	14	15	16
My	17	18	19	20
Mx	21	22	23	24

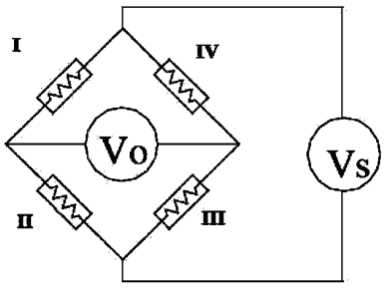

Figure 3.3: Strain gauges relative position in the Wheatstone bridge.

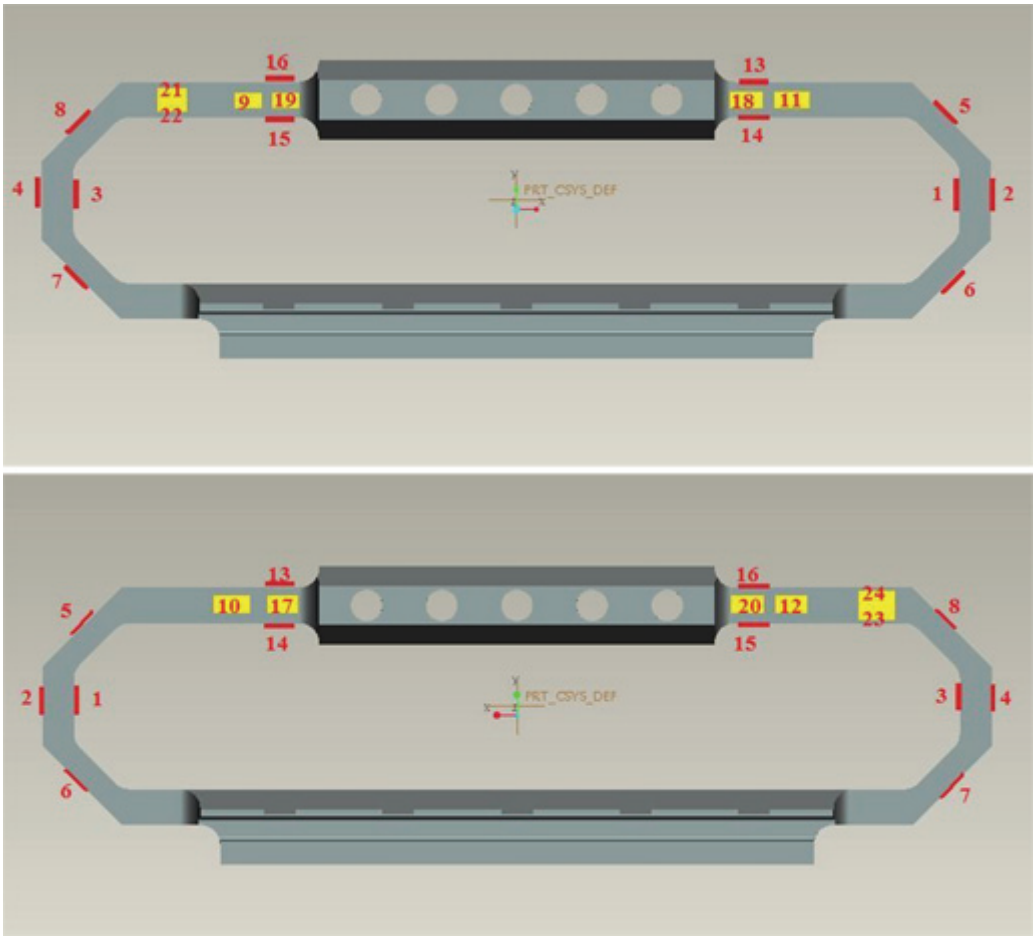

Figure 3.4: Sensors positioning on the handle. Top view: XY plane, X towards the left, Z going into the plane. Bottom view: XY plane, X towards the right, Z coming out.

Full scale values considered for the analysis were: Fx, Fz = 500 N (antero-posterior and medio-lateral axes), Fy = 1100 N (vertical axis), with Mx, My, Mz = 20 Nm.

Preliminary analysis of the load cell behaviour in order to evaluate cell dimensions, static

resistance and the best strain gauge positioning related to the magnitude of measurable strains was performed via Finite Element (FEM) Analysis Software (ANSYS, Inc., Canonsburg, Pennsylvania, USA).

Handle dimensioning was done considering that the handles need to be fixable to the tubes that form the handling part of normal walkers. Tube diameters normally have sizes that vary from 20 to 22 mm, depending on the walker. The part of the tube which can be used for handle placement is about 150 mm.

The handling part of the instrumented handle has a length of 100 mm, with a squared section of 20 x 20 mm (Fig. 3.5).

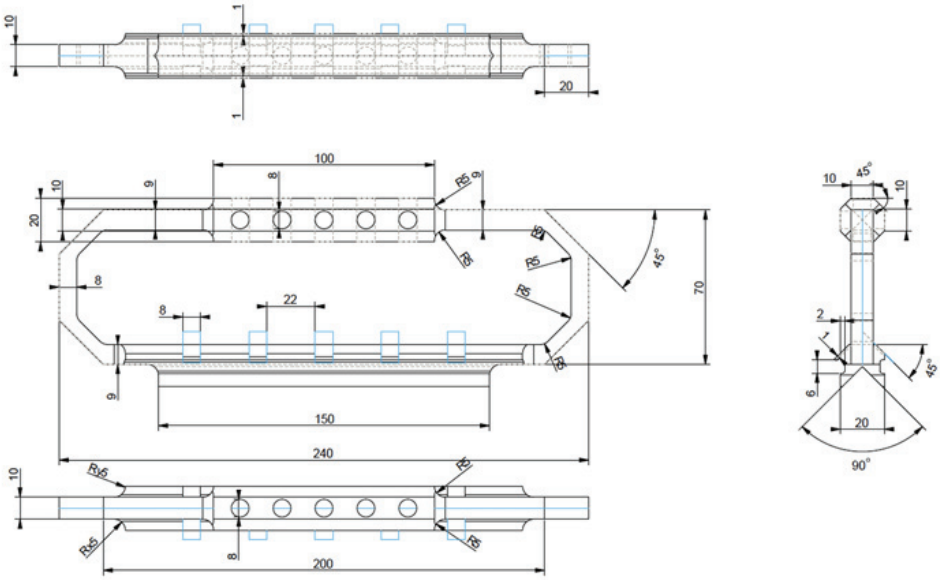

Figure 3.5: Technical drawing of the handle.

The handle is fixable to the walker by means of metal bands. The handle and the metal bands can be adapted to different tube diameters, thanks to the particular reversed *V-shaped* inner surface of the cell (Fig. 3.7).

FEM analysis

Material

7075 T6 Alluminium alloy (Maximum stress $\sigma_{yield} = 503MPa$)

Elastic modulus: $E = 71700MPa$

Poisson's ratio: $\nu = 0.33$

Mesh definition

Element: SOLID45 (8 nodes)

Element dimensions: 2mm

The mesh was refined around the extremities of the handling part, because that is expected to be structurally the most critical area.

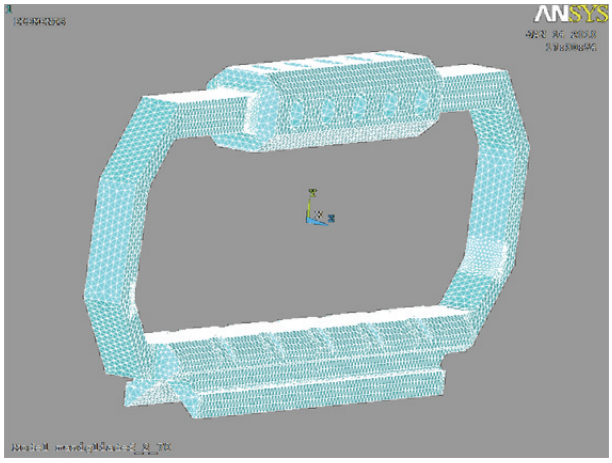

Figure 3.6: Mesh structure.

Constrain conditions for all the analyses

No movement along the lines of contact between the lower surface of the handle and the walker tube (the contact is not possibile with all the inner surface of the handle support).

Loads application

Three orthogonal forces and three moments were separately applied to the handle in this way (Fig. 3.8):

Fy and Fz loads were applied as uniform pressure loads on the correspondent faces of the handling area;

Fx was applied as a system of parallel forces uniformly distributed on the handling surface;

Mx, My, Mz were applied as a system of forces uniformly distributed on the handling surface, with resultant force equal to zero and ideal application point of the moment considered at the center of the handle.

For a preliminary static analysis the following static loads were applied to the handle as

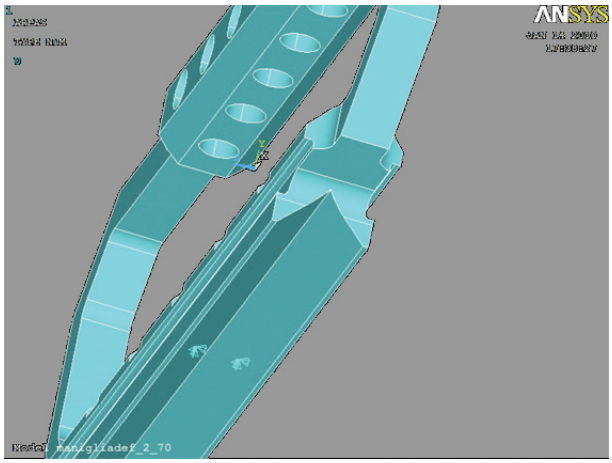

Figure 3.7: Graphical representation of the inner surface of the handle.

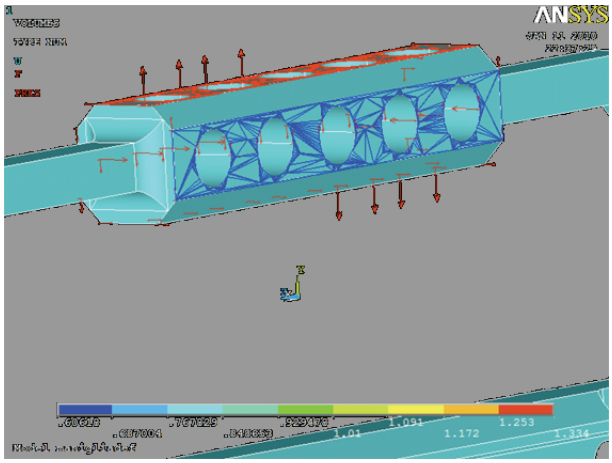

Figure 3.8: Graphical representation of the systems of forces applied.

maxima of the pure forces:

Fx =500N

Fy = 1100N

Fz = 500N

Figure 3.9 is a graphical representation of the FEM analysis results in terms of magnitude of the von Mises σ parameter, which is an index used to analyze critical stress conditions in the structure.

Considering the typical *real* loading conditions of the handles, for the static analysis we hypothesized the contemporaneous action of only pure forces acting at their maximal values. It is unlikely to happen a loading condition with both all forces and moments

acting at the same time at their maximum.

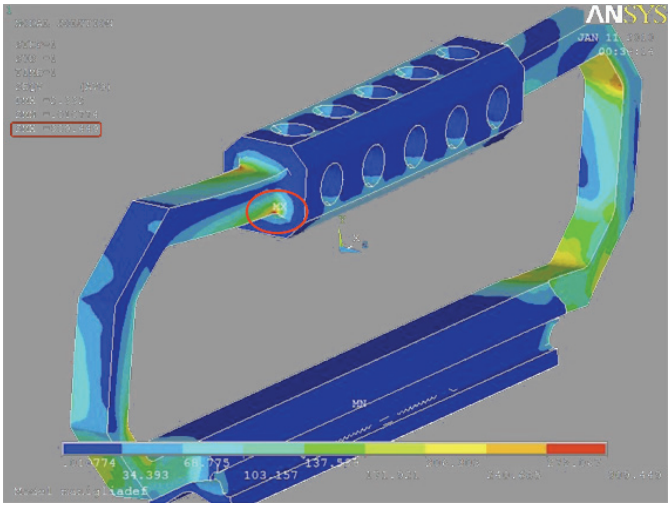

Figure 3.9: Graphical representation of the magnitude of the von Mises σ.

FEM analysis results

Fig. 3.9 evidences the area experiencing the highest stress (σ_{MAX} = 309,5 MPa) under the loading conditions described above.

The tensile strength limit for the 7075 T6 aluminium alloy is 503 MPa. With a static safety coefficient k=1.5 we get a σ_K= 335 Mpa. Since $\sigma_{MAX} < \sigma_K$, the structure is validated with these loading conditions.

For the estimation of strains measured by each single strain gauge bridge, every pure loading condition was separately simulated at its full scale value, in order to graphically and quantitatively evaluate the magnitude of the deformations measured by the correspondent sensor in the area where it should be applied.

Horizontal force Fx, full scale loading (Fx = 500N)

Strain gauges for the Fx channel should be placed in the middle of the external faces of the oblique sides of the octagonal structure, which are inclined of about 45° with respect to the horizontal. For every area we obtain the following strains along the X and Y directions, with principal strains being maximal, ε_1, along the faces that are experiencing a tensile force, and minimal, ε_3, along the faces that are experiencing a compressive force

(Figg. 3.10, 3.11).

$5 : \varepsilon_x = +340\mu\varepsilon;\ \varepsilon_y = +250\mu\varepsilon;\ \varepsilon_1 = +900\mu\varepsilon$

$6 : \varepsilon_x = -400\mu\varepsilon;\ \varepsilon_y = -350\mu\varepsilon;\ \varepsilon_3 = -1100\mu\varepsilon$

$7 : \varepsilon_x = +360\mu\varepsilon;\ \varepsilon_y = +330\mu\varepsilon;\ \varepsilon_1 = +1000\mu\varepsilon$

$8 : \varepsilon_x = -350\mu\varepsilon;\ \varepsilon_y = -250\mu\varepsilon;\ \varepsilon_3 = -870\mu\varepsilon.$

Vertical force Fy, full scale loading (Fy = 1100N)

Values of ε_y estimated in the areas where strain gauges 1-2-3-4 should be placed for the measurement of the vertical force are shown. Loading conditions are symmetrical, therefore the strain values are identical between sensors 1 and 3, and between sensors 2 and 4 (Fig. 3.12).

1-3: $1000\mu\varepsilon$

2-4: $-1100\mu\varepsilon$.

Horizontal force Fz, full scale loading (Fz = 500N)

To measure this force component we are interested in measuring the mean magnitude of the strain along the X direction, ε_x, in the area where mono-axial strain gauges 9-10-11-12 should be placed (Fig. 3.13).

9-11: $\varepsilon_x = -750\mu\varepsilon$

10-12: $\varepsilon_x = +750\mu\varepsilon$.

Twisting moment, full scale loading (Mx = 20Nm)

In pure twisting loading conditions, shearing stress brings to the development of principal stresses in the two directions inclined by 45° from their axial line, whose strains can be measured by a strain gauge rosette configuration, with two sensors coupled together and inclined by ±45° with respect to the horizontal axis.

In the area interested by sensors placement, we measured a mean strain of $\varepsilon_{xy} = +/-1450\mu\varepsilon$. The estimation of principal strains gives approximately the same magnitude, with opposite sign, for the first and third components, while the second principal strain remains very close to 0 (Fig. 3.14).

$\varepsilon_1/\varepsilon_3 = +/-660\mu\varepsilon$.

Bending moment, full scale loading (My = 20Nm)

In this case we are interested in the ε_x strain component. Under strain gauge ideal placement areas the following deformations are estimated (Fig. 3.15):

17-19: $\varepsilon_x = 480\mu\varepsilon$

18-20: $\varepsilon_x = -480\mu\varepsilon$.

Bending moment, full scale loading (Mz = 20Nm)

Sensors to measure this loading component should be placed over the upper horizontal beam of the octagon, therefore the strain componenent we are interested in is again ε_x, with the following strains being measured in the selected areas (Fig. 3.16):

13-15: $\varepsilon_x = 450\mu\varepsilon$

14-16: $\varepsilon_x = -450\mu\varepsilon$.

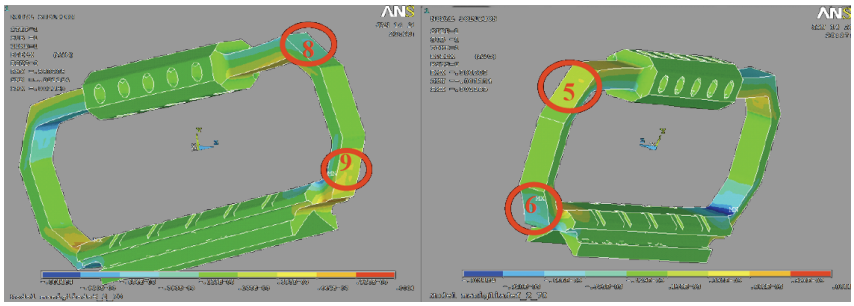

(a)

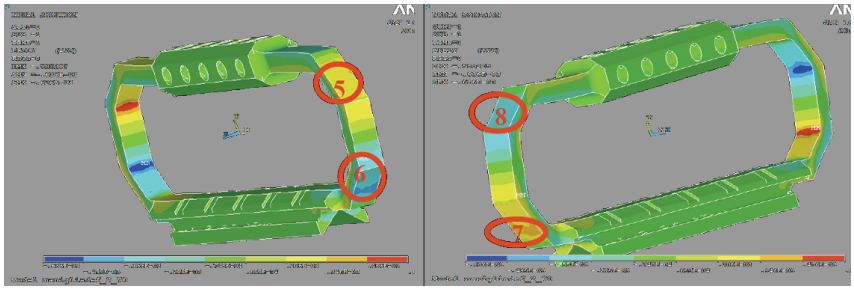

(b)

Figure 3.10: Fx, strains a) ε_x, b) ε_y.

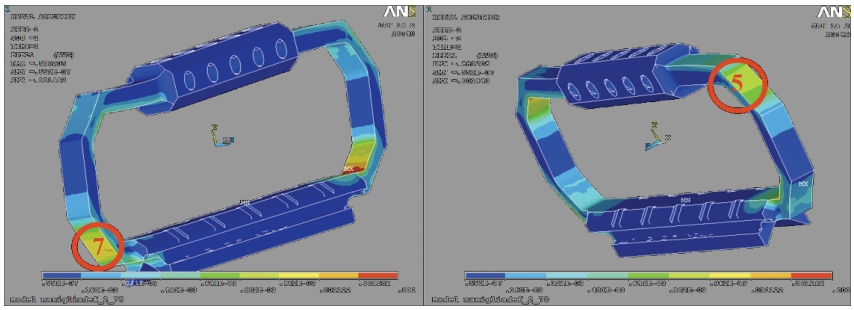

(a)

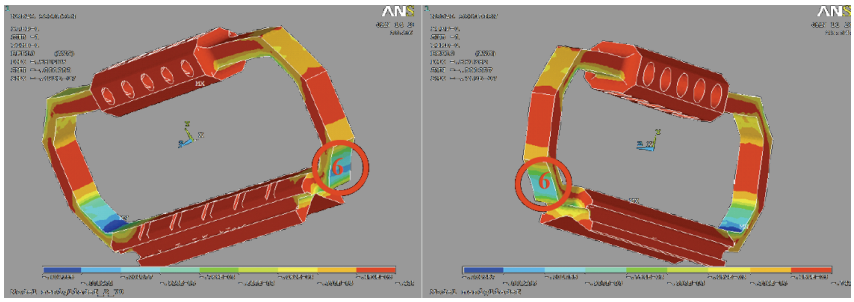

(b)

Figure 3.11: Fx, principal strains a) ε_1, b) ε_3.

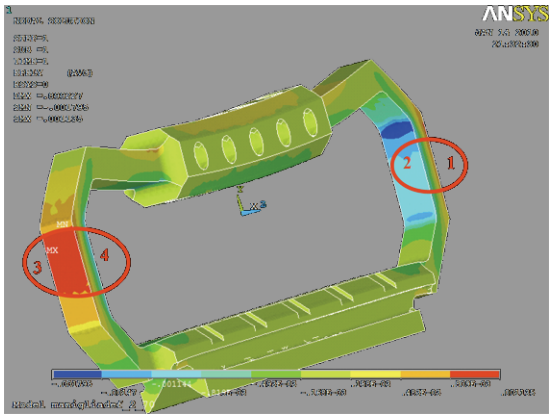

Figure 3.12: Fy: handle deformation ε_y under vertical compressive load.

Discussion of FEM results

Results of the simulations show that the cell structure and the strain gauge positioning chosen were effective for the measurement of all applied loading components.

The following resistive EA series strain gauges (Vishay GmbH, Germany) were chosen for cells instrumentation:

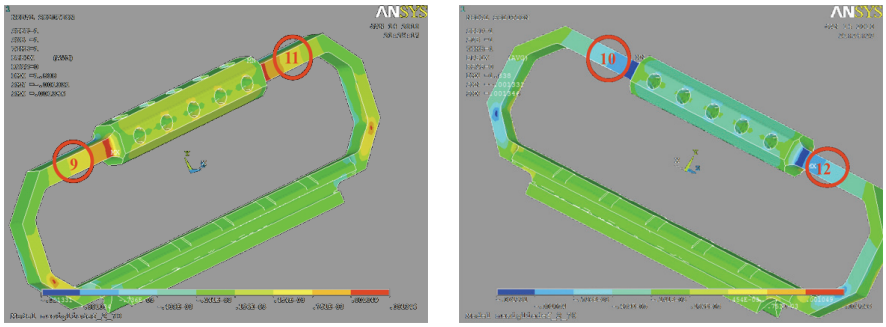

(a) (b)

Figure 3.13: Fz: handle deformation ε_x under lateral force directed towards positive Z direction.

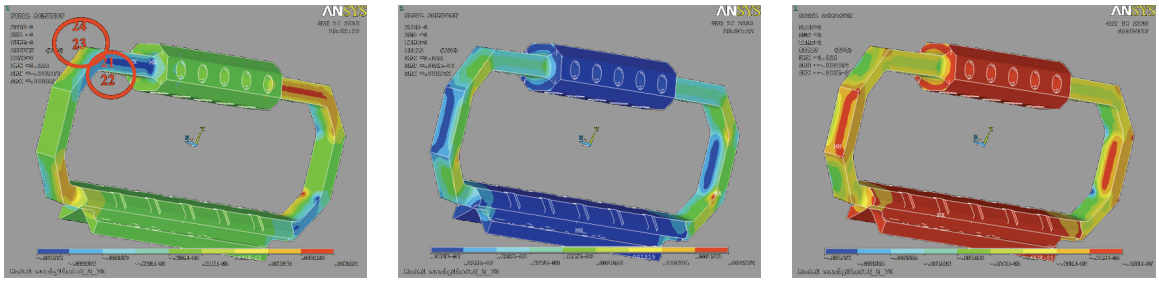

(a) (b) (c)

Figure 3.14: Mx: handle deformation under pure twisting moment: a) ε_{xy}, b) ε_1, c) ε_3.

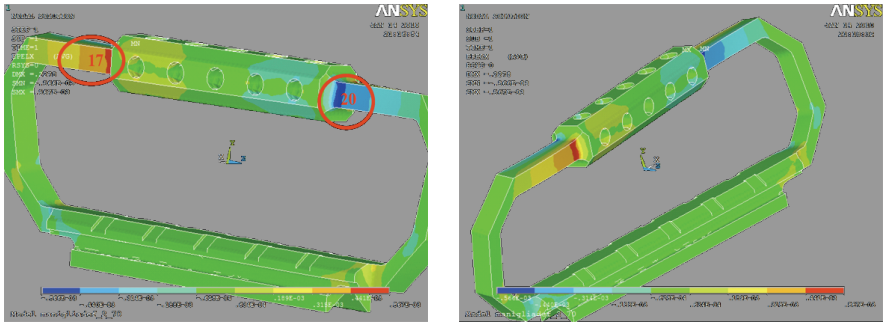

(a) (b)

Figure 3.15: My: handle deformation ε_x under bending moment My.

Vishay Micro-Measurements CEA-13-062UW-350Ω for linear stresses
Vishay Micro-Measurements CEA-13-062UV-350Ω for shearing stresses
which have a polyamide baking, copper solder tabs, constantan alloy grid in self temperature-compensated form related to the structural material on which the gauge is to be used, gauge length of 1.57 mm, Gauge Factor @24°C equal to 2.170 for the UW model e 2.135

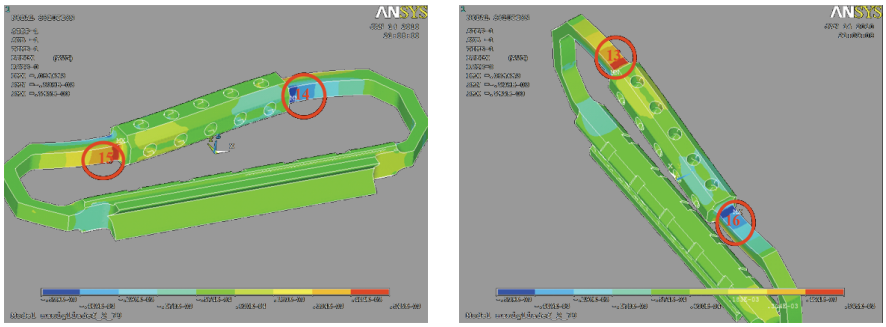

(a) (b)

Figure 3.16: Mz: handle deformation ε_x under bending moment Mz.

for the UV model, resistance equal to 350 $\Omega \pm 0.3\%$. Wheatstone bridges were powered at Vs = 5V.

From these data it was possible to get a preliminary estimate of full scale channel output and channel sensitivity, since each strain gauge bridge of the cell is directly associated to a single load component.

Channel	I (με)	II (με)	III (με)	IV (με)	ε tot (με)	Capacity*	Sens (mV/V)	Output (mV)	Unit Sens**
Fx	418,44	-531,91	531,91	-513,91	2014,18	500	1,09	5,46	2,19
Fy	900	-1100	900	-1100	4000	1100	2,17	10,85	1,97
Fz	750	-750	750	-750	3000	500	1,63	8,14	3,26
Mx	660	-660	660	-660	2640	20	1,41	7,05	70,46
My	480	-480	480	-480	1920	20	1,04	5,21	52,08
Mz	450	-450	450	-450	1800	20	0,98	4,88	48,83

* Capacity in N for forces and Nm for torques
** Unit sensitivity in (μV/V N) for forces and (μV/V Nm) for torques

Gauge Factors:

K lin	2,170
K torc	2,135

It is also necessary to point out that, theoretically, there is a good mechanical uncoupling among the majority of the channels, since sensors disposition in the bridges leads to reciprocal cancellation of spurious strain terms.

3.4 Handles realization and instrumentation

Two octagonal shaped 7075 T6 aluminium alloy cells were realized by means of a CNC (computer numerical control) milling machine, after the final cell dimensioning obtained considering the FEM analysis outcomes (Fig. 3.17). Each aluminium cell had a mass of 0.270 Kg.

Sensors were positioned in the areas that FEM analysis highlighted as the most sensi-

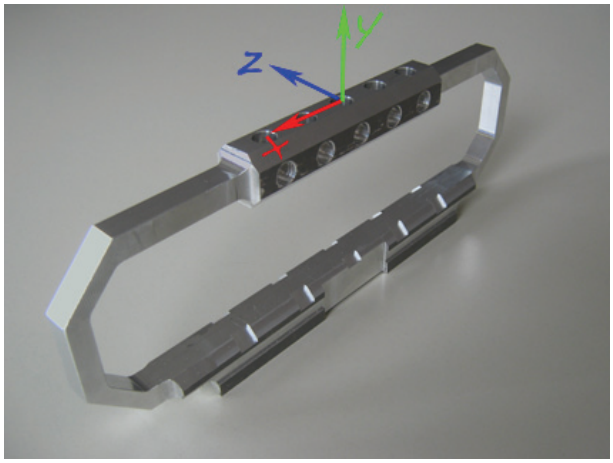

Figure 3.17: Aluminium frame of the handle.

tive to deformations. Aluminium surface was smoothed with very fine sand paper (up to P1000) and deoiled with solvent. Strain gauges were attached to the substrate with a special cyanoacrylic glue, after engraving thin crossing lines on the octagonal faces to help the aligment. Every gauge was positioned by using special transparent adhesive tape which allowed to check proper aligment of the sensor with the engraved lines. Once the proper position was found, the tape was raised from one side and the aluminium surface was quickly cleaned with solvent before placing a drop of glue on it and pressing down the tape with the gauge (Fig. 3.18(a)).

After checking proper fixation and alignment, strain gauges were connected in Wheatstone bridge configuration, by straighforwardly soldering on the tabs the extremities of the cables leading to the excitation and measuring points of the bridge amplifier (Fig. 3.18(b)).

Each cell was cabled with two 25-conductor shielded cables, necessary to connect the

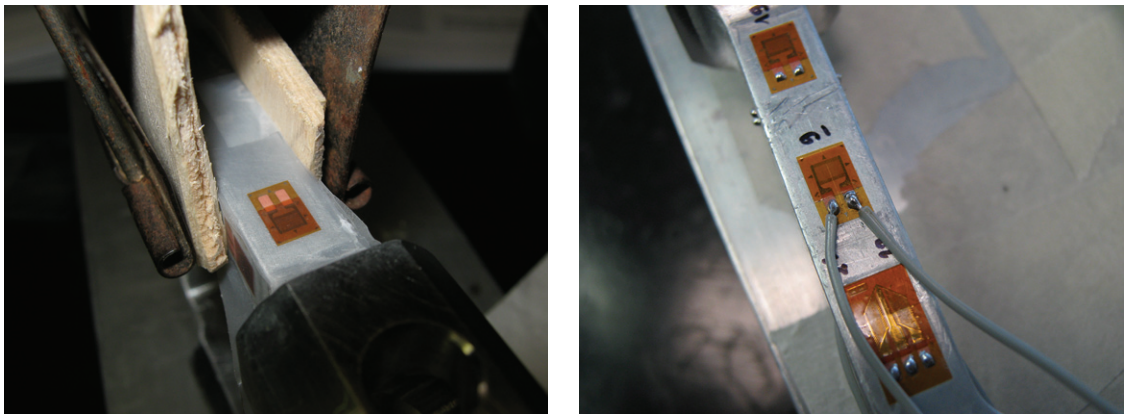

(a) (b)

Figure 3.18: (a) Strain gauge fixation and (b) electric connection.

soldering tabs of the 24 straing gauges which constitute the six bridges. The two extra free leads were used to connect to the ground the aluminium structure of the cell.

3.5 Handles static calibration setup

Before final cable fixation to the amplification devices and protection of the strain gauges with a silicon layer, all force and moment channels were statically calibrated, in order to determine the linear coefficients which relate static loads applied to the handle (forces, in N and moments, in Nm) to the straing gauge deformation (in $\mu\varepsilon$) or straightforwardly to the bridge voltage output (in mV).

The two handles were statically calibrated using a cubed frame (Fig. 3.19(a)) designed to position pulleys around the handle to apply three-axial bilateral known forces and moments by means of a system of cables and incremental weights. The handle was rigidly fixed on a full steel tube with a diameter of 20mm, to simulate a walker tube, at the center of the cubed frame (Fig. 3.19(b)).

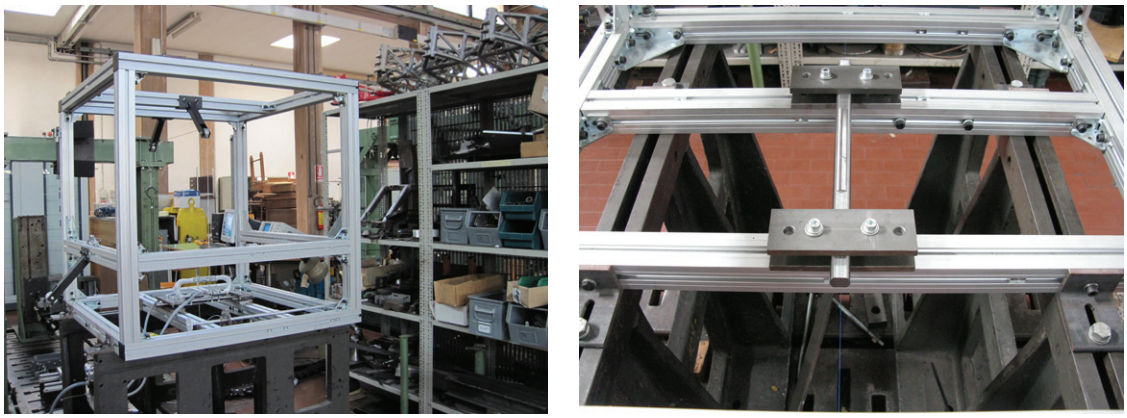

(a) (b)

Figure 3.19: Details of the calibration frame.

Two different methods to bind the handles on the horizontal tube were evaluated: The first one, based on five metal bands for each handle, is the solution which allows more lightness (Fig. 3.20(a)); the second choice is based on three aluminium brackets with U shaped bolts for each handle, a solution which can provide stronger fixation and therefore more stability even when loaded by larger subjects.(Fig. 3.20(b)).

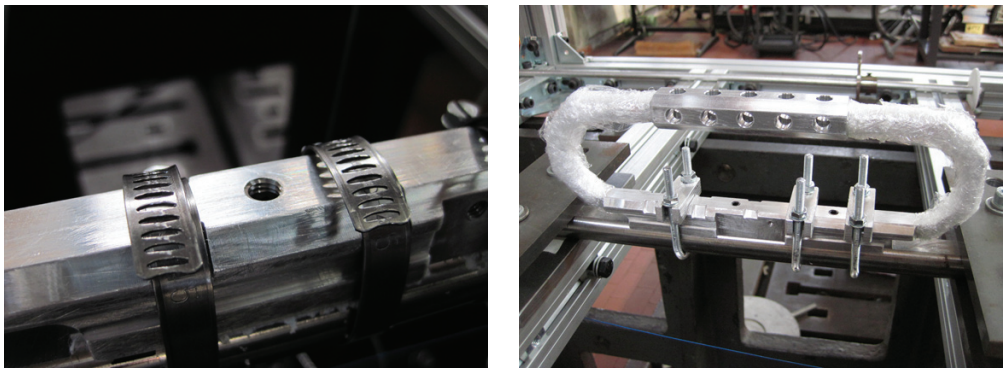

(a) (b)

Figure 3.20: Different systems for handle fixation to the walker tube.

Weights were applied incrementally until reaching approximately 70% of full scale for that considered load, both in the positive and in the negative directions, to evaluate

non-linearity and hysteresis. Bridges excitation and output voltages were applied and measured via a HBM Multipoint Measuring Unit UPM100 station, with a $V_0 = 5$ V excitation voltage, output measured in mV/V, full scale output signal limited between $\pm$ 10 mV/V, integration time for the output measures equal to 20 or 100 ms, sensitivity equal to 0.001 mV/V.

Incremental weights were independently applied to the handle for each degree of freedom, as shown in Fig. 3.21.

For all the channels at least five loading steps were applied along both positive and negative directions, including the unloaded condition, for three times. The second and third trials data were used to estimate sensitivity and calibration matrices. As zero-load condition we considered the situation with the support for the weights empty and already connected to the handles via the steel cables. Measured data were then processed using custom MATLAB functions.

(a) (b)

(c) (d)

(e) (f)

Figure 3.21: Loads application for (a) Fx, (b) Fy, (c) Fz, (d) Mx, (e) My, (f) Mz.

3.6 Handles static calibration results

Sentitivity and calibration matrices were computed for both handles. After that, a few trials were realized by applying multiple combined loads on the handle, to check system capability to distinguish and correctly estimate the different loads.

Matrices were obtained following this conditions: raw data (in mV/V) were obtained as mean values of the second and third loading sequences. If there were channels reading raw data with absolute values always less than 0.003 mV/V in all loading conditions, they were considered as equal to zero.

Calibration matrix S was obtained from the angular coefficients of the linear interpolation curves. The coefficient of multiple determination R-square was computed for all matrix elements: Elements of S associated to R^2 values < 0.75 were defined equal to zero, since they give evidence of a random correlation between voltage output and applied load.

Parameters which determine cell accuracy

Cross-Talk: Effect measured as a voltage output on an unloaded channel while a different channel is being loaded. It is normally expressed as percentage of the full-scale value of the unloaded channel.

Hysteresis: Evaluated, for every single channel, as the maximum difference between output readings for the same applied load, with one value obtained when increasing the loads from zero and the other one when decreasing the loads from 70% of maximum capacity of the channel. The value is expressed as a percentage of the full-scale value.

Non-linearity: Evaluated as the maximum deviation of load estimates from the line representing the true applied loads, expressed as a percentage of the full-scale value for each channel (Fig. 3.22).

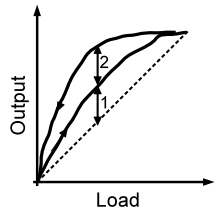

Figure 3.22: Non-linearity (1) and Hysteresis (2)

3.6.1 Handle A

Sensitivity matrix

(output in mV/V = S_{Aij} by input load in N or Nm)

S_A =

	Fx	Fy	Fz	Mx	My	Mz
Vfx	**0.00527**	-0.00001	0.00006	0.00138	0.00000	0.00037
Vfy	0.00001	**0.00236**	-0.00008	-0.00266	0.00000	0.00000
Vfz	-0.00003	0.00000	**0.00318**	0.00164	0.00000	-0.00034
Vmx	0.00002	0.00008	-0.00001	**0.10888**	-0.02211	0.00000
Vmy	-0.00007	-0.00001	-0.00001	-0.00036	**0.05042**	0.00030
Vmz	0.00187	-0.00002	0.00015	0.00000	0.00000	**0.04794**

Calibration matrix

(output in N or Nm = C_{Aij} by input in mV/V)

C_A =

	Vfx	Vfy	Vfz	Vmx	Vmy	Vmz
Fx	**190.24321**	0.86975	-3.62737	-2.33689	-1.02470	-1.49659
Fy	-0.51601	**423.56357**	11.22406	10.18476	4.46592	0.05525
Fz	0.88451	0.16569	**314.23404**	-4.74047	-2.07865	2.22010
Mx	0.02757	-0.28469	0.03301	**9.18969**	4.02959	-0.02510
My	0.29191	0.04439	0.05517	0.06246	**19.86009**	-0.12566
Mz	-7.42704	0.10738	-0.83306	0.10937	0.04796	**20.91045**

Matrix of R^2

R^2 =

0.9999	0.8270	0.9977	0.9749	NaN	0.9849
0.7920	**0.9998**	0.9821	0.8453	0.6179	0.1221
0.9732	0.5665	**0.9999**	0.9923	0.2454	0.8071
0.7901	0.8098	0.8918	**0.9996**	0.9999	0.2807
0.8903	0.9413	0.8833	0.9865	**0.9999**	0.9157
0.9997	0.7840	0.9969	0.0131	NaN	**1.0000**

Results for calibration step sequences: for each channel, loaded with pure force or pure moment, all the six channels output readings (in mV/V) were measured (Fig. 3.23).

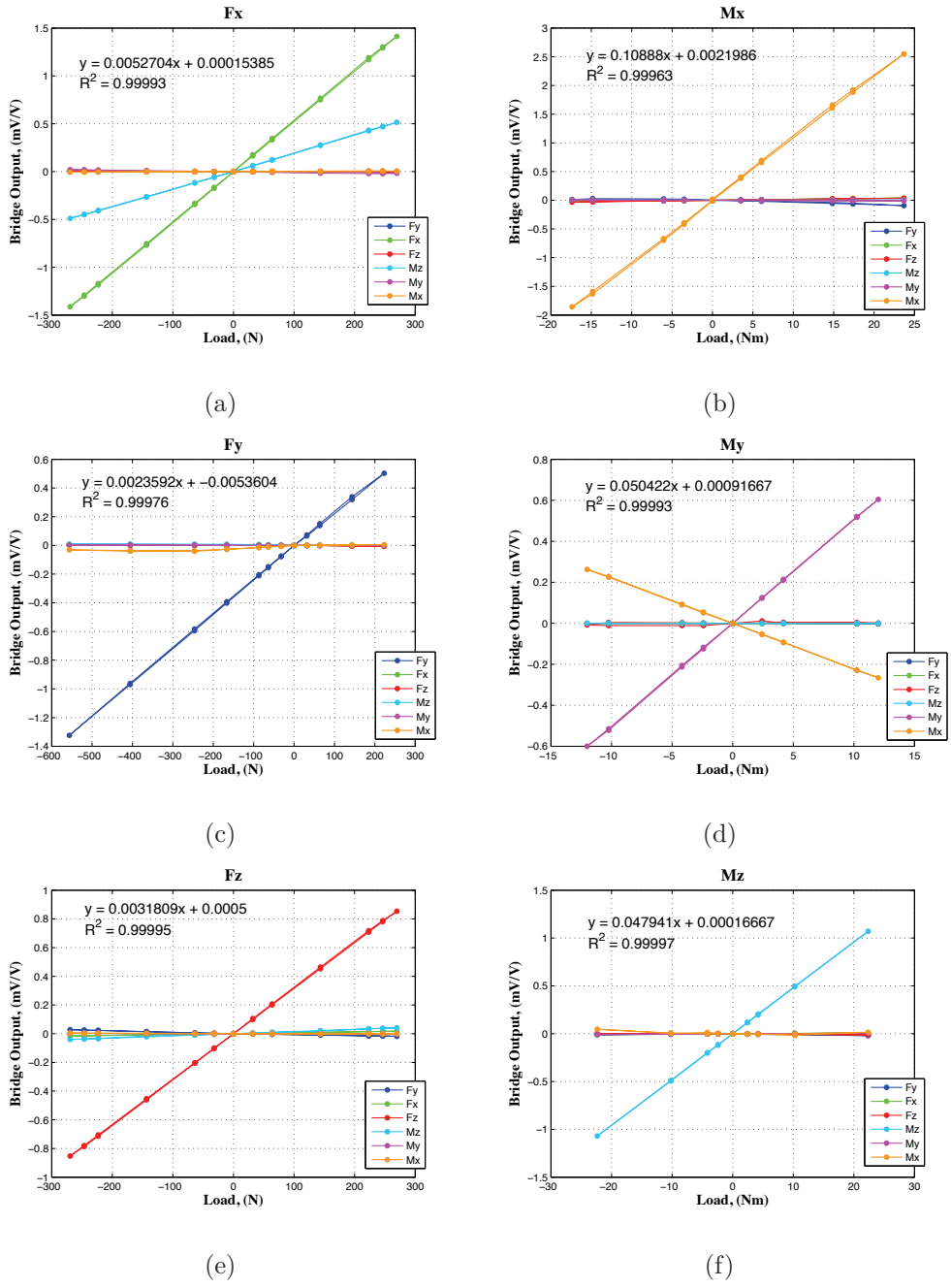

Figure 3.23: Calibration curves for (a) Fx, (b) Fy, (c) Fz, (d) Mx, (e) My, (f) Mz.

The following table shows the results of multiple loading trials with contemporaneous application of positive Fx and Fz and negative (compressive) Fy.

Real load (Fx, Fy, Fz)

Fx	Fy	Fz
0	0	0
31.8825	-57.3885	31.8825
111.5789	-137.0849	111.5789
134.8286	-160.3346	134.8286

Estimated load

Fx	Fy	Fz	Mx	My	Mz
0	**0**	**0**	0	0	0
29.6903	**-56.1186**	**31.3242**	0.0724	0.0398	-0.2320
108.6676	**-135.6878**	**110.8782**	0.1386	0.1689	-0.4178
132.2601	**-158.6753**	**134.0354**	0.1368	0.1813	-0.4379

Relative error % (estimate-true)/true

Fx	Fy	Fz	Mx	My	Mz
NaN	NaN	NaN	Inf	Inf	Inf
6.8759	**2.2128**	**1.7511**	Inf	Inf	Inf
2.6093	**1.0192**	**0.6280**	Inf	Inf	Inf
1.9051	**1.0349**	**0.5884**	Inf	Inf	Inf

% error with respect to full-scale

Fx	Fy	Fz	Mx	My	Mz
0	0	0	0	0	0
0.4384	**0.1154**	**0.1117**	0.3620	0.1989	1.1601
0.5823	**0.1270**	**0.1401**	0.6929	0.8445	2.0892
0.5137	**0.1509**	**0.1587**	0.6841	0.9067	2.1897

3.6.2 Handle B

Sensitivity matrix

(output in mV/V = S_{Bij} by input load in N or Nm)

SB =

	Fx	Fy	Fz	Mx	My	Mz
Vfx	**0.00521**	-0.00001	0.00006	-0.00106	0.00000	0.00017
Vfy	0.00000	**0.00238**	0.00000	0.00000	0.00000	0.00000
Vfz	0.00001	-0.00003	**0.00301**	0.00055	-0.00060	0.00000
Vmx	0.00002	0.00000	-0.00006	**0.10366**	-0.02238	0.00000
Vmy	0.00000	0.00003	0.00000	0.00000	**0.04926**	0.00064
Vmz	0.00185	0.00005	0.00017	0.00000	0.00022	**0.04682**

Calibration matrix

(output in N or Nm = C_{Bij} by input in mV/V)

CB =

	Vfx	Vfy	Vfz	Vmx	Vmy	Vmz
Fx	**192.05887**	1.15549	-3.79853	1.98332	0.85766	-0.71760
Fy	0.00000	**420.43069**	0.00000	0.00000	0.00000	-0.00000
Fz	-0.49187	3.49711	**331.93264**	-1.75539	3.27331	-0.04281
Mx	-0.00972	-0.04597	0.18414	**9.64586**	4.38451	-0.05972
My	0.09847	-0.22091	0.01392	0.00093	**20.30387**	-0.27710
Mz	-7.60015	-0.50404	-1.07430	-0.07203	-0.14259	**21.38751**

Matrix of R^2

R^2 =

0.9999	0.8270	0.9977	0.9749	NaN	0.9849
0.7920	**0.9998**	0.9821	0.8453	0.6179	0.1221
0.9732	0.5665	**0.9999**	0.9923	0.2454	0.8071
0.7901	0.8098	0.8918	**0.9996**	0.9999	0.2807
0.8903	0.9413	0.8833	0.9865	**0.9999**	0.9157
0.9997	0.7840	0.9969	0.0131	NaN	**1.0000**

Results for calibration step sequences: for each channel, loaded with pure force or pure moment, all the six channels output readings (in mV/V) are measured (Fig. 3.24).

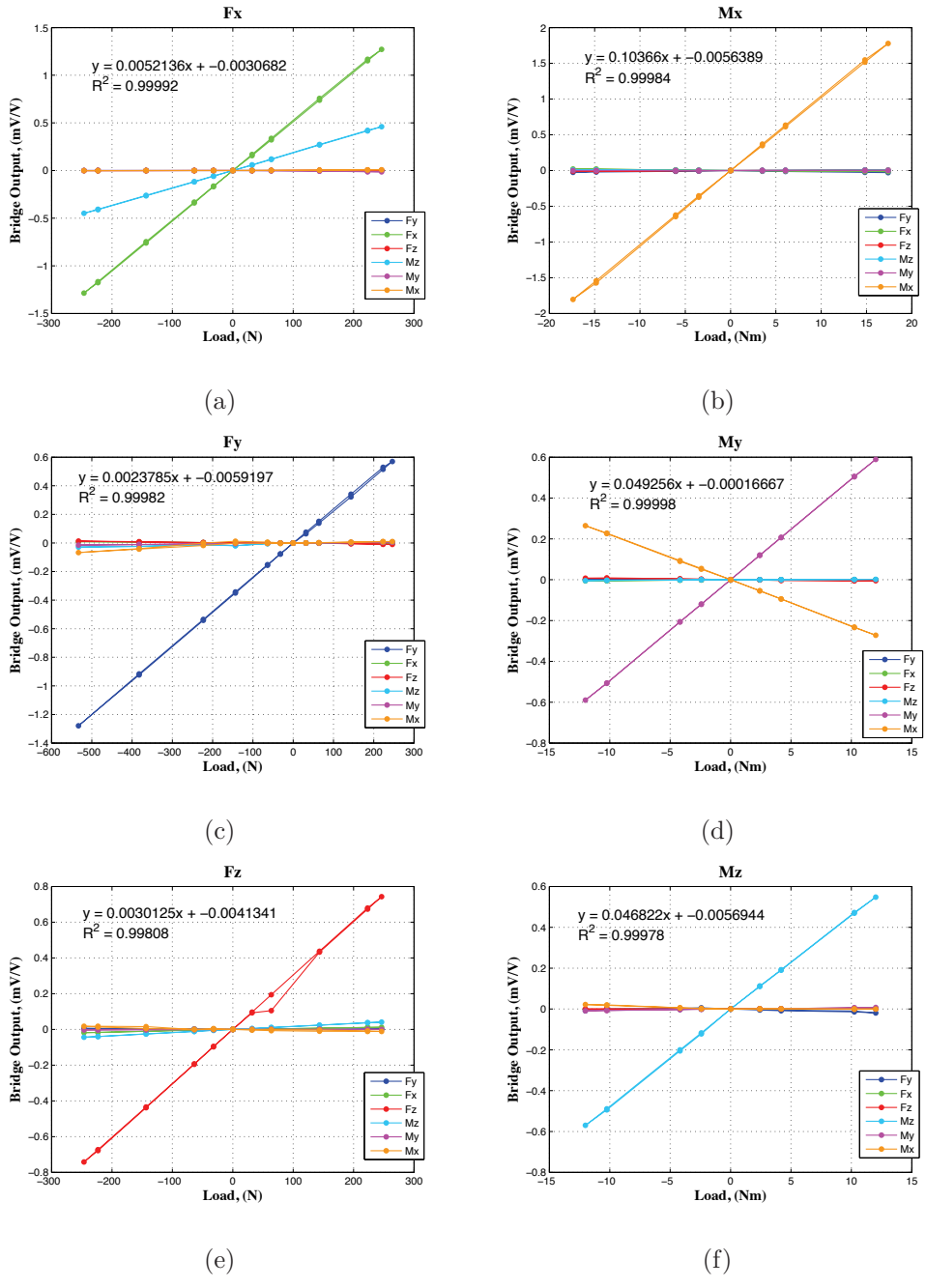

Figure 3.24: Calibration curves for (a) Fx, (b) Fy, (c) Fz, (d) Mx, (e) My, (f) Mz.

In the figures 3.25, 3.26, 3.27 are represented the results of multiple loads trials, obtained with the following loading conditions: 1) Fx positive, My clock-wise; 2) Fy negative (compression), My clock-wise; 3) Mx clock-wise, My clock-wise). The larger errors were noticed with the Fx-My loading combination.

Real load (Fx, My)

Fx	My
0	0
79.6964	-2.4231
79.6964	-4.1900
79.6964	-5.9570
79.6964	-4.1900
79.6964	-2.4231
0	0

Estimated load

Fx	Fy	Fz	Mx	My	Mz
0	0	0	0	**0**	0
76.1515	0	-0.2861	0.0176	**-2.0512**	0.0510
75.9709	0.4204	-0.6373	0.0457	**-3.7973**	0.0459
75.9811	0.4204	-0.9925	0.0738	**-5.5431**	0.0338
75.9803	0.4204	-1.3061	0.0506	**-3.8174**	0.0267
76.1491	0.4204	0.0410	0.0186	**-2.0920**	0.0496
-0.0024	0	0.1295	-0.0043	**-0.0203**	-0.0003

Relative error % (estimate-true)/true

Fx	Fy	Fz	Mx	My	Mz
NaN	Inf	Inf	Inf	NaN	Inf
4.4480	Inf	Inf	Inf	**15.3485**	Inf
4.6747	Inf	Inf	Inf	**9.3733**	Inf
4.6618	Inf	Inf	Inf	**6.9482**	Inf
4.6629	Inf	Inf	Inf	**8.8947**	Inf
4.4510	Inf	Inf	Inf	**13.6641**	Inf
Inf	Inf	Inf	Inf	Inf	Inf

% error with respect to full-scale

Fx	Fy	Fz	Mx	My	Mz
0	0	0	0	**0**	0
0.7090	0	0.0572	0.0880	**1.8595**	0.2548
0.7451	0.0382	0.1275	0.2284	**1.9637**	0.2295
0.7431	0.0382	0.1985	0.3690	**2.0695**	0.1688
0.7432	0.0382	0.2612	0.2532	**1.8635**	0.1337
0.7095	0.0382	0.0082	0.0931	**1.6555**	0.2479
0.0005	0	0.0259	0.0216	**0.1015**	0.0014

Figure 3.25: Results for handle B under multiple loading: Fx, My

Real value (Fy, My)

Fy	My
0	0
-150.5835	0
-150.5835	-2.4231
-230.2799	-4.1900
-253.5296	-10.2470
-412.9421	-10.2470
-253.5296	-10.2470
-230.2799	-4.1900
-150.5835	-2.4231
-150.5835	0
0	0

Estimated load

Fx	Fy	Fz	Mx	My	Mz
0	**0**	0	0	**0**	0
-0.5405	**-148.4120**	-1.3014	0.2978	**-0.0028**	0.1411
-0.9393	**-149.2529**	-0.7939	0.2644	**-2.4386**	0.1461
-2.2796	**-228.2939**	-2.1550	0.3229	**-4.2206**	-0.0451
-3.3053	**-251.4176**	-1.9108	0.3285	**-10.3188**	-0.0587
-4.6138	**-408.6586**	-4.9419	0.5803	**-10.3521**	-0.3198
-3.4992	**-253.0993**	-3.2485	0.2847	**-10.3397**	0.0626
-2.4739	**-231.6573**	-3.5185	0.2995	**-4.2812**	0.0782
-1.1476	**-150.9346**	-1.4657	0.1876	**-2.4798**	0.2656
-0.5658	**-150.5142**	-1.3083	0.2163	**-0.0231**	0.2299
0	**0**	0	0	**0**	0

Relative error % (estimate-true)/true

Fx	Fy	Fz	Mx	My	Mz
Inf	NaN	Inf	Inf	NaN	Inf
Inf	**1.4420**	Inf	Inf	Inf	Inf
Inf	**0.8836**	Inf	Inf	**0.6411**	Inf
Inf	**0.8625**	Inf	Inf	**0.7280**	Inf
Inf	**0.8331**	Inf	Inf	**0.7007**	Inf
Inf	**1.0373**	Inf	Inf	**1.0263**	Inf
Inf	**0.1697**	Inf	Inf	**0.9053**	Inf
Inf	**0.5981**	Inf	Inf	**2.1763**	Inf
Inf	**0.2332**	Inf	Inf	**2.3432**	Inf
Inf	**0.0460**	Inf	Inf	Inf	Inf
Inf	NaN	Inf	Inf	NaN	Inf

% error with respect to full-scale

Fx	Fy	Fz	Mx	My	Mz
0	**0**	0	0	**0**	0
0.1081	**0.1974**	0.2603	1.4892	**0.0138**	0.7054
0.1879	**0.1210**	0.1588	1.3218	**0.0777**	0.7306
0.4559	**0.1806**	0.4310	1.6147	**0.1525**	0.2256
0.6611	**0.1920**	0.3822	1.6424	**0.3590**	0.2933
0.9228	**0.3894**	0.9884	2.9015	**0.5258**	1.5989
0.6998	**0.0391**	0.6497	1.4233	**0.4638**	0.3131
0.4948	**0.1252**	0.7037	1.4974	**0.4559**	0.3912
0.2295	**0.0319**	0.2931	0.9380	**0.2839**	1.3281
0.1132	**0.0063**	0.2617	1.0814	**0.1153**	1.1494
0	**0**	0	0	**0**	0

Figure 3.26: Results for handle B under multiple loading: Fy, My

Real load (Mx, My)

Mx	My
0	0
-2.5575	-2.4231
-8.8702	-4.1900
-17.6368	-16.3054
-8.8702	-4.1900
-2.5575	-2.4231
0	0

Estimated load

Fx	Fy	Fz	Mx	My	Mz
0	0	0	**0**	**0**	0
-0.3296	-2.5226	1.5897	**-2.4392**	**-2.4552**	0.0002
-0.2837	-5.0452	1.3699	**-8.8056**	**-4.2397**	-0.0537
-1.3244	-9.2495	1.5111	**-17.7459**	**-16.4300**	-0.7408
-0.2748	-2.1022	-1.8948	**-8.9953**	**-4.2612**	-0.0878
-0.3268	-0.8409	-0.0449	**-2.5454**	**-2.4965**	-0.0168
0.0078	0	-0.3354	**0.0191**	**-0.0000**	0.0009

Relative error % (estimate-true)/true

Fx	Fy	Fz	Mx	My	Mz
Inf	Inf	Inf	NaN	NaN	Inf
Inf	Inf	Inf	**4.6259**	**1.3253**	Inf
Inf	Inf	Inf	**0.7283**	**1.1850**	Inf
Inf	Inf	Inf	**0.6185**	**0.7644**	Inf
Inf	Inf	Inf	**1.4103**	**1.6970**	Inf
Inf	Inf	Inf	**0.4706**	**3.0295**	Inf
Inf	Inf	Inf	Inf	Inf	Inf

% error with respect to full-scale

Fx	Fy	Fz	Mx	My	Mz
0	0	0	**0**	**0**	0
0.0659	0.2293	0.3179	**0.5915**	**0.1606**	0.0009
0.0567	0.4587	0.2740	**0.3230**	**0.2483**	0.2687
0.2649	0.8409	0.3022	**0.5454**	**0.6232**	3.7042
0.0550	0.1911	0.3790	**0.6255**	**0.3555**	0.4389
0.0654	0.0764	0.0090	**0.0602**	**0.3670**	0.0842
0.0016	0	0.0671	**0.0955**	**0.0001**	0.0047

Figure 3.27: Results for handle B under multiple loading: Mx, My

Numerical results for the parameters that describe the two cells specifications and accuracy are listed in Tables 3.2 and 3.3.

Static calibration process confirmed a reasonable accuracy for the cell sensitivity parameters. Crosstalk compensation obtained through the calibration matrix provides good uncoupling among different channels. Channels measuring axial forces and bending forces and moments demonstrate low hysteresis and non-linearity between $\pm 0.5\%$ and $\pm 1.0\%$ of full-scale. A lower accuracy is evident with the torsional load channel Mx, and overall accuracy of the cells demonstrates a lower performance compared to the commercially available AMTI load cells for walker instrumentation. However, cell accuracy under concurrent channels static loading conditions demonstrated that the accuracy is adequate for our purposes and lightness and adaptability of the handles realized will allow to have a versatile instrument, easily usable for both research and clinical purposes in standard gait analysis laboratories.

Table 3.2: Load cell specifications. Sensitivity was computed as $[S]*[fullscale]./[fullscale]$, with fullscale being a column vector containing all the six channels full-scale values, and the symbol ./ indicating element-by-element division.

		Handle A	**Handle B**
Load	**Capacity**	**Sensitivity**	**Sensitivity**
Fx	500 N	5.4 $\mu V/V\ N$	5.2 $\mu V/V\ N$
Fy	1100 N	2.3 $\mu V/V\ N$	2.4 $\mu V/V\ N$
Fz	500 N	3.2 $\mu V/V\ N$	3.0 $\mu V/V\ N$
Mx (tor.)	20 N	91.1 $\mu V/V\ Nm$	80.3 $\mu V/V\ Nm$
My (bend.)	20 N	48.2 $\mu V/V\ Nm$	51.4 $\mu V/V\ Nm$
Mz (bend.)	20 N	97.6 $\mu V/V\ Nm$	100.4 $\mu V/V\ Nm$

Table 3.3: Load cell non-linearity and hysteresis expressed as % full-scale values for each channel.

	Handle A		**Handle B**	
Load	**Non-linearity**	**Hysteresis**	**Non-linearity**	**Hysteresis**
Fx	± 0.52	± 0.0006	± 0.53	± 0.0006
Fy	± 0.92	± 0.0014	± 0.74	± 0.0010
Fz	± 0.45	± 0.0024	± 0.52	± 0.0020
Mx (tor.)	± 1.83	± 0.2150	± 1.69	± 0.1500
My (bend.)	± 0.67	± 0.0150	± 0.28	± 0.0100
Mz (bend.)	± 0.51	± 0.0150	± 1.52	± 0.0250

3.7 Handle protection and signal amplification

Once results provided by FEM analysis were confirmed by the static calibration of the handles, we could prepare the instrument for being used with the walker. Cell faces with strain gauges and cables were covered with a protective layer of silicon rubber to isolate the sensors and prevent damages to the circuits (Fig. 3.28).

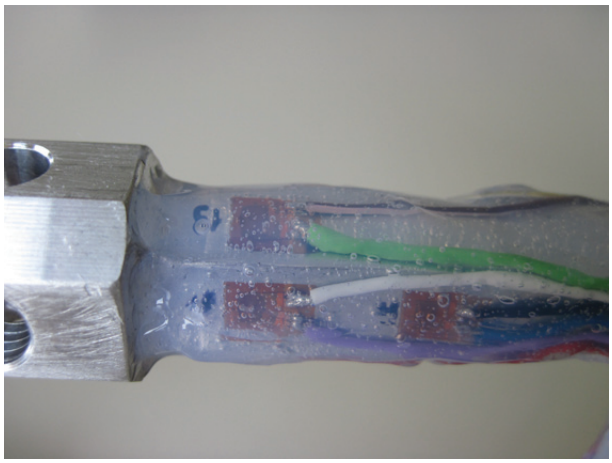

Figure 3.28: Sensors covered with silicon rubber.

The original idea was to connect the strain gauges with thinner wire, and connect these wires with external cable in the middle of the handle, in order to be able to keep all the cables under the metal bands used to fix the handle on the walker. However, the final choice led to larger wires and this solution was no longer applicable. Therefore, the four cable branches were maintain external to the cell surface and fixed with epoxy resin at the two end points of the octagon to avoid unintentional tearings (Figg. 3.29(a),3.29(b)).

After the silicon layer was completely dry, the sensing part of the handles was covered with a thin plastic layer and then with an aluminium adhesive tape for electromagnetic (EM) noise shielding (Fig. 3.30).

Signals from the Wheatstone bridges we amplified very close (40 cm) to the handles (Fig. 3.31). A small shielded box contained a fixed-voltage regulator, six amplifiers with zero-adjustment to provide exitation voltage to the bridges and amplify their output after

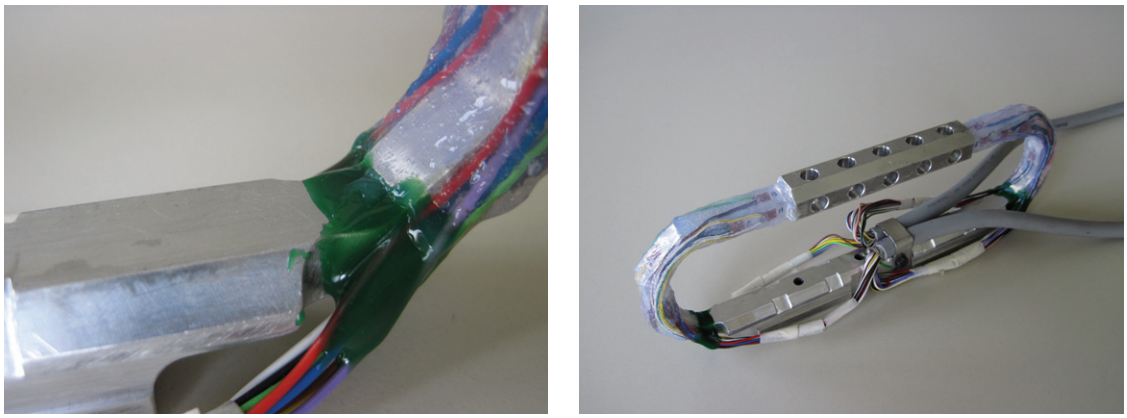

(a) (b)

Figure 3.29: Reinforcement of cable fixation at the extremities and plastic covering of the whole handle.

Figure 3.30: Shielding from EM noise.

a low pass filtering @ 250 Hz (BA660 amplifiers, Vishay GmbH, Germany). The box with the amplifiers can be connected to a 22 meters-long shielded cable via a 'D' connector, and signals can be sent to the Vicon AD converter input board (Fig. 3.32).

Through the same cable, amplification devices are provided with power and with an external trigger signal to store the zero reading (Fig. 3.33(a)).
Figure 3.33(b) summarizes the corresponce between the 22 meters colored cable conductors and the connector pins on the amplification boxes. The same color code has been used for both cables. Two of the '*Power*-' terminals are used for connection to the GND terminals of the ADC board.

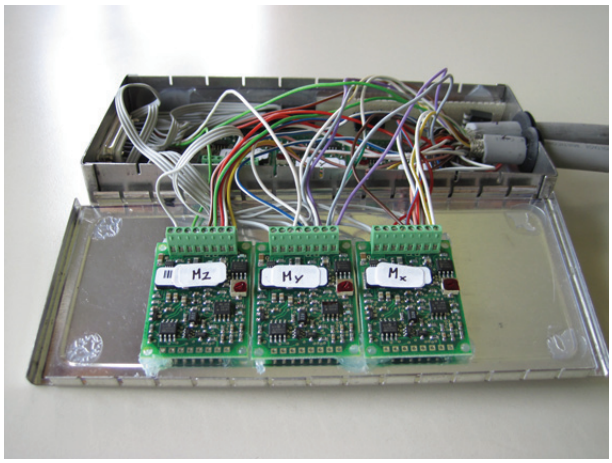

Figure 3.31: Metal box with amplifiers.

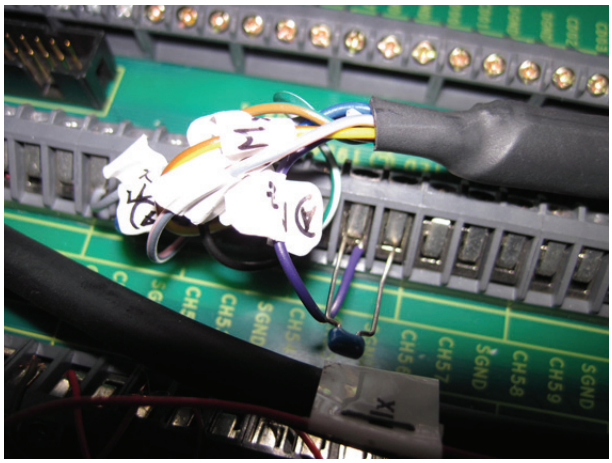

Figure 3.32: Final connection of the cables with Vicon system hardware.

The whole handles were finally wrapped with road bicycle handlebar rubber tape. Two different colors were used to highlight hand holding areas (Fig. 3.34).

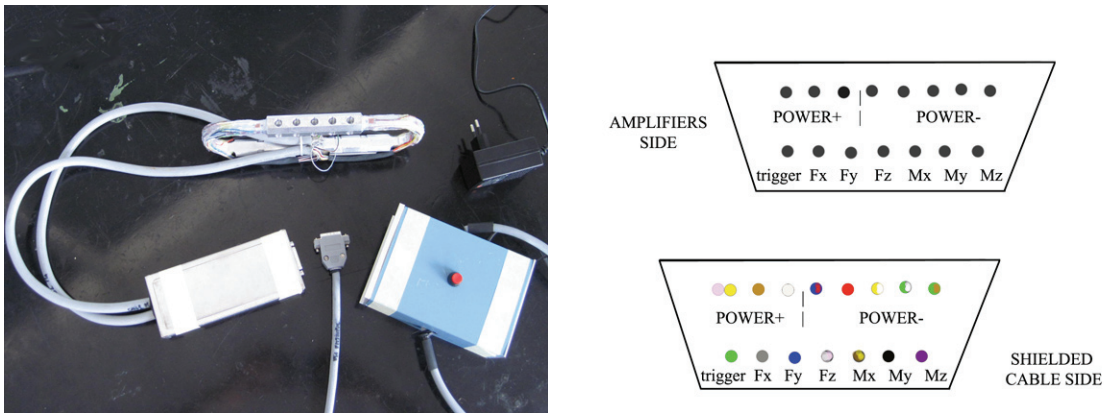

(a) (b)

Figure 3.33: a) Handle with the signal conditioning box, extremity of the shielded cable with connector, trigger switch and power transformer with its plug; b) Association of box connector pins to the signals. Due to a connection error, for the handle B the output cable for the amplified signals Mx and Mz were swapped, and therefore at the end of the 22-meters cable the label 'Mz' is associated to the yellow-brown cable and the label 'Mx' to the violet cable.

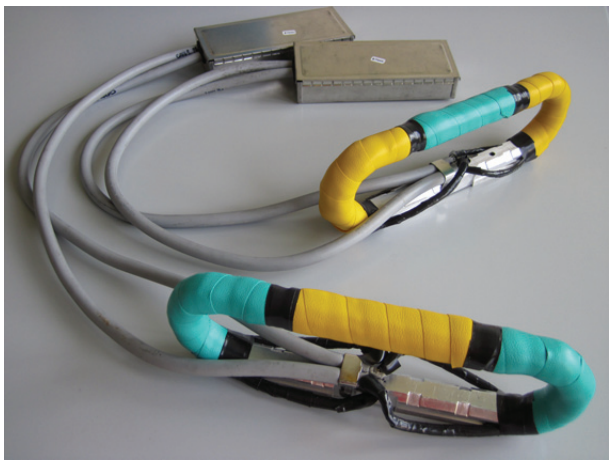

Figure 3.34: Handles with final covering.

3.8 Connection with the motion-capture system

The two instrumented handles were included in the sofware Vicon Nexus as if they were 6 channels AMTI strain gauge force plates, in order to get real-time information about forces and moments applied on the handle. The handle is seen from the system as a forceplate fixed on a specific point in space. Reflective markers will be later placed on the handle to register its position at every time instant. A few parameters are needed by Nexus to correctly process the input signals.

Sensitivity matrix. Sensitivity matrix (which is uncorrectly called '*calibration matrix*' in Nexus) was required in SCS units, therefore we had to convert Newtons and Newton-meters into pounds-force and pound-force by inches, remembering the equivalences:

$$\begin{aligned} 1\,Kg &= 2.20462262\,lb \\ 1\,N &= 0.224808943\,lbf \\ 1\,m &= 39.3700787\,inches \end{aligned} \tag{3.2}$$

Moreover, it was necessary to re-arrange matrix elements following AMTI internal axes convention (Fig. 3.35) and, for the same reason, it was necessary to follow a precise order to label the channels in Vicon Nexus after connection of the handle cables to the ADC input board (Tab. 3.4).
Sensitivity matrix values were given to the system through a text file with extension .plt, that we generated by modifying the file of the previously installed AMTI force plate.

Correction factor. The value of the correction factor CF, required in Nexus as 1/CF, is used to scale appropriately the numerical values obtained after multiplication of the calibration matrix by the voltage input signals. The correction factor is computed as:

$$CF = V_{EXC} * G * 10^{-6} \tag{3.3}$$

where V_{EXC} is the bridges excitation voltage, equal to 5V, G is the amplifier gain (in our situation it is equal to 500), and term 10^{-6} is needed because the values of the sensitivity matrix in the calibration file were expressed in μV/V.

Amplitude of signal input. To make the most of the ADC capabilities, it is necessary to provide Nexus with the maximum value ($\pm$ 5V) achievable from the input signals.

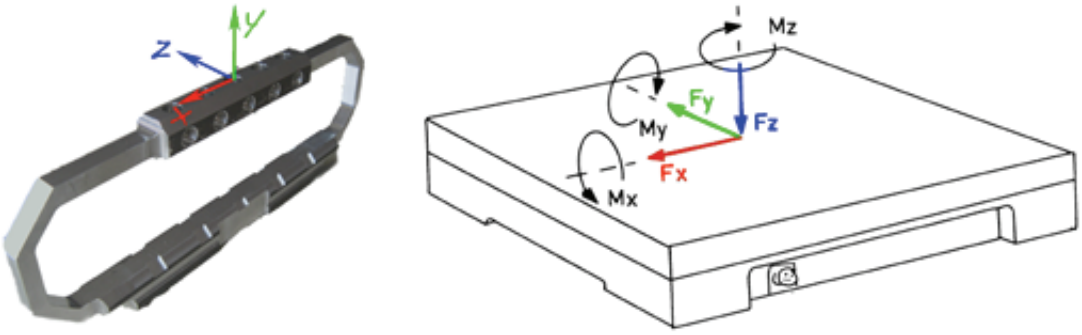

Figure 3.35: Reference systems for the handle and for an AMTI force plate.

Table 3.4: Association of original handle signals with associated labels given in Vicon Nexus.

Handle signal	**Vicon Nexus labels**
Fx	Fy
Fy	Fz
Fz	Fx
Mx	My
My	Mz
Mz	Mx

Observations after completing the connections.

Signal to noise ratio (SNR): approximately 100 (5V/0.05V).

Electric current absorbed by handle A before the voltage regulator: 250-260 mA, which confirms expectations, since each one of the six amplifiers needs 30 mA plus the current of the bridge, 14 mA.

3.9 Handles dynamic calibration

As a further check, instrumented handles were dynamically validated using a floor-mounted AMTI BP900900-2K force plate (AMTI, Watertown, USA) .
Handles were placed on a rigid frame fixed by means of screws on the superior plate of the force plate to compare forces measured by both systems along the three reference axes when the handle was loaded in static and dynamic conditions, as highlighted in Fig. 3.36.

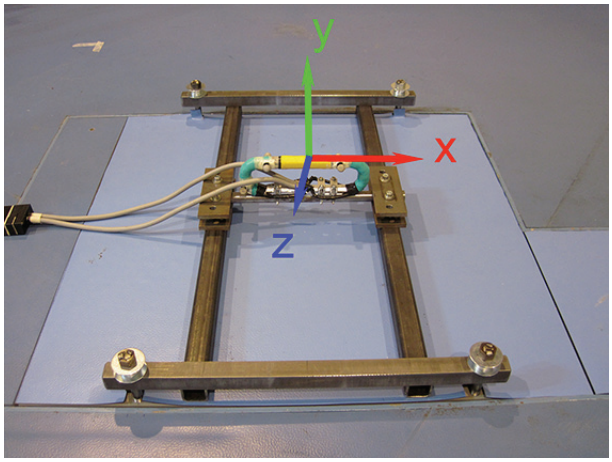

Figure 3.36: Handle fixed on the superior plate of the force plate.

Results of the comparison during a dynamic cyclic loading test in all directions are summarized in Fig. 3.37 and in Tab. 3.5. The best accuracies were measured for the anterior-posterior (Fx) and vertical (Fy) forces, while the larger difference was measured along the medial-lateral axis (Fz), that gave anyway a mean relative error below 5%.

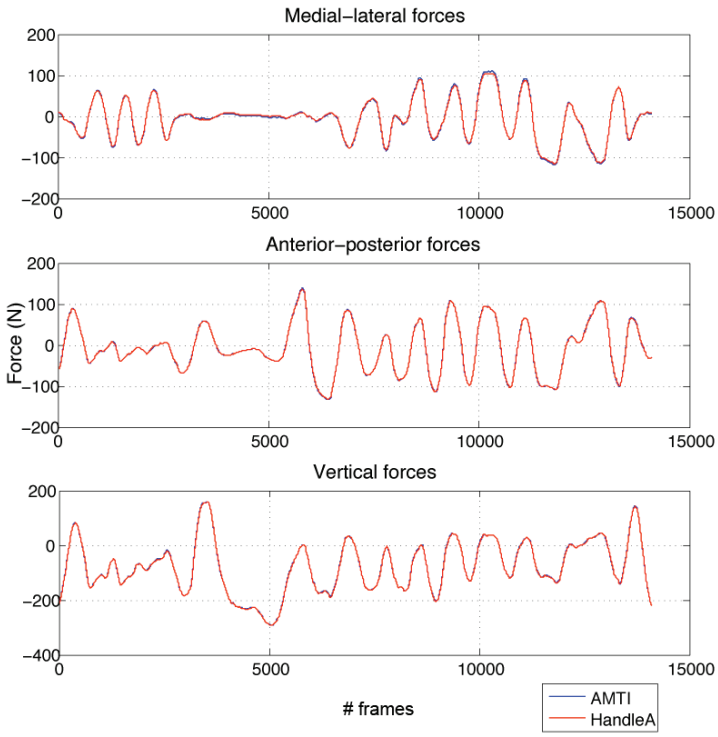

Figure 3.37: Forces comparison along the three orthogonal axes.

Table 3.5: Evaluation of differences in dynamic loading conditions between AMTI force plate and handles, with the axes convention used in Fig. 3.36.

	Fx	**Fy**	**Fz**
Error due to noise (N)	0.3	0.8	0.4
Mean abs Force (N)	49.2	98.2	35.2
Max error (N)	2.4	4.3	6
Mean error (N)	0.6	1.3	1.6
Mean relative error (%)	1.3	1.3	4.7

3.10 First tests on walkers

Handles were tested on a posterior paediatric walker driven by an healthy child (Figures 3.38(a) and 3.38(b)).

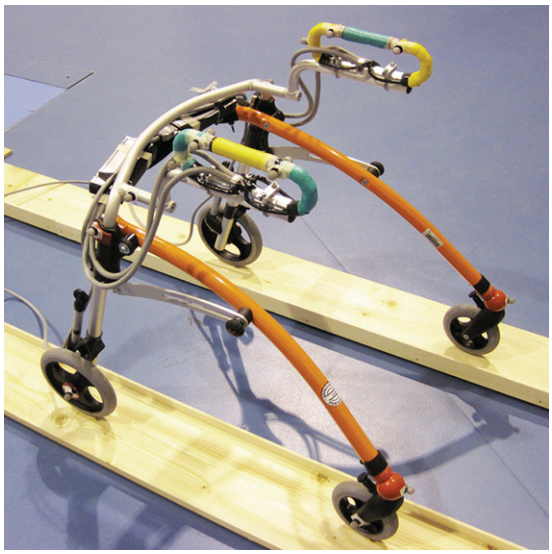

(a)

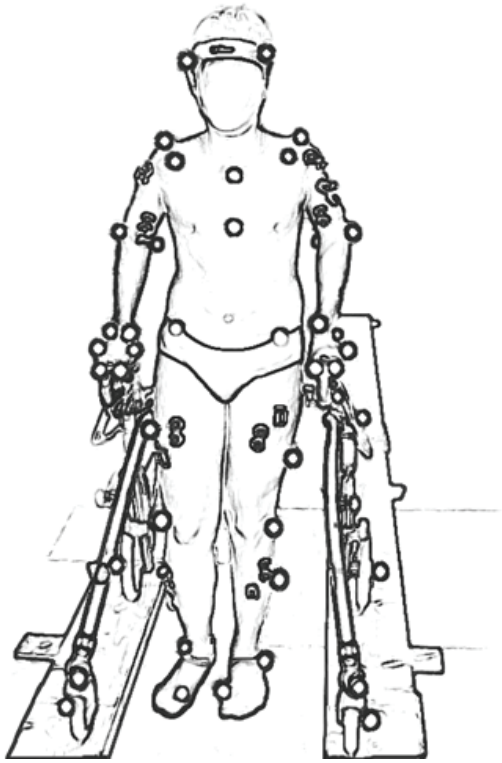

(b)

Figure 3.38: (a) Instrumented handles positioned on a posterior paediatric walker. Walker was placed over two rails in order to be able to measure ground reaction forces at the feet without walker wheels interaction with the force plates; (b) Drawing of a healthy children with markers and surface EMG sensors while using the posterior walker with instrumented handles during a test trial.

Figure 3.40 is an example of the information provided by the two instrumented handles during the test on the posterior walker: the plots show the raw measured handle reaction forces along the three reference axes for the right and left sides, superposed to a scaled copy of the vertical component of the ground reaction forces, in order to have an idea of the loading strategy followed by the subject. Figure 3.39 shows the graphical three-dimensional representation of force plates, handles and measured force vectors in Vicon Nexus. As with the normal force plates positioned on the ground, also handle position

is fixed. A proper biomechanical model (see chapter 4) can be used to associate handles forces and moments to their true point of application registering the position of markers attached to the handles.

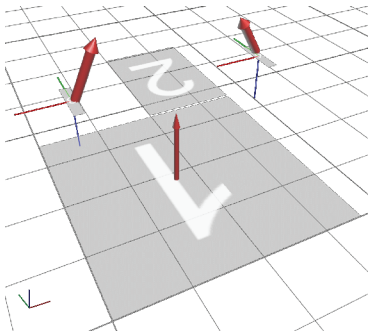

Figure 3.39: Graphical representation of HRFs and GRF in Vicon Nexus during the test.

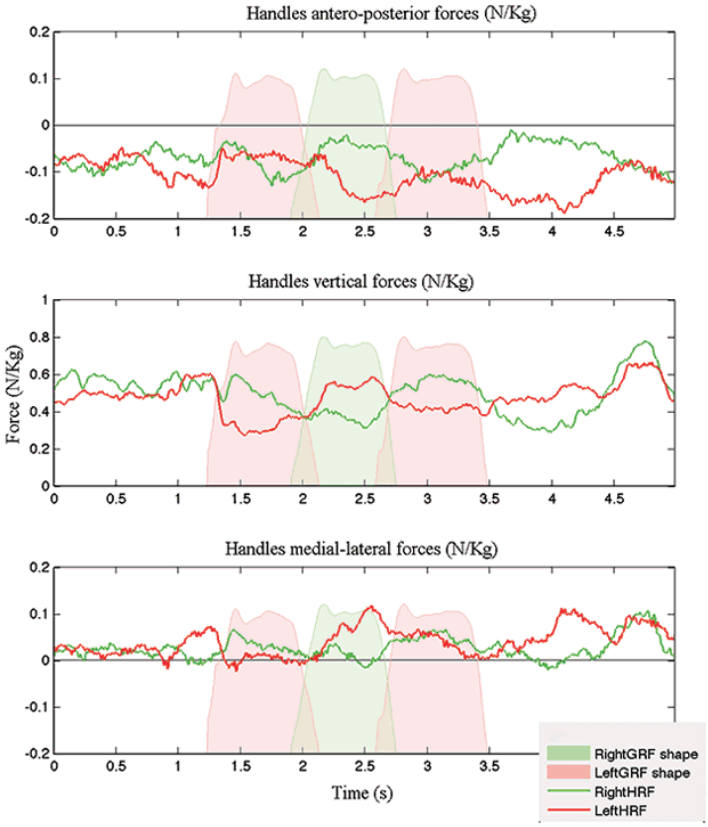

Figure 3.40: Handle Reaction Force (HRF) components measured by the right (green) and left (red) handles. The shape of the vertical Ground Reaction Force (GRF) component is shown, for the right (green) and left (red) sides.

Chapter 4

Full-body model

In order to estimate the whole body muscle mechanical work during normal walking and walker-assisted locomotion, a full-body 3-dimensional kinematic and kinetic model was developed.

To compute muscle work following the joint power approach described in section 1.2.1, external Ground Reaction Forces (GRFs) and Handle Reaction Forces (HRFs) interacting with the body have to be measured and included in the analysis.

The model consists in 16 segments, connected by 15 ideal ball-and-socket joints, for a total 51 degrees of freedom, integrating an Upper Limb (UL) model with a 2-segments trunk, pelvis, head and a traditional kinetic lower limbs (LL) model. The overall marker-set is made by 41 markers placed on anatomical landmarks. Five markers were also positioned on each of the two instrumented handles.
This chapter describes in more detail the full-body model developed and its validation.

4.1 The Upper-Body

The upper part of the model is composed by a right and left Upper Limb (UL) model including hand, forearm and upper-arm, a head-neck segment, a trunk divided in thorax and abdomen segments.

Additionally to the use of the model for the computation of joint powers, UL kinetic assessment is important to understand gait strategies and joint loading to improve walker

ergonomics and prevent joint damage.

Several models for UL movement evaluation exist in the literature (Bachschmidt et al., 2001; Konop et al., 2009b; Rettig et al., 2009; Garofalo et al., 2009; Mackey et al., 2005; Slavens et al., 2010), but the criteria for the present study were to: i) have an accurate but easy-to-place marker set, ii) avoid functional calibrations of joint centres and axes due to possible patient movement limitations, iii) allow muscles surfaces to be free for additional electromyographic recording.

Therefore, we developed a new protocol for assessing UL kinematics and kinetics in adults and children using their own walkers and we tested it on an adult healthy subject. The UL marker-set was chosen after evaluation and comparison of four models performance in estimating wrist, elbow and shoulder joints movement against manual goniometric measures. Our proposed marker-set, similar to the one presented in (Slavens et al., 2010) gave results comparable to the marker-set presented in (Rettig et al., 2009) and was highly better than that presented in (Mackey et al., 2005) and an additional one based on marker clusters for upperarm, forearm and hand. None of the models implemented from the four marker-sets, however, had internal-external rotation of the humerus related to the forearm reference frame.

Upper body segments were defined using 20 reflective markers placed on anatomical landmarks (Fig. 4.1). Head markers were placed anteriorly over the temples (RFHD, LFHD) and posteriorly on the back of the head, roughly defining a horizontal plane with the front head markers (RBHD, LBHD). Thorax markers were placed on T2, T6, T12 and sternal notch (CLAV) following the Oxford Trunk Model (Bates et al., 2010); an additional marker was placed on the xiphoid process of the sternum (STRN). UL markers were placed on the acromion process (AC), anteriorly and posteriorly on the shoulder (AA, AP), medial (ME) and lateral (LE) humeral epicondyles, ulnar (US) and radial (RS) styloid processes, 3rd metacarpal head (HAND). The four pelvis markers were placed on the anterior and superior iliac spines (RASI, LASI, RPSI, LPSI).

Five markers were also positioned on each of the two load cells, since at least 3 markers are needed to define a plane in a 3D space, but we used 2 additional markers for redundancy (to overcome the problem of markers occlusions) and one for asymmetry (to avoid

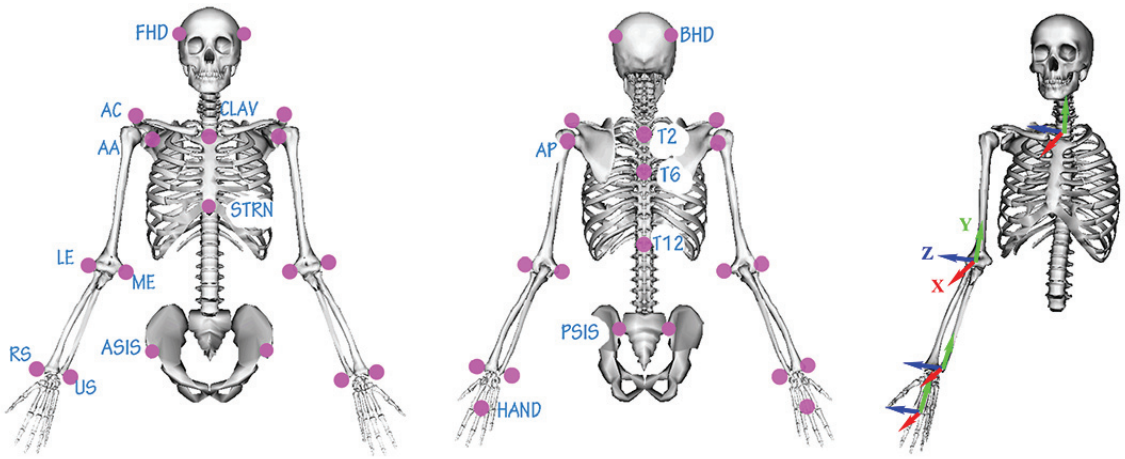

Figure 4.1: Upper body markers placement and coordinate systems for hand, forearm, upper arm and thorax.

errors during automatic markers labelling by the Vicon system).

The gleno-humeral joint centre (GH) was defined as the centre of a circle encompassing the three markers on the shoulder, revising the seminal idea in Mackey et al. (2005), Fig.4.2.

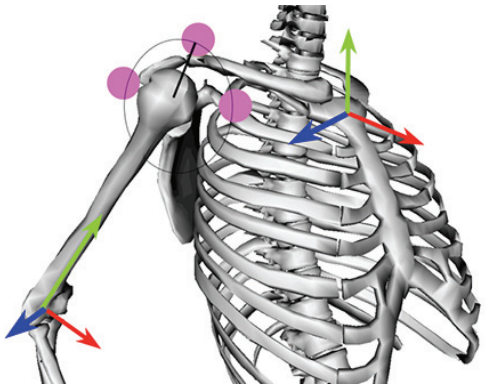

Figure 4.2: Gleno-humeral joint centre as the centre of a circle encompassing the 3 shoulder markers.

4.1.1 Segments definitions

Coordinate systems were defined following ISB guidelines (Wu et al., 2005).

mm = markers diameter. **Head**

Origin: HO = (LFHD+LBHD+RFHD+RBHD)/4

Other points: LHead = (LFHD+LBHD)/2

RHead = (RFHD+RBHD)/2

BHead = (LBHD+RBHD)/2

FHead = (LFHD+RFHD)/2

C7 = T6 + 1.5*(T2-T6)

NeckOrigin = NO = C7 + 0.3*(CLAV-C7)

UpHead = direction normal to the plane containing head markers

VertexHead = VX = $HO+$ UpHead$*0.9*$ $\parallel RFHD - HO \parallel$ (0.9 found by checking outputs superposed to digital video of the subject).

$Zhd = RHead - LHead / \parallel Rhead - Lhead \parallel$, medio-lateral axis

$Yhd = \frac{Zhd \wedge (FHead - BHead)}{\parallel Zhd \wedge (FHead - BHead) \parallel}$, vertical (longitudinal) axis

$Xhd = Yhd \wedge Zhd$, antero-posterior axis

Thorax

Origin: T2

$Yt = (T2 - T6) / \parallel T2 - T6 \parallel$, with correction for the offset T2-T12 from static trial

$Zt = \frac{(CLAV - T2) \wedge Yt}{\parallel (CLAV - T2) \wedge Yt \parallel}$, medio-lateral axis

$Xt = Yt \wedge Zt$, antero-posterior axis

Abdomen

Origin: A = (T12 + STRN)/2

SACR = (LPSI+RPSI)/2

$Ya = (T12 - SACR) / \parallel T12 - SACR \parallel$ longitudinal axis

$Za = \frac{Yt \wedge (STRN - T6)}{\parallel Ya \wedge (STRN - T6) \parallel}$ medio-lateral axis

$Xa = Ya \wedge Za$, antero-posterior axis

Upper arm (Humerus), (right side, ISB guidelines 1st option)

Origin: E = (EL+EM)/2 , elbow joint centre

$Yh = \frac{(GH - E)}{\parallel GH - E \parallel}$, longitudinal axis

$Xh = \frac{Yh \wedge (EL - EM)}{\parallel Yh \wedge (EL - EM) \parallel}$, antero-posterior axis

$Zh = Xh \wedge Yh$, medio-lateral axis

Forearm (right side)

Origin: US, ulnar styloid

$Yf = (E - US)/ \parallel E - US \parallel$, longitudinal axis

$Xf = \frac{Yf \wedge (RS-US)}{\|Yf \wedge (RS-US)\|}$, antero-posterior axis

$Zf = Xf \wedge Yf$, medio-lateral axis

Hand (right side)

Origin: HND $= HAND - mm \perp planeby(RS, US, HAND)$

WR $= (US + RS)/2$, wrist centre

$Ym = \frac{(WR-HND)}{\|WR-HND\|}$, longitudinal axis

$Xm = \frac{Ym \wedge (RS-US)}{\|Ym \wedge (RS-US)\|}$, antero-posterior axis

$Zm = Xm \wedge Ym$, medio-lateral axis

For the left limb, the orientation of the coordinate systems is the same, with the difference that Z axis points medially instead of laterally. Therefore, with the subject in anatomical neutral position, with hand palm facing forward, X-axis is anterior, Y-axis is superior and Z-axis lateral towards the right for all segments.

When using the walker, the forearm is pronated and therefore forearm and hand coordinate systems are internally rotated of about 80-100 degrees with respect to the neutral position.

4.2 The Lower Body

As Lower Limb (LL) model the traditional Newington-Davis marker set was chosen, to allow clinical integration of this model with a traditional Vicon Lower Limbs Plug-in Gait protocol, if needed.

Markers were placed on the pelvis and lower limbs anatomical landmarks, as described in Fig.4.1 and 4.3. The knee markers (KNE) were placed on the lateral epicondyles of the

knee, the ankle markers (ANK) were placed on the lateral malleoli along an imaginary line that passes through the transmalleolar axis. Foot markers were placed over the second metatarsal head (TOE) and on the calcaneous (HEE) at the same height above the ground surface as the toe marker. Thigh and leg wands were not used, to avoid interactions with the walker frame. These markers (RTHI, LTHI, RTIB, LTIB) were therefore attached directly on the skin. Since the aim of this study was to compute net joint powers, Cardan-Euler angles cross-talk effect has no effect on this parameter and therefore the precision in the definition of the frontal plane of thigh and leg segments is not so stringent.

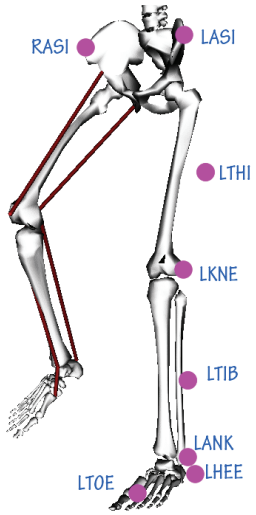

Figure 4.3: Lower body markers placement.

4.2.1 Segments definitions

mm = marker diameter.

Pelvis

The Newington - Gage model is used to define the positions of the hip joint centres (HJCs) in the pelvis segment (Davis et al., 1991).

PELF = (LASI+RASI)/2

SACR = (LPSI+RPSI)/2

L5 = SACR + 0.2*(PELF-SACR)

Origin: MidHJC = (LHJC+RHJC)/2

$Zp = (RASI - LASI)/ \parallel RASI - LASI \parallel$ medio-lateral axis

$Yp = \frac{(SACR-PELF)\wedge Zp}{\|(SACR-PELF)\wedge Zp\|}$ vertical axis

$Xp = Yp \wedge Zp$, antero-posterior axis

Thigh (femur), (right side)

In both the static and the dynamic model, the knee joint centre (KJC) is determined as a point belonging to the plane defined by the hip joint centre (HJC), the thigh marker (THI), and the knee marker (KNE), placed medially with respect to KNE of a knee offset (KO), a parameter computed using the *knee width* value measured on the subject. KO = (mm + knee width)/2

Origin: KJC, knee joint centre

$Yth = (HJC - KJC)/ \parallel HJC - KJC \parallel$, longitudinal axis

$Xth = \frac{(KJC-THI)\wedge Yth}{\|(KJC-THI)\wedge Yth\|}$, antero-posterior axis

$Zth = Xth \wedge Yth$, medio-lateral axis

Shank (tibia) (right side)

In both the static and the dynamic model, the ankle joint centre (AJC) is determined as a point belonging to the plane defined by the knee joint centre, the tibia marker, and the ankle marker (ANK), placed medially with respect to ANK of an ankle offset (AO), a parameter computed using the *ankle width* value measured on the subject. AO = (mm + ankle width)/2

Origin: AJC, ankle joint centre

$Ys = (KJC - AJC)/ \parallel KJC - AJC \parallel$, longitudinal axis

$Xs = \frac{(AJC-TIB)\wedge Ys}{\|(AJC-TIB)\wedge Ys\|}$, antero-posterior axis

$Zs = Xs \wedge Ys$, medio-lateral axis

Foot (right side)

Origin: TOE

$Yft = (HEE - TOE)/ \parallel HEE - TOE \parallel$, longitudinal axis

$Zft = \frac{(KJC-AJC)\wedge Yft}{\|(KJC-AJC)\wedge Yft\|}$, medio-lateral axis

$Xft = Yft \wedge Zft$, antero-posterior axis

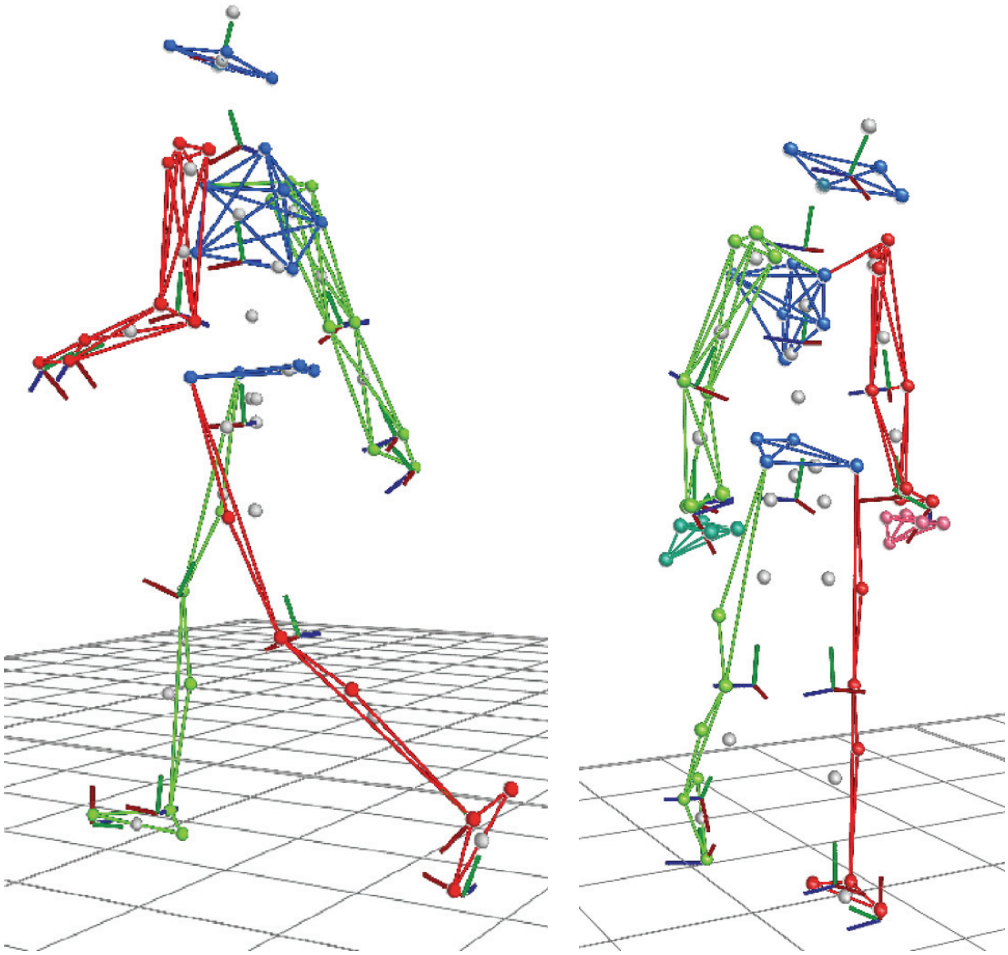

(a) (b)

Figure 4.4: Full-body model during normal gait and during walker locomotion, with markers on the handles. Together with the acquired markers, in the figures are shown other computed points, as the center of mass of the segments, and of the segment local reference systems.

4.3 Inertial properties of the model

The definition of inertial properties is needed for the body segments in order to be able to define the connection between measured kinematics and applied forces, following the basic equations of mechanics:

$$\mathbf{F} = m\mathbf{a} \tag{4.1}$$

$$\mathbf{M} = \mathbf{I}\alpha \tag{4.2}$$

Inertial parameters of the model were defined considering the anthropometric tables of Zatsiorsky-Seluyanov (De Leva, 1996) for male adults and from Jensen (1986) for children, with some adaptations related to our segments definitions based on the surface reflective markers used.

The moment of inertia $\mathbf{I}$ for a segment is expressed by mean of its components related to three orthogonal axes of rotation passing through the segment centre of mass. In the tables the values normally represented are the three *radii of gyration*, r_{XX}, r_{YY}, r_{ZZ}, expressed as fractions of the segment length. The moment of inertia around the x axis, for a segment with mass m and length L is then computed as:

$$I_{XX} = m\,(r_{XX}\,L)^2 \tag{4.3}$$

Since the radii of gyration and the COM positions do not change substantially with age (Jensen, 1986), regression equations with respect to age were used for the relative mass of the segments only (Tab.4.2).

In (Jensen, 1986) the trunk consisted of one segment only, therefore thorax, abdomen and pelvis equations were corrected here by partitioning the original mass of the whole segment in three parts following the relative ratios given in Tab.4.1.

4.4 Body centre of mass

From markers and internal points defined in sections 4.1 and 4.2 the whole body centre of mass (BCOM) was computed by finding, first, the single centers positions of all the 16 segments (Tab.4.3) from (De Leva, 1996) tables, and then computing their weighted mean using the regression equations described, alternatively for adults or children.

The main concern with these definitions has been the correct positioning of the centers of mass of the trunk segments in the transversal plane, since tables from (De Leva, 1996)

Table 4.1: Inertial properties of the body segmentsfor adult male subjects, adapted from (De Leva, 1996). COM position is expressed as a % of the segment length from distal end. Radii of gyration are expressed as % of the segment length, with AP being the antero-posterior axis, ML the medio-lateral axis, LG the longitudinal axis.

Segment	**Length**	**% Bodymass**	**COM**	r_{AP}	r_{ML}	r_{LG}
Head+Neck	$\parallel VX - NO \parallel$	6.9	50.0	30.3	31.5	26.1
Thorax	$\parallel T12 - T2 \parallel$	16.3	50.7	50.5	32.0	46.5
Abdomen	$\parallel T12 - L5 \parallel$	16.0	45.0	48.2	38.3	46.8
Pelvis	$\parallel MidHJC - L5 \parallel$	11.2	50.0	61.5	55.1	58.7
Upperarm	$\parallel GH - E \parallel$	2.7	42.3	28.5	26.9	15.8
Forearm	$\parallel E - WR \parallel$	1.6	54.3	27.6	26.5	12.1
Hand	$\parallel WR - HND \parallel$	0.6	21.0	62.8	51.3	40.1
Thigh	$\parallel HJC - KJC \parallel$	14.2	59.0	32.9	32.9	14.9
Shank	$\parallel KJC - AJC \parallel$	4.3	56.1	25.1	24.6	10.2
Foot	$\parallel 0.8\,(HEE - TOE) \parallel$	1.4	0.5	25.7	24.5	12.4

and (Jensen, 1986) do not provide this information. The final positioning was therefore based on empirical assumptions, later qualitatively verified on a few static trials by observing the projection of the BCOM on the ground versus the position of the center of pressure provided by the forceplate.

Table 4.2: Segments relative masses as a function of age, expressed as fractions of the total body bass, adapted from (Jensen, 1986)

Segment	**% Bodymass**
Head	(0.2376-0.0114*age)
Thorax	(-0.0006*age+0.157)
Abdomen	(-0.0006*age+0.154)
Pelvis	(-0.0006*age+0.114)
Upperarm	(0.00084*age+0.022)
Forearm	(0.00018*age+0.01469)
Hand	(-0.00003*age+0.00898)
Thigh	(0.00364*age+0.06634)
Shank	(0.00122*age+0.03809)
Foot	(0.00015*age+0.0187)

Table 4.3: Definition of the center of mass position of the body segments.

Segment	**COM definition**
Head	(RBHD+LBHD+RFHD+LFHD)/4
Thorax	(T2+CLAV+T12+STRN)/4
Abdomen	(SACR+T12+STRN+PELF)/4
Pelvis	(RHJC+LHJC+SACR+PELF)/4
Upperarm	E + 0.423*(GH-E)
Forearm	WJC + 0.543*(E-WJC)
Hand	Hand origin
Thigh	HJC + 0.41*(KJC-HJC)
Shank	KJC + 0.45*(AJC-KJC)
Foot	HEE + 0.5*(TOE-HEE)

4.5 Model implementation in Vicon BodyBuilder

Vicon BodyBuilder 3.6 software was used to implement the kinematic and inverse dynamics model (Vicon Motion Systems, Oxford, UK).

The five markers on the handle were used to compute the handle centre and apply the measured forces and moments to that point. Reactions measured at the handles were applied to the hand segments while reactions measured on the ground were applied to the proper foot segment.

Joint rotations were described using Cardan-Euler Z-X-Y (flexion-extension, ab-adduction, internal-external rotation) sequences for all joints. Joint angles are positive for flexion, adduction, and internal rotation. The three internal joint reaction force components (anterior-posterior, medial-lateral, longitudinal) are represented in the local coordinate system of the proximal segment, with signs following this convention: positive internal reaction component pointing towards X and Y axes positive direction for both sides, Z axis positive direction for the right side and Z axis negative direction for the left side. The three internal joint reaction moment components (flexion-extension, ab-adduction, internal-external rotation) are expressed as internal moments in the coordinate system of the proximal segment connecting to that joint and are defined positive for internal actions towards extension, abduction and external rotation (Kirtley, 2006).

Hierarchical relationships between the segments were defined as in Fig.4.5, with the pelvis segment considered as the root segment. Joint reactions were computed at the points connecting two adjacent segments. Using the definitions given in sections 4.1 and 4.1, neck reaction was computed with respect to the neck origin point; wrist, elbow and shoulder reactions were computed with respect to the wrist joint centre (US), the elbow joint centre (E), the humerus head (GH); trunk reaction were computed at the thoracolumbar joint (T12, approximation of T12-L1 joint) and at the lumbosacral joint (L5, approximation of L5-S1 joint); lower limb reactions were computed with respect to the hip joint centre (HJC), the knee joint centre (KJC) and the ankle centre (AJC).

Bodybuilder REACTION and POWER functions were used to compute joint reactions and joint power flows for all considered body joints.

Model outputs were normalized by bodymass (forces and powers) and by bodymass

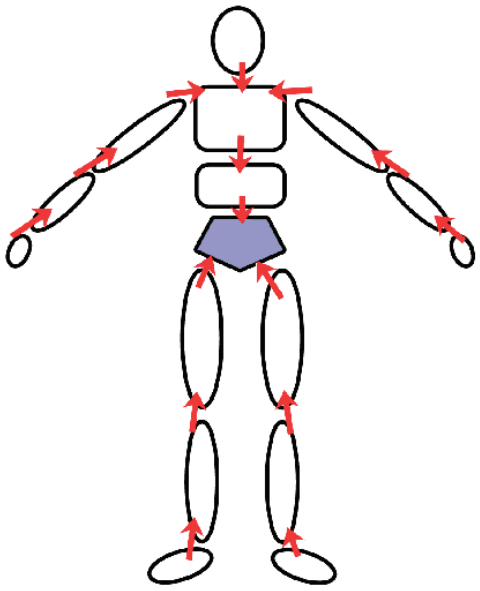

Figure 4.5: Hierarchical relationships between body segments for kinematics and kinetic computations. When forces from force plates and/or handles are available, they are applied to the correspondent foot or hand segment.

times height (joint moments). Height was preferred to leg length since joint moments are computed at both the upper and lower limbs. Fig.4.6 shows the results of a simple check test on the POWER function. The plot includes the values of the rotational (or *active*) and the linear (or *passive*) power curves at the lower limb joints during a gait cycle for a young adult subject.

The aims of this simple validation were:

(1) To qualitatively check the power outputs provided by the standard Vicon Plug-In Gait (PiG) model to verify that the power values provided are relative to the rotational components of joint powers only, which is confirmed by the blue and red lines in the figure;

(2) To compare our (Verona) model power results (greeen line) with the Vicon PiG results, since the Vicon PiG model is based on Dempster's anthropometric regression equations (Winter, 2005), which have slightly different parameters with respect to the equations we used in our model. In this way we could also check that the BodyBuilder function POWER output gives the rotational component of the joint power;

(3) To evaluate the magnitude of the linear (*passive*) power transferred from the distal to the proximal segment (dotted magenta line).

The output of the two models are comparable: Differences appear mainly around the toe-off phase (60% of the gait cycle), probably related to differences in segments inertial parameters.

The values of the linear power components are consistent with results published in (Robertson and Winter, 1980), considering that the model used in that publication was only sagittal.

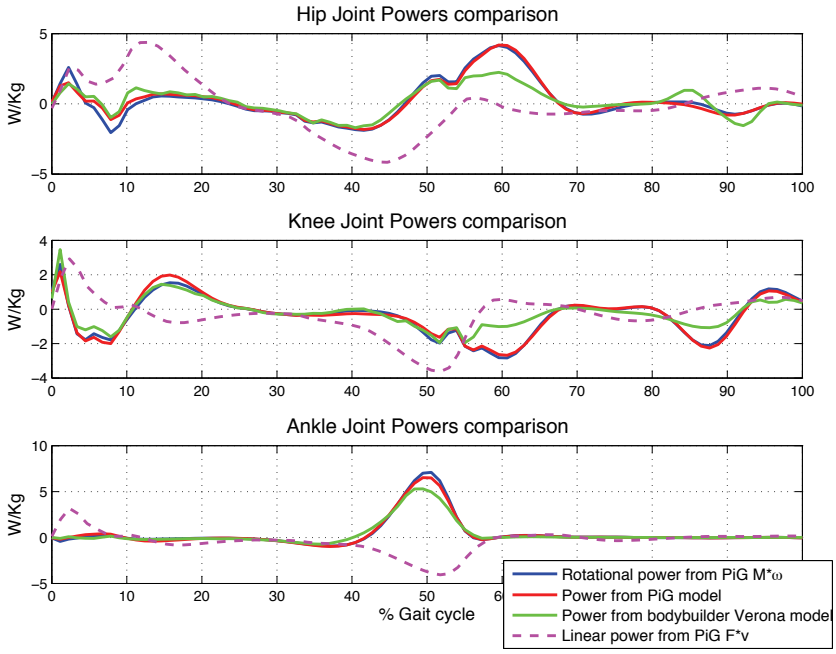

Figure 4.6: Different computations of lower limbs joint powers during one gait cycle (see text for details).

4.6 Full-body model validation

While validating the model, two errors, due to wrong explanations on how to define inertial properties of a segment given in the BodyBuilder technical manual (Vicon), final examples, pages 136-137, were found and corrected. The mistake was communicated to Vicon staff. Since we developed a full-body dynamic model, a criterion to evaluate the quality of inverse dynamics computations was needed.

Inverse dynamics approaches suffer from error propagation, and therefore proximal joint loads estimations might evidence larger errors (Winter, 2005).

Errors may depend on uncorrect estimation of the inertial properties of body segments (relative mass, centre of mass position, moments of inertia), uncorrect estimation of joint centers and joint axes of rotation, noise in the stereophotogrammetric measures, markers misplacement and tissue artifacts, inaccuracy in determining the point of application of external forces (Zatsiorsky, 2002).

For the final purposes of our study we need to study locomotion in two conditions, with and without walking aids. Therefore, in the first situation the body is interacting only with the ground, while in the second case we have to take into account also forces and moments coming from interaction with the handles.

To evaluate the reliability of the results provided by the model, we compared *hip* reactions computed via a *bottom-up* or a *top-down* approaches (Kingma et al., 1996; Robert et al., 2007).

In the first case, the pelvis brings to the hip the overall loads coming from the upper body and also from the contralateral leg. With the *bottom-up* approach, hip loads were estimated as pelvis segment reactions to loads applied by the femur segment at the hip joint.

In the second case, the equations of motions are solved starting from the most distal segments of the upper body (hands and head) and going proximally at each iteration, while in the second case the starting point is the foot in contact with the ground. Therefore, with the *top-down* approach, hip loads are estimated as thigh segment reactions to loads applied by the pelvis segment to the hip joint.

Differences in outputs computed with the two methods are presented in the following

figures as magnitude of joint forces and moments components computed for all the good trials acquired from the 10 healthy children during normal walking and during walker locomotion.

For all the trials, left hip reactions were computed via the *top-down* and *bottom-up* approaches during the left single support phase.

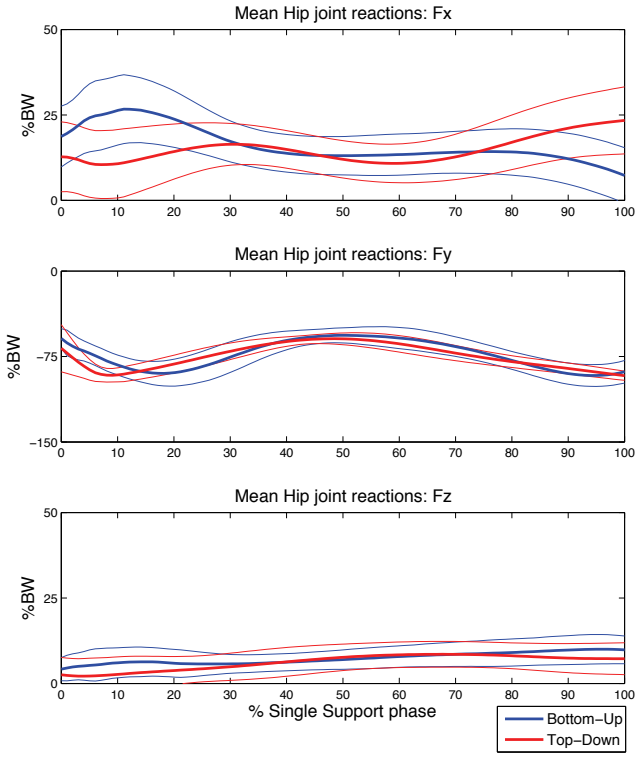

Figure 4.7: Left hip joint reaction forces during *normal gait*, computed with bottom-up and top-down inverse dynamics computations. Results are presented as mean values ± 1 SD, expressed in the pelvis reference system.

Results from figures 4.7, 4.8, 4.9, 4.10 show, for both gait conditions, a good correspondence between the two models in terms of estimated hip joint reaction forces and moments, except for some differences evident at the antero-posterior force Fx during gait and at the flexion-extension moment Mz in both conditions.

Besides differences due to a low-pass filtering effect on the reactions estimated with the *top-down* approach (Cappozzo, 1983), which might explain the differences measured at Fx at the beginning and at the end of the single support phase during gait due to important

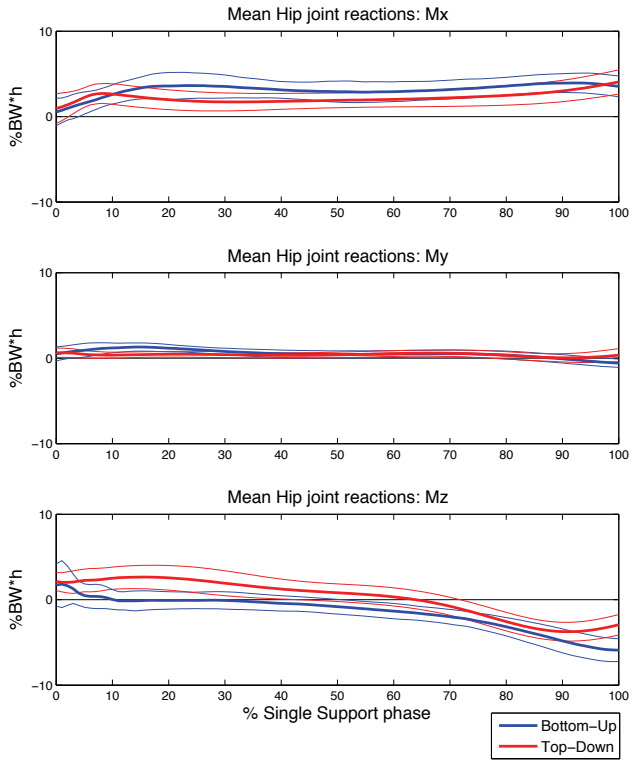

Figure 4.8: Left hip joint reaction moments during *normal gait*, computed with bottom-up and top-down inverse dynamics computations. Results are presented as mean values ± 1 SD, expressed in the pelvis reference system.

force transients happening at the impact of the foot with the ground, discrepancies found may entail wrong definitions of anthropometric properties of the segments and particularly of the head and trunk. Regression equations extrapolated by (Jensen, 1986) considered trunk and pelvis as a unique segment, while our choice was to divide the trunk in three segments (thorax, abdomen and pelvis), with the need to subdivide the whole trunk mass into the different parts. Errors might also depend on improper definitions of the trunk moments of inertia.

A further parameter of evaluation of the model, as suggested in (Robert et al., 2007) could be to compare the estimated COM range of movement on the horizontal plane with the centre of pressure (COP) range of movement, computed from the forceplates. We have not numerically performed this evaluation. From a simple visual inspection of a static standing trial (one video frame is visualized in Fig.4.11 for an adult subject and a child)

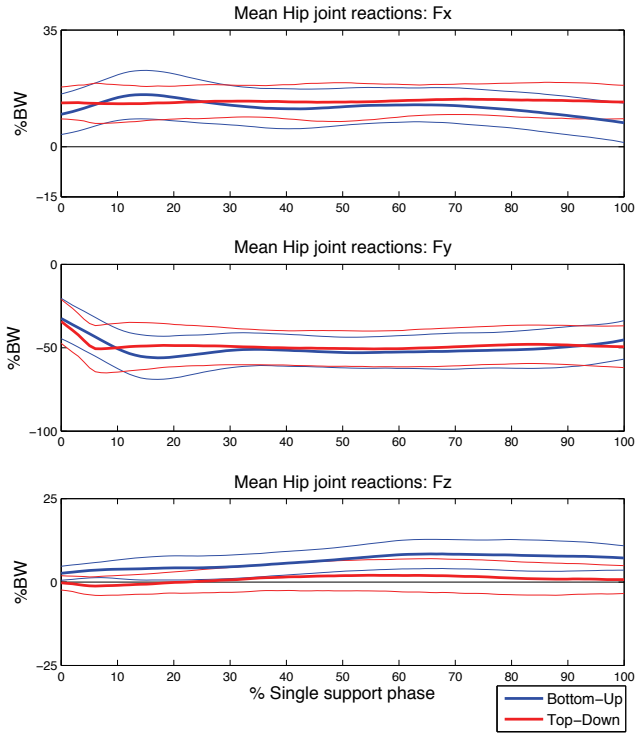

Figure 4.9: Left hip joint reaction forces during *walker gait*, computed with bottom-up and top-down inverse dynamics computations. Results are presented as mean values ± 1 SD, expressed in the pelvis reference system.

it is possible to see that the GRF vector tends to remain slightly posterior to the COM during all the 2 seconds of the trial, expecially for the child: a difference that, although small, might explain the Mz discrepancy towards flexion.

As a further check, the model was applied on data acquired on an adult subject standing with the feet on two separate force plates. The subject performed lateral bendings of the trunk, and flexion, extension and bendings of the head. Forces and moments computed both at the left hip joint and at the L5-S1 joint with *bottom-up* and *top-down* approaches are presented (Fig. 4.13, 4.15, 4.14, 4.16, 4.17).

The different movement phases highlighted in the graphs correspond to:

A-B: left lateral bending (up to 40 deg.) and back

B-C: right lateral bending (up to 40 deg.) and back

C-D: neck and trunk extension and back

D-E: neck forward flexion and back

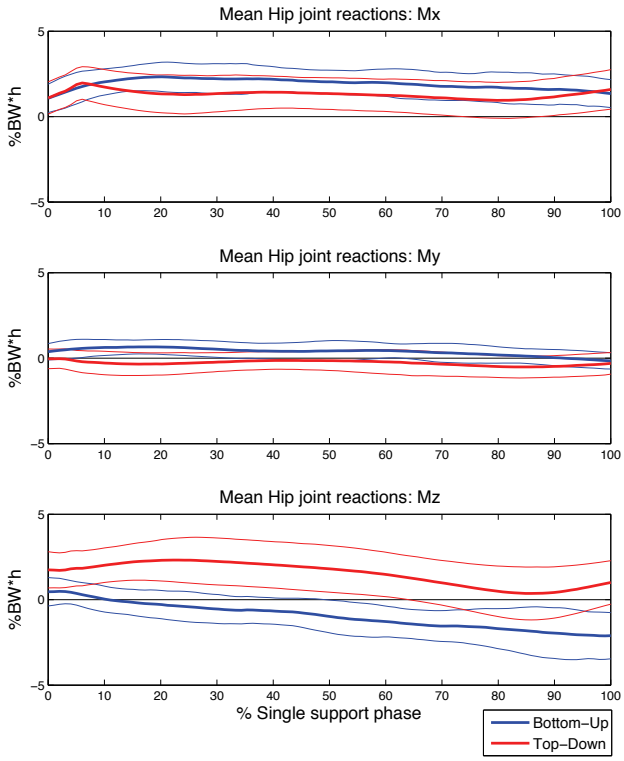

Figure 4.10: Left hip joint reaction moments during *walker gait*, computed with bottom-up and top-down inverse dynamics computations. Results are presented as mean values ± 1 SD, expressed in the pelvis reference system.

E-F: neck left bending (with slight trunk bending) and back
F-G: neck right bending (with slight trunk bending) and back
G-end: neck extension and back.
The position of the subject during the phases A-B and C-D are illustrated in Fig.4.12(a) and 4.12(b).

Force and moment components are expressed in the pelvis reference system, with hip lateral reaction force Fz considered positive when directed laterally, and lumbar loads considered in the right side convention, with positive internal moments towards extension, flexion to the left, anti-clockwise internal rotation.

Some artefacts can be seen in the forces graphs, respectively for the L5-S1 bottom-up approach and for hip top-down approach which depend on flickering of back pelvis markers, that produces alterations in the internal points L5 and HJCs, whose compu-

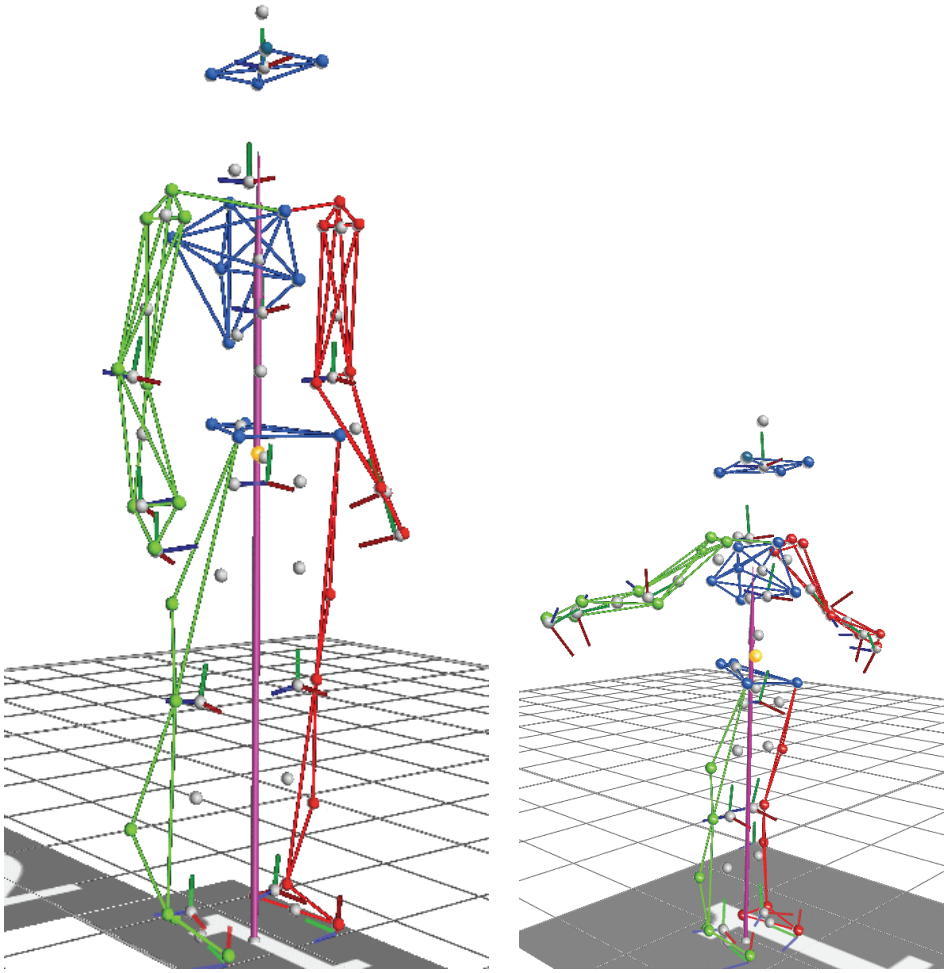

(a) (b)

Figure 4.11: Body centre of mass on adult (a) and child (b) evidenced in orange color. Grey points represent segment origins, joint centers or local segments COMs.

tation is based on those markers. Data were filtered only with Vicon Woltring filtering routine, with Generalized Cross Validation option. A stronger smoothing would reduce the problem.

Comparing the two methods, all the three force components agree very well, for both the left hip and the L5-S1 joints. As for the moments, they show large differences in the forward and lateral flexion-extension components, with differences reduced at smaller angles. Since the zero-crossings are the same for both approaches, this differences might be related with inaccuracy in the estimated body segment inertial parameters of the segments, and not with joint misplacement. The very good correspondence in the forces

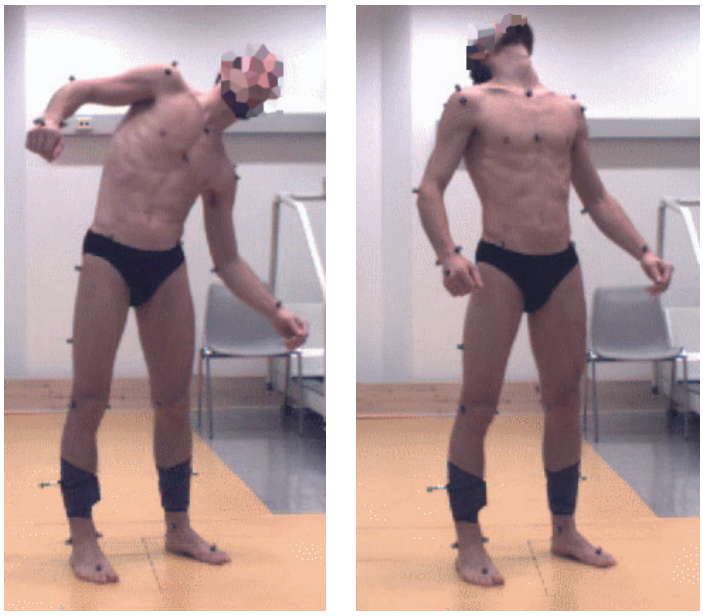

(a) (b)

Figure 4.12: Left trunk bending and head extension movements.

estimation demonstrates that masses distributions between upper body and lower body are correct, but, still, there might be a wrong distribution of masses between the different parts of the trunk.
Possible causes of errors could be:

- hypothesis of rigid body segments not valid for larger movements of trunk and head
- inaccuracy in the magnitude of segments moments of inertia
- inaccuracy in segment COM position in the transverse plane of the segments

Segments moments of inertia are defined as a percentage of the segment length, therefore precise definition of segments extremities have a great influence on the final results. To check this hypothesis, we processed the data with a modified model with the size of the head being half of the original: Results are shown in Fig.4.17, but interpretation is not so immediate. Moments values are actually decreased, but not so much as expected, considering that the moment of inertia of the head has been diminished by a factor of 4.

As pointed out in (Kingma et al., 1996), it is debatable which of the two approaches, *bottom-up* or *top-down* is the most accurate. The authors suggest that the best estimates

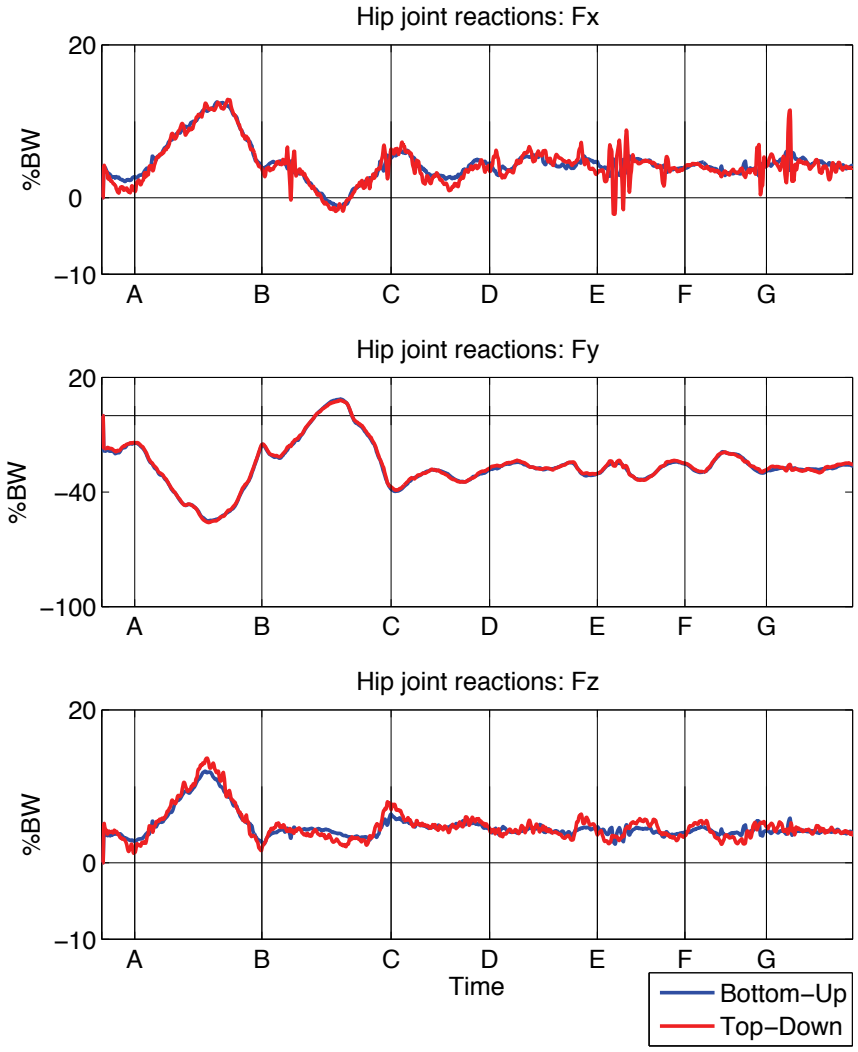

Figure 4.13: Left hip joint reaction forces during movements over two forceplates, expressed in the pelvis reference system.

are given by the *bottom-up* because the trunk is excluded from the computation. The role of the trunk is critical, since it is a segment with large mass and low rigidity. In our model we tried to consider thorax and abdomen as two separate segments, a choice that would allow a more realistic representation of trunk movement in flexion and lateral bendings, but that is also critical for th definition of the correspondent inertial properties, since more separate segments have to be defined and this might increase errors in joint centers and segments lengths estimations.

Our model is based on 41 anatomical markers used to define 16 segments whose inertial

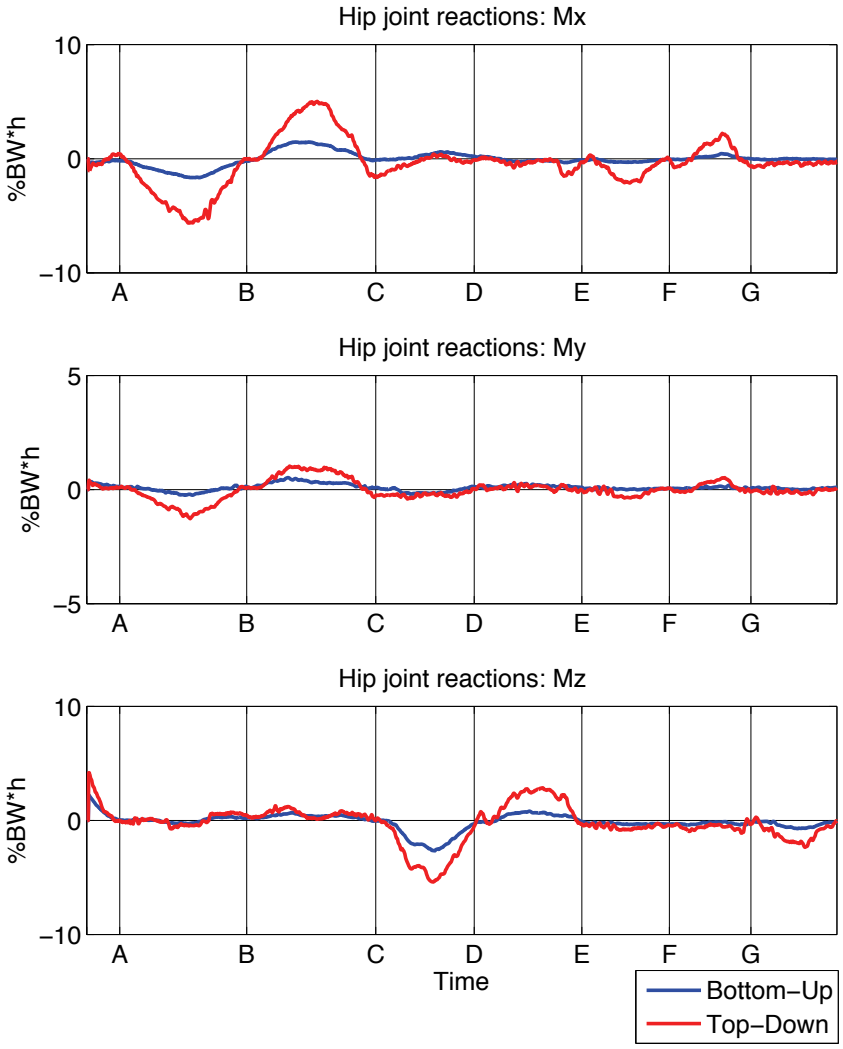

Figure 4.14: Left hip joint reaction moments during movements over two forceplates, expressed in the pelvis reference system.

properties are determined from (De Leva, 1996), while the model in (Kingma et al., 1996) is based on clusters made by 69 markers used to build 14 segments whose properties are defined measuring 75 anthropometric parameters and equations by (McConville et al., 1980). They asked the subjects to raise from a squat position while abducting one arm and holding a 5 Kg barbell on the hand.

The lower detail and precision in the definition of the inertial parameters of our model is probably the reason of the larger errors we found between *top-down* and *bottom-up* approaches, even if for a fair comparison we should have reproduced the same movement

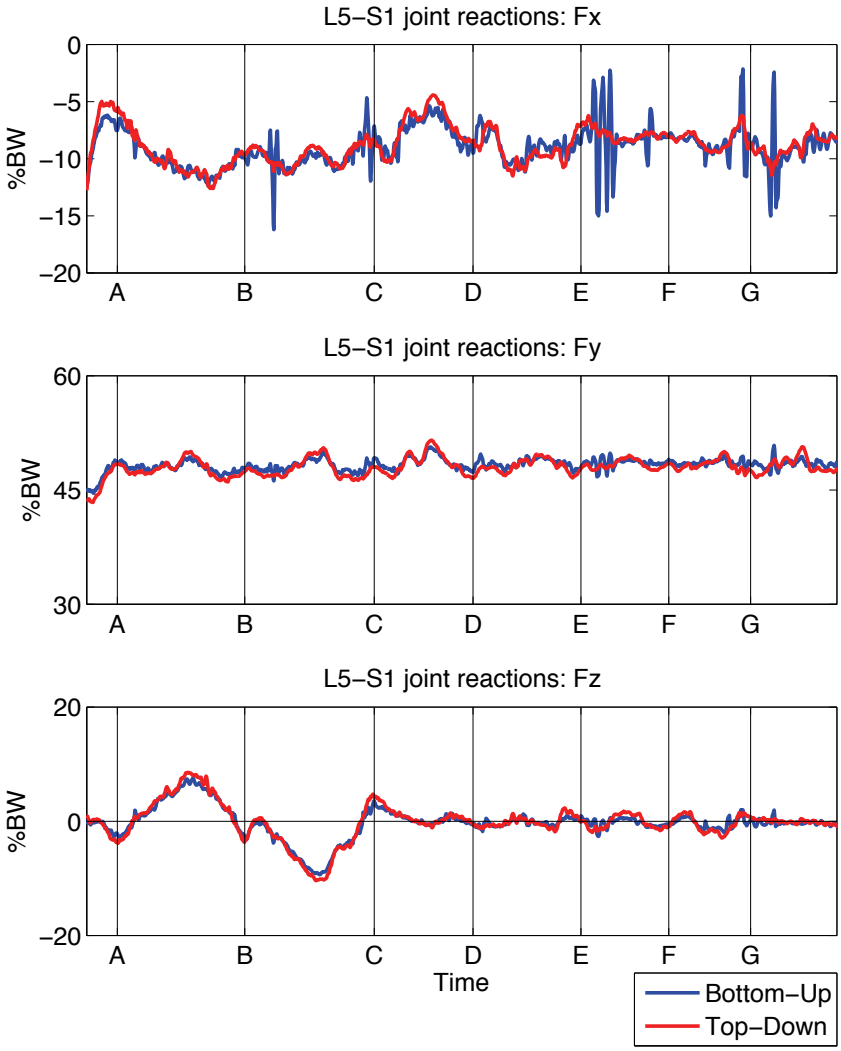

Figure 4.15: Lumbar (L5-S1) joint reaction forces during movements over two forceplates, expressed in the pelvis reference system.

task. Moreover, the moment generated at the waist by holding a 5 Kg barbell on the hand with straight abducted arm might be able to hide smaller discrepancies related to segments definitions.

We chose anthropometric values from (De Leva, 1996) because they provide distinct parameters for the thorax and the abdomen. But for future work an integration of those data with the scaling equations proposed by (Dumas et al., 2007), adjusted from the data of (McConville et al., 1980) would probably improve the precision of the model, as was demonstrated by the same authors in (Robert et al., 2007).

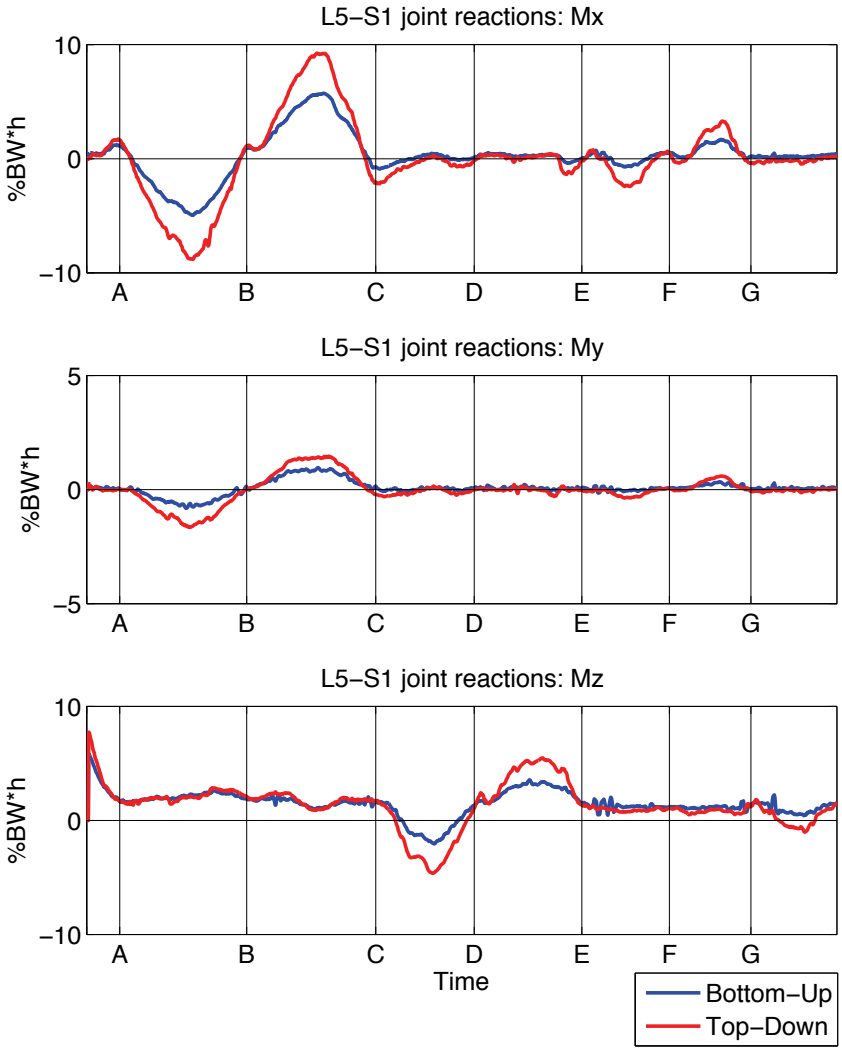

Figure 4.16: Lumbar (L5-S1) joint reaction moments during movements over two forceplates, expressed in the pelvis reference system.

However, the acquisition of 75 anthropometric measures in a clinical environment represents a very demanding task, if the model has to be used for clinical evaluations.

Our model therefore is an attempt to obtain a compromise between simplicity and precision, even though future refinement of inertial parameters is recommended. Being aware of the limitations of the actual model, we think that it can be used for the aims of this work: if the errors mainly depend on incorrect definition of inertia parameters, all muscle mechanical work measures will be similarly affected (Joint powers, Segmental powers, External/Internal powers).

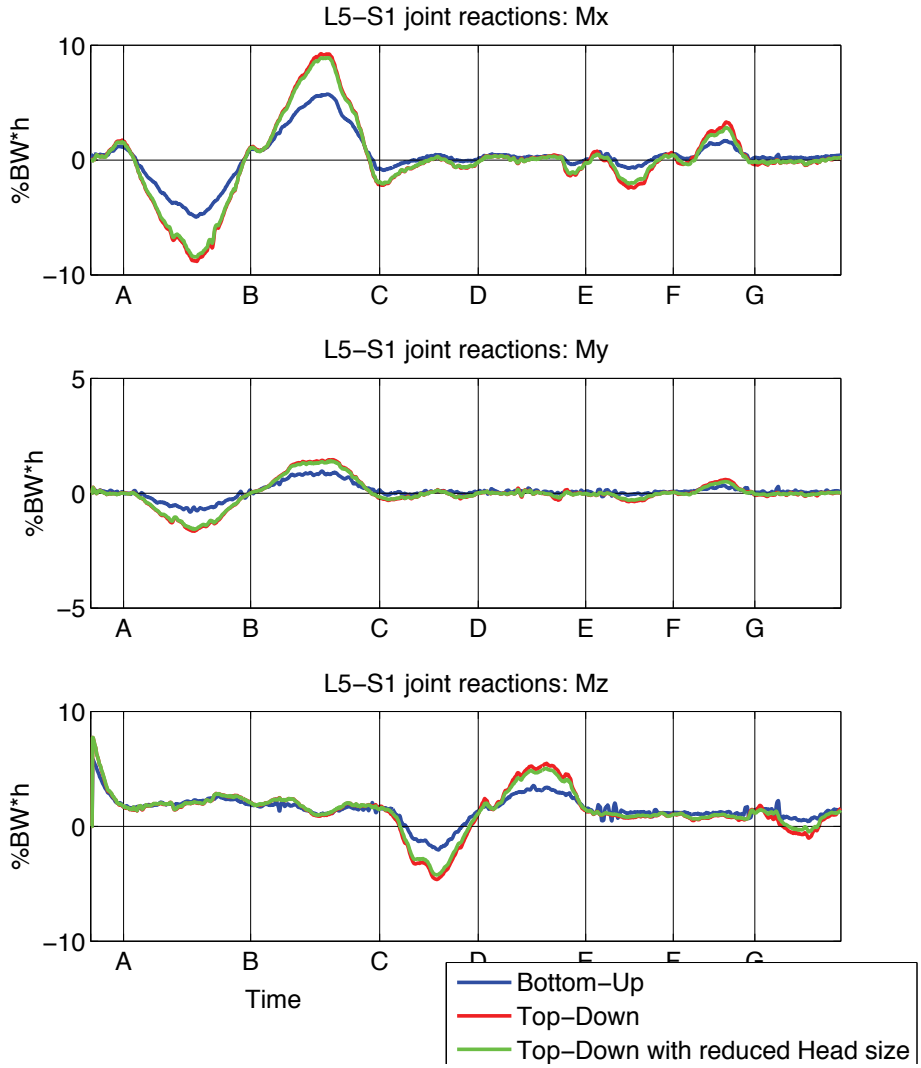

Figure 4.17: Lumbar (L5-S1) joint reaction moments during movements over two forceplates, expressed in the pelvis reference system, as in the previous figures, compared with moments estimated while dividing head segment length by 2.

As final decision, the model was built with separate head, thorax, abdomen and pelvis, with reactions computed with a *bottom-up* approach from GRFs until the hip joints, while upper-body joint reactions down to L5-S1 joint were computed with a *top-down* approach.

During normal gait and walker locomotion, trunk and head movements are likely to be smaller than those produced during this last test, and therefore their overall contribution in terms of joint power is expected to be smaller compared to the lower and, with the walker, to the upper limbs.

4.7 UL model test with walker

To test the upper-limbs part of the model, we collected data from a female healthy young adult (29 years, 158.5 cm, 64.6 Kg).

Ground Reaction Forces (GRFs) were recorded using two adjacent floor-mounted forceplates, while Handle Reaction Forces (HRFs) and Moments (HRMs) were recorded using the two instrumented handles fixed on an anterior walker (Fig. 4.18).

Figure 4.18: Handles fixed on an anterior adult walker frame.

The subject loaded the anterior walker with 50% body weight (BW) when stepping forward. Handles were placed at the 60% of the subject's height and the first step after placing the walker forward was always with the right foot. A right and left gait cycle were selected from one trial, when the subject placed both feet over the same forceplate while unloading the previous one. Walker wheels in this situation were larger than the forceplates, allowing measurement of the GRFs as resultant of the loading of one or both feet.

Kinematic data were filtered (Vicon Woltring filtering routine, *Generalized Cross Validation* option) before and after inverse dynamics computations.

Bilateral UL joint angles, forces, moments and powers at the shoulder, elbow and wrist were computed by the UL model.

4.7.1 Test results

The following figures represent bilateral UL kinematics (joint angles) and kinetics (joint forces, moments and powers) for shoulder, elbow and wrist for the adult subject with anterior walker (Fig.4.19, 4.20, 4.21) during a full right and a full left gait cycles.

The bottom row of all graphs represents the vertical components of HRFs and GRFs. This information is provided for a better interpretation of the kinematic and kinetic results. From these two plots it can be noticed that when stepping forward, the subject was symmetrically loading the two handles with approximately the 50% of body weight, while unloading the feet.

As a subject might use different strategies to load the walker and distribute body weight between the two sides, a time window including contemporaneous visualization of both a full right and a full left gait cycles was assessed. This representation will provide slightly redundant information, due to the repetition of the time interval between ipsilateral and contralateral heel-strikes, but this repetition can be useful to assess data consistency between adjacent gait cycles.

Continuous vertical bars represent right (green) and left (red) heel-strike events, while segmented vertical bars represent toe-off events.
Joint angles and joint reactions follow the conventions described in section 4.5.
Forces were normalized by body weight (%BW), moments by body weight times height (%BW·h), while powers were normalized by body mass (W/Kg).

The redundant information at the beginning and at the end of all graphs shows slight differences between different gait cycles, compatible with the fact that we asked a healthy subject to mimic walking conditions she actually does not experience normally.

Kinematics

All three joints had a large range of movement, due to the high position of the handles as percentage of the body height, and also due to the necessity of moving the walker forward at every step.
The shoulder and the wrist were constantly extended and elbow constantly flexed, with a flexion pattern occurring at all joints while moving the walker forward. Maximum

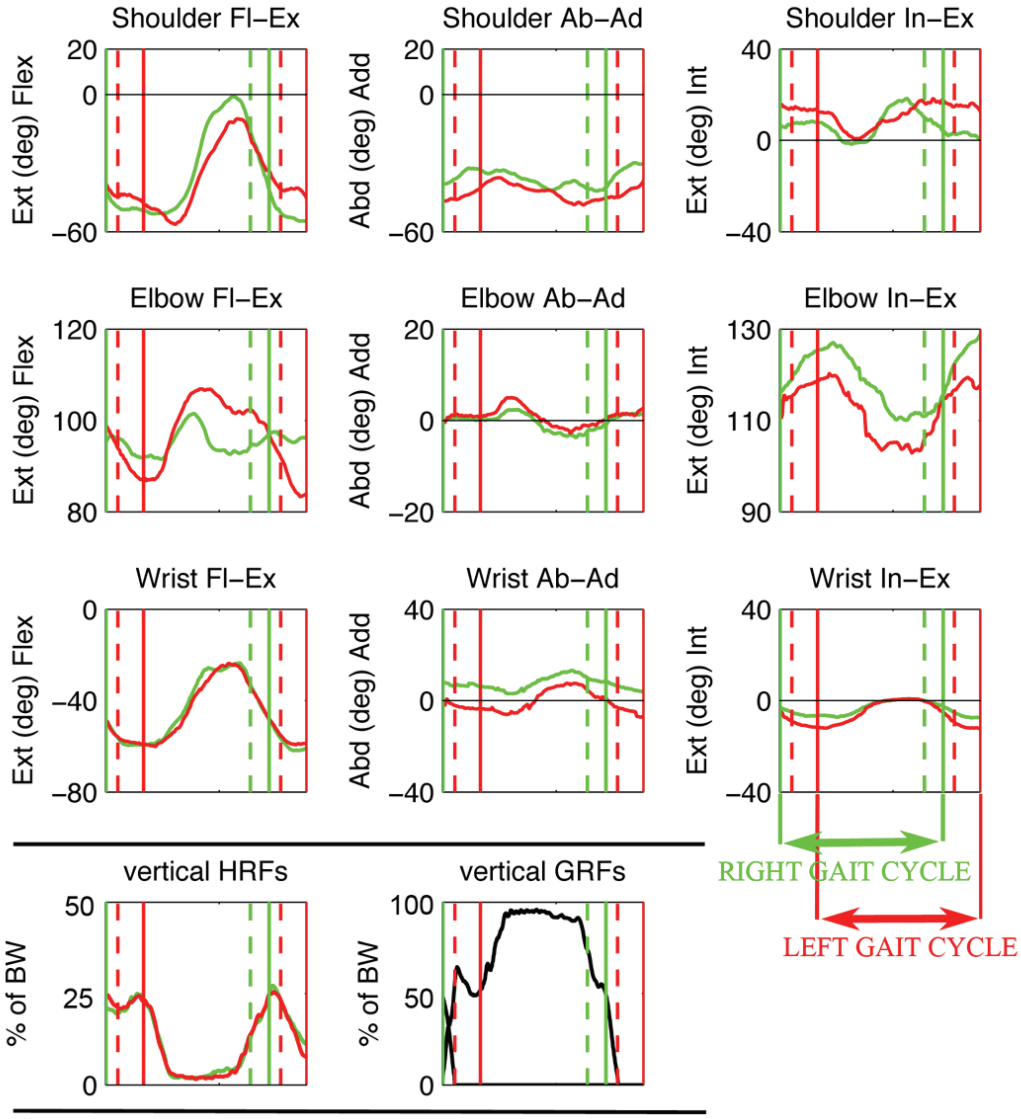

Figure 4.19: Right (green) and left (red) UL joint kinematics.

elbow flexion was obtained on the left side, as the subject prepared for right stepping. Shoulder abduction was observed throughout the whole gait cycle; elbow ab-adduction was measured and the model correctly gave a value close to 0°, with a small variation corresponding to pushing the walker forward; wrist adduction (correspondent to ulnar deviation) increased when moving the walker forward. The shoulders were internally rotated, with a neutral value reached when beginning to move the walker forward. The elbow was pronated more than 90°, with maximum pronation occurring just after stepping with the left foot. A wrist internal-external rotation of about 10° was noted correspondent

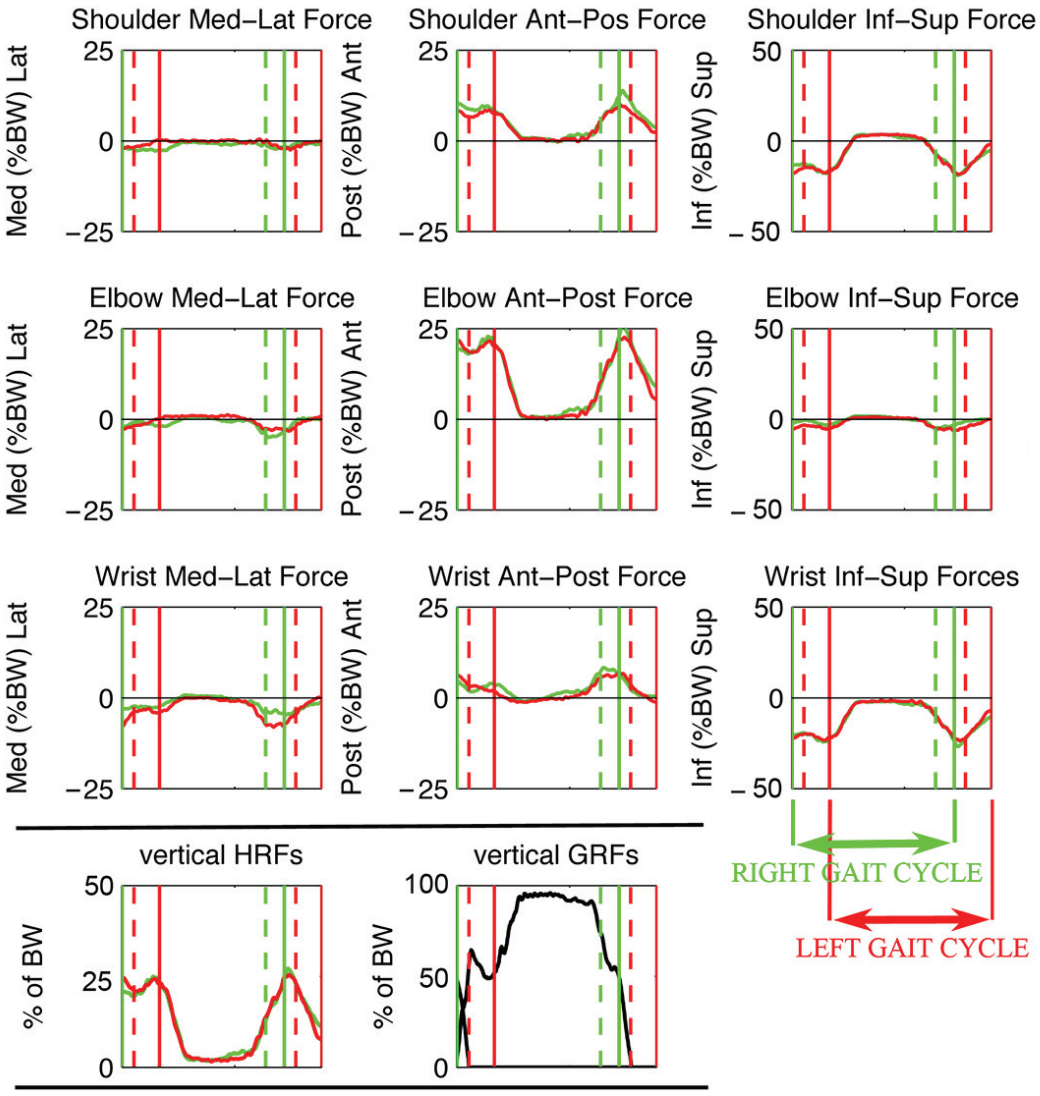

Figure 4.20: Right (green) and left (red) UL internal joint forces.

to maximum wrist extension when loading and stepping into the walker.

Kinetics-Forces

Walker loading by the subject was very symmetrical, as shown by the vertical components of the HRFs. For shoulder and elbow, the main joint loads occurred in the sagittal plane when stepping forward. For the wrist, due to its particular orientation, reactions distributed along all three directions.

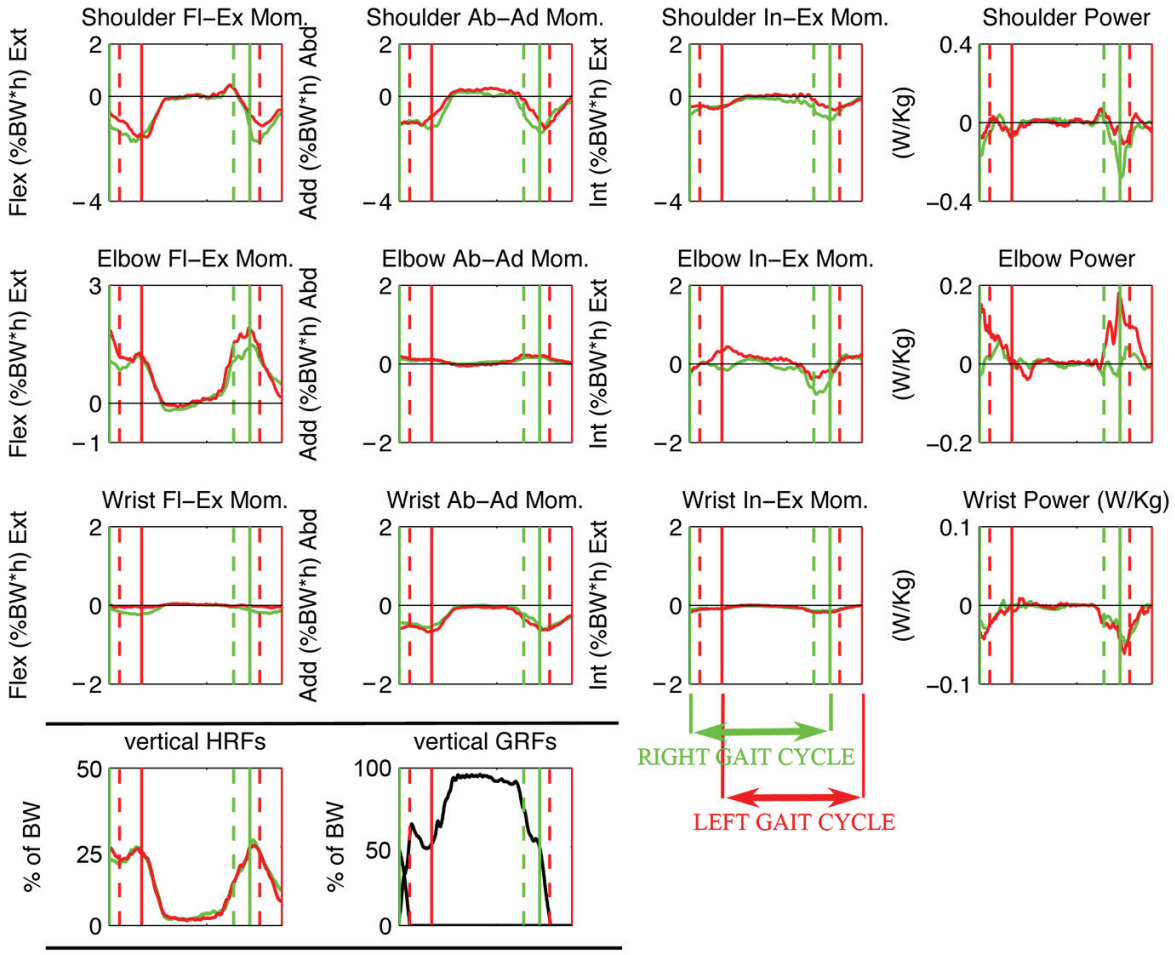

Figure 4.21: Right (green) and left (red) UL internal joint moments and powers.

Kinetics-Moments

Internal moment generation was mainly required from shoulder flexors and adductors, elbow extensors, with the highest demand recorded in the sagittal plane for the right shoulder and left elbow, approximately 2% BW·h, equivalent to 20 Nm. Minor demands were noticed at the shoulder internal rotators, elbow pronators/supinators and wrist ulnar deviators.

Kinetics-Powers

With anterior walker, power was mainly absorbed (shoulder and wrist) and produced (elbow) bilaterally during stepping movement.

4.7.2 Discussion of test results

The protocol is feasible to be used to study upper-limb kinematics and kinetics during walker-assisted gait. Joint angles, forces, moments and powers can be computed. Considering the differences in walking conditions (walker model, weight bearing, handle height and orientation), model conventions and data normalizations, a comparison with findings in (Bachschmidt et al., 2001) is not fully applicable. However, common kinematic and kinetic patterns are evident across all joints. As a global finding, the highest net joint moment was noted in the sagittal plane at the elbow for this subject and this walker model.

Chapter 5

Results

A 16 segments full body three-dimensional model has been used to study normal gait and walker locomotion in healthy children and then applied to children with cerebral palsy. The model provided kinematics of body segments, segments centres of mass and whole body centre of mass (BCOM, or COM), joint kinetics in terms of intersegmental forces, joint moments and joint powers.
Data were then used to estimate whole-body muscle mechanical work during locomotion with the different approaches (or methods) described in chapters 1 and 2.

Details on the subjects involved in the study, on data collection protocols and on data processing were described in chapter 2.

This chapter describes the results obtained. Further details on numerical results and statistical analysis are presented in the appendix. A preliminary discussion of some intermediate results is also presented in this chapter, for a better understanding of results description, while the critical analysis of the overall results is left to the final Discussion (chapter 6).

In order to compare muscle work values for subjects with large differences in body size, work was normalized by bodymass and the ratio between stride length and subject's height (see section 2.6.3). Work results are therefore expressed in J*m/Kg*m and power results in W/Kg.

5.1 Analysis of joints and segments powers

As described in chapter 1, muscle actuators produce net moments around a joint, causing movement and mechanical energy change of the segments.

In the following figures, joint powers ($P_i = \int \mathbf{M}_i \cdot \boldsymbol{\omega}_i \, dt$) and rates of change of segment's mechanical energy ($P_i = \frac{dE_i}{dt}$) are shown as an example for a single gait cycle during normal gait (Figure 5.1) and during walker locomotion (Figure 5.2) of a healthy child.

During normal gait the predominant power production and absorption happens at the lower limb joints (Fig. 5.1(a)). Action of upper limb muscles is minimal, since the arm is normally kept straight, acting as a pendulum. At the trunk, we can notice a synchronized action at the neck and lumbarsacral (L5-S1) joints, while the curve behaviour at the thoracolumbar (T12-L1) joint is out of phase with respect to the previous two.

Fig. 5.1(b) shows the variation of mechanical energy of the body segments. Again, the major changes involve the lower limb segments, and the curves allow to investigate the cause-effect relationship between muscle action at the joints and movement of the body segments. For example, positive ankle power production at push-off contributes to increase leg and thigh mechanical energy. Further increase in energy of these segments, together with increase in energy of the foot, are obtained during the initial swing phase by the positive action of the hip flexors, while the power pattern is reversed in terminal swing, when there is negative power measured at the hip and knee. It is interesting to notice that during the positive joint power production phase at the ankle, there is a decrease in the energy of the trunk segments.

The analysis becomes more complicated when considering walker locomotion. As expected, amplitude of power components of the lower limbs decrease with respect to normal gait, while amplitude of power contributions from upper limb joints and trunk joints increase. There is less synchronization of hip, knee and ankle action, because the supporting function is now divided among upper and lower limbs. Considering segment powers, during this selected trial we can notice large, and not symmetric during right and left steps, energy variations of the head (a segment which has a considerable relative weight for a 6 years old boy).

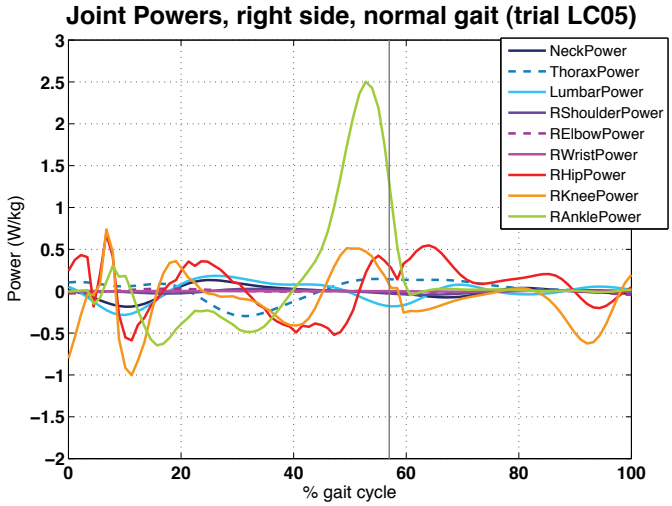

(a)

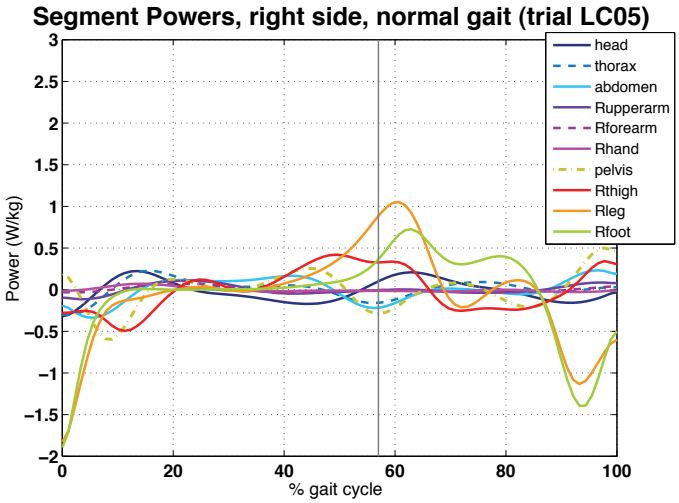

(b)

Figure 5.1: (a) Joint power curves and (b) rate of change of segments energy (segment power curves), during a right gait cycle for all body joints/segments during normal walking (for simplicity, powers from left side limbs are not shown). Curves are computed from a single trial of LC subject, walking at the normalized speed of 0.357. The vertical gray line represents the toe-off event.

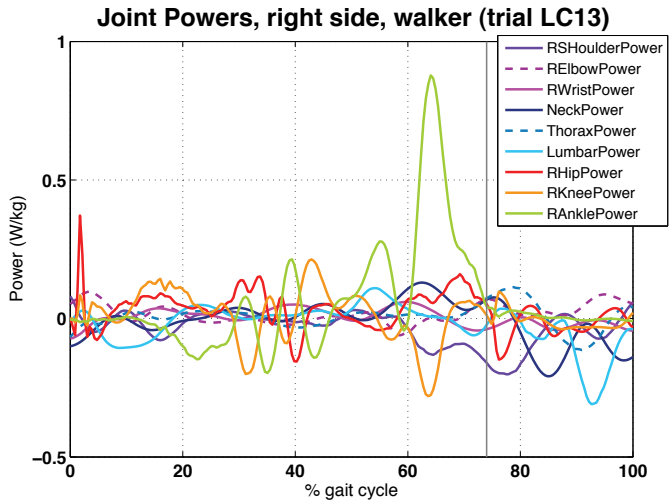

(a)

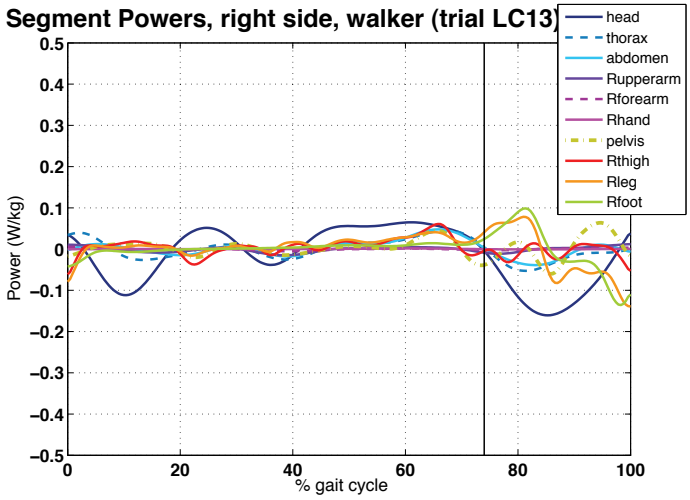

(b)

Figure 5.2: (a) Joint power curves and (b) segment power curves during a right gait cycle for all body joints/segments during walker locomotion (for simplicity, powers from left side limbs are not shown). Curves are computed from a single trial of LC subject, walking at the normalized speed of 0.092. The vertical gray line represents the foot-off event.

Mean values among all healthy subjects' trials are shown in Fig. 5.3, for normal gait, and in Fig. 5.4 for walker locomotion.

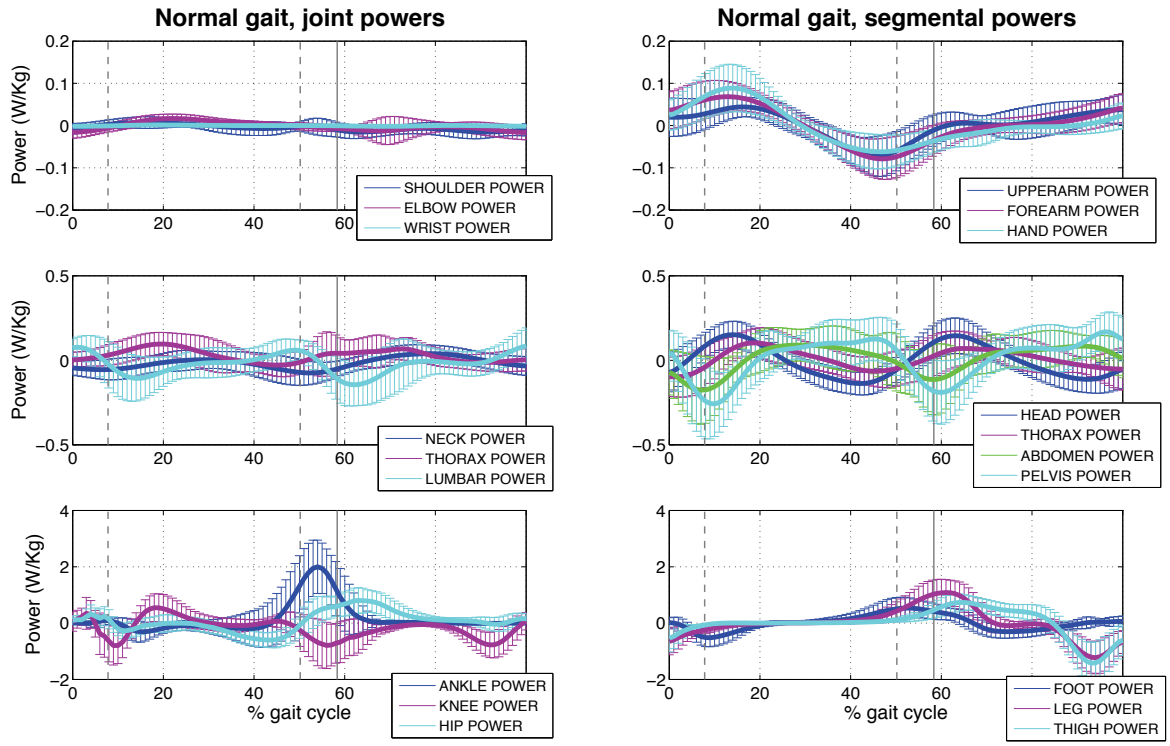

Figure 5.3: Powers curves for the right upper limb, trunk, right lower limb computed as joint powers and segmental powers during normal gait. Plots represent the mean ± 1 SD values among all healthy subjects trials for a right gait cycle. The continuous vertical line represents the mean ipsilateral (right) foot-off event, while dashed lines represent the mean contralateral (left) foot-off and foot-strike events.

During normal gait timing and amplitude of the lower limb joints power peaks during normal gait at non-dimensional self selected walking speed are consistent with previous publications on healthy children's gait (Schwartz et al., 2008).

Despite lower joint power production at the upper limb, there is a large variation of mechanical energy of the related segments, due to a pendulum-like movement of the limbs with respect to the trunk.

At the trunk level, power production/absorption appears to happen mainly at the lumbosacral joint, out of phase with respect to the behaviour of the thoracolumbar and neck joints. This action is reflected in the segments power curves, with energy variations of abdomen and pelvis out of phase with the variations of head and thorax, with the

overall result of mantaining almost constant both the mechanical energy of the whole trunk plus head (HAT) and, possibily, the whole body angular momentum. The result is consistent with previous observations about trunk movement strategies during walking (Cappozzo et al., 1976; Perry, 2005).

The large energy variations observed at the level of the trunk depend not only on the action of trunk joints, but also on the propulsive action of the lower limbs joints, especially the ankle at the end of the support phase.

During walker locomotion upper limbs are used for support, with joint power production and absorption at the elbow during the ipsilateral foot-off and leg swing phases, and almost no power fluctuations evident for the segmental powers plots during the whole gait cycle. With respect to normal gait (note the difference in graph scales between figures 5.3 and

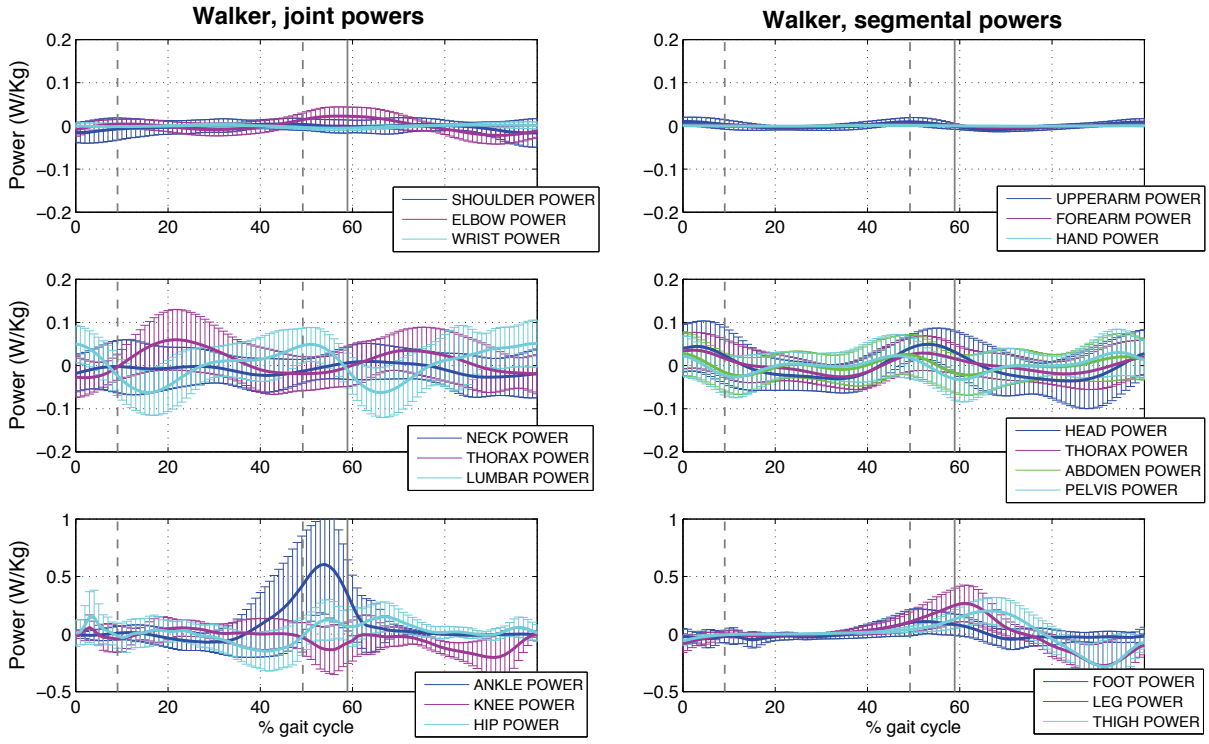

Figure 5.4: Power curves for the right upper limb, trunk, right lower limb computed as joint powers and segmental powers during walker locomotion. Plots represent mean ± 1 SD values among all healthy subjects trials for a right gait cycle. The continuous vertical line represents the mean ipsilateral (right) foot-off event, while dashed lines represent the mean contralateral (left) foot-off and foot-strike events. For a better visualization, scales are reduced with respect to Fig. 5.3.

5.4), trunk and pelvis energy variations show here a more *in-phase* pattern, with reduced amplitude of joint and segmental power curves of the trunk. At the lower limbs, knee joint power production/absorption during the single support phase is strongly reduced and the overall amplitude of the curves is also reduced, while keeping a similar pattern during the terminal stance, push-off and swing phases.

5.2 Whole-body power during normal gait

Figures 5.5 and 5.6 represent the whole-body power curves computed, for a gait cycle extracted from a single trial of subject GZ, following the definitions described in section 2.6.

Positive and negative power components obtained from separate summation, across all segments or all joints, of all positive or negative values of External power, Internal powers, Joint powers and Segmental powers at the different time instants of a normal gait cycle are shown in Fig. 5.5(a). External power, being a value relative to one point only, has a single value (positive or negative) at every time instant. This description, coming from separate computation of all positive and negative simultaneous power contributions, allows to evidence, at the whole-body level, the phases where either energy generation or absorption is predominant and the possibilities for possible energy transfers (with energy corresponding to fractions of the area under the power curve).

In the example considered, two main phases of energy generation and two main phases of energy absorption appear during the gait cycle.

This behaviour is common to all the different methods, even if a slightly different timing is evident. Energy generation is associated with the push-off and early swing phases, while energy absorption is associated mainly with terminal stance phases.

During energy generation phases the power values computed with the Joint method reach the highest values, around 5 W/Kg, occurring exactly at the foot-off instant. A contemporaneous small peak of power absorption is also evident.

A smoother power curve is instead provided by the Segmental method, with a maximum positive peak that is slightly delayed from its equivalent Joint power peak, a possible

indication that energy generated at the level of the ankle has been transferred to more proximal segments, incrementing their mechanical energy.

External power curve and Internal power curves are in-phase, and their peaks follow the same timing as the Segmental method.

Little differences between the two steps which compose a full gait stride are observable, an index of a slightly asymmetric walking for this subject.

A point-by-point summation of the positive and negative components described above, with their sign, gives the *net* power curves for the different methods (external and internal power values are summed together, thus allowing for all possible energy transfers between segments).

Not surprisingly, Segmental and External/Internal power curves are perfectly superposed, thus revealing their equivalence when all possibile energy transfers between segments are allowed. These last two approaches slightly differ from the Joint power approach mainly in the distribution of the positive peaks area, while the negative parts of the curves look very similar.

Average *net* power curves from all healthy subjects trials during gait are shown in Fig. 5.6. Standard deviation (SD) is almost uniform along all the gait cycle for the Segmental power and the External/Internal power curves, while it is larger for the Joint power curve during the double support phases and immediately after, a possible effect of larger variability in the ground reaction forces data during the foot-off and foot-strike events.

Observations from Fig. 5.5 which regarded a single trial only are still valid here with, additionally, improved symmetry between the two steps. Scales are slightly different between the previous and present figures.

Around the foot-off events the curves display the larger differences among the methods: the Joint power positive maximum occurring during the double support phase is followed by a negative local minimum, possibly correlated with the weight acceptance phase by the support limb, while Segmental and External/Internal powers are equal to zero at the beginning of the double support phase, and then reach their maximum during ipsilateral

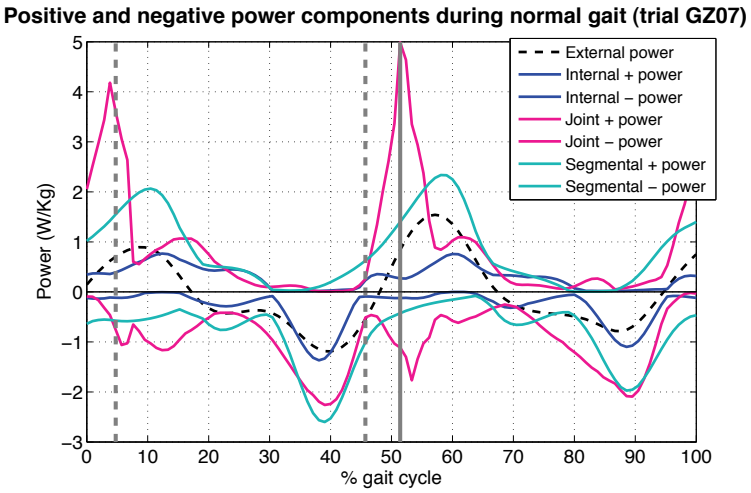

(a)

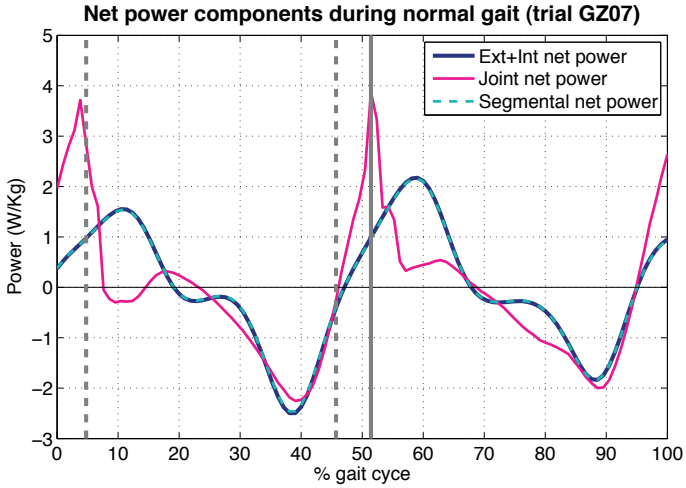

(b)

Figure 5.5: (a) Positive and negative power components of external power, internal powers, joint powers and segmental powers during one gait cycle. Vertical grey dashed lines represent, from left to right, contralateral foot-off, contralateral foot-strike, ipsilateral foot-off (data from trial GZ07). (b) *Net* power curves for external+internal powers, joint powers, segmental powers during one gait cycle, after summation of the components in (a).

early swing phase (when lower limb segments are being accelerated) and their minimum at the end of the swing phase (when lower limb segments are being decelerated). The behaviour of the different curves highlights the different information that the two methods can provide: the Joint power curve represents the *cause*, the kinetic propulsive and braking

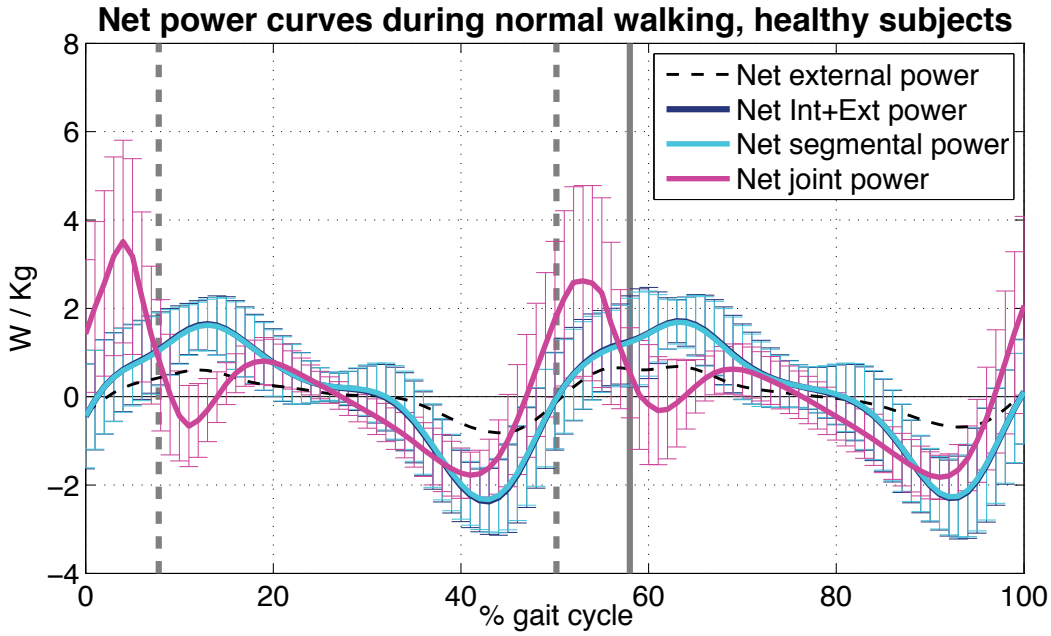

Figure 5.6: Relationship between net power curves during a complete gait cycle computed with the three different methods during trials at self-selected walking speed, for healthy subjects, plotted as mean values ± 1 SD. The curve representing *external* power was also added to the plot as mean value only. Vertical lines represent ipsilateral foot-off (continuous line) contralateral foot-off and foot-strike (dashed lines).

action, while the Segmental power curve information comes from the kinematic *effect* of those forces on the body segments. If the dissipation of mechanical energy produced by the joint actuators is minimal, we would expect that, despite the local differences in net power curve paths, their integration will give the same results in terms of muscle mechanical work.

External power curve has been added to the graph, to show how much the energy variations of the centre of mass can be descriptive of the overall negative and positive energy variations phases of the whole body segments. Amplitude differences from the Segmental power curve depend on the additional *internal* work done by the body segments with respect to the centre of mass. Despite amplitude differences, however, the power curve associated to the centre of mass confirms the ability to condense on one point the movement of the whole body and its possibile asymmetries.

From the *net* power plots above we verified the equivalence between the net Segmental power curve and the net External/Internal power curve. However, if we do not consider

net power values, as in figure 5.5(a) and especially during the double support phases, we can easily notice that the summation of the positive (or negative) External and Internal power values does not reach the correspondent value of the Segmental power curve. As described in chapter 1 and in section 2.6, in this case the use of the centre of mass as a global representation of the body power does lead to reciprocal cancellation of power terms not measurable any more even as Internal power.

The results of the computation of the simultaneous external power performed by the individual lower limbs on the COM during the step-to-step transition is shown in figure 5.7. Results are very similar to those obtained by (Donelan et al., 2002) on adult subjects and confirm that a considerable amount of positive and negative power is reciprocally cancelled out when external power on the COM is computed instead with the original *combined limbs approach*.

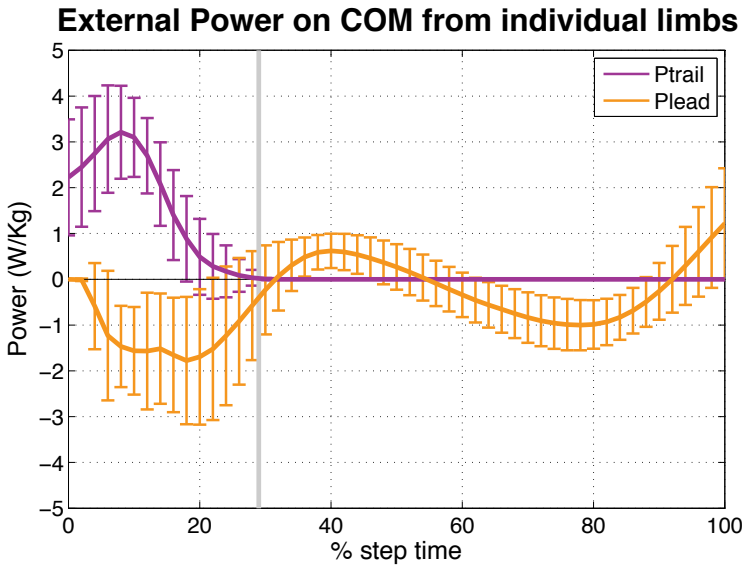

Figure 5.7: External mechanical power on the COM done separately by the trailing and leading lower limbs during a step. Curves are obtained from all the collected trials and represent mean ± 1 SD values. The vertical line represents the transition between double support and single support phases.

5.3 Muscle mechanical work during normal gait

Once joints power, segments power, COM power plus segments power relative to the COM have been computed at the different time instants, it is possible to estimate muscle mechanical work by integrating the different power components along the gait cycle.
It could be interesting to analize how the whole-body muscle mechanical work production is shared between the upper body and the lower body, and therefore split the total work value in two components, computed with both the Joint and the Segmental powers approaches (this kind of analysis cannot be applied to the External/Internal approach). The values computed with the two approaches will likely not be equal, since the joint chosen to divide the body in two parts (the lumbosacral joint) is shared between two segments, pelvis and middle trunk (abdomen), which will be assigned respectively to the upper and the lower body, with these resulting subdivisions:
Upper body joints: Wrists, elbows, shoulders, neck, thoracolumbar, lumbosacral.
Lower body joints: Ankles, knees, hips.
Upper body segments: Hands, forearms, upperarms, head, thorax, abdomen.
Lower body segments: Feet, legs, thighs, pelvis.

Bar plots in Fig. 5.8 show the fractions of whole-body positive and negative work performed by the upper and lower body joints or segments, under the condition of no energy transfers between segments.

The predominant action is done by the lower body. At the upper body, the Joint power approach gives lower values with respect to the Segmental approach for both positive and negative work, as expected from the observation of the upper limb power curves in Fig. 5.3.

At the lower body, both methods provide positive and negative work magnitude approximately equal to 1.2 J*m/Kg*m, with a higher value of 1.3 for the joint positive work, that is surprisingly not symmetrical with its negative conterpart.

Fig. 5.9 illustrates the total work results obtained by computing the different measures of muscle mechanical work (*Wtot+*, *Wtot-*, $|Wtot|$, *Wnet*, *Wabsnet*) with the three different methods plus, for some of the measures, the External/Internal work with external work

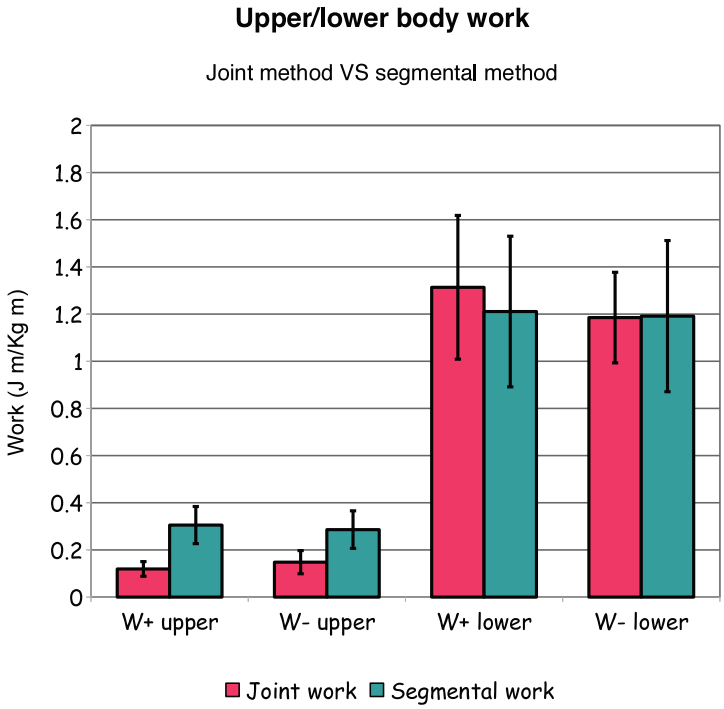

Figure 5.8: Positive and negative components of muscle mechanical work done by the upper and lower body, computed with the Joint and Segmental powers methods, during walker locomotion. Results are presented as mean values ± 1 SD.

computed by using the *individual limbs* approach. Mean normalized walking speed was 0.335 ± 0.047. Data relative to all single trials are presented in appendix, figures A.1 and A.2.

To give a graphical idea of the mathematical operations performed, the first four work measures were computed from separate integration, for all trials, of positive and negative power curves like those in Fig. 5.5(a), while *Wabsnet* was obtained from the integration of the absolute value of the curves like those in Fig. 5.5(b).

The results show that, during walking, the three methods are equivalent ($F(2,18) = 0.165, p = 0.849, \eta^2 = 0.018$) when all possible energy transfers between segments are allowed (*Wabsnet*). With no transfers (*Wtot+*, but also *Wtot-* and their absolute values summation, $|Wtot|$), Joint and Segmental methods give equivalent results, both differing significantly ($p < 0.01$) from work values computed via the External/Internal method.

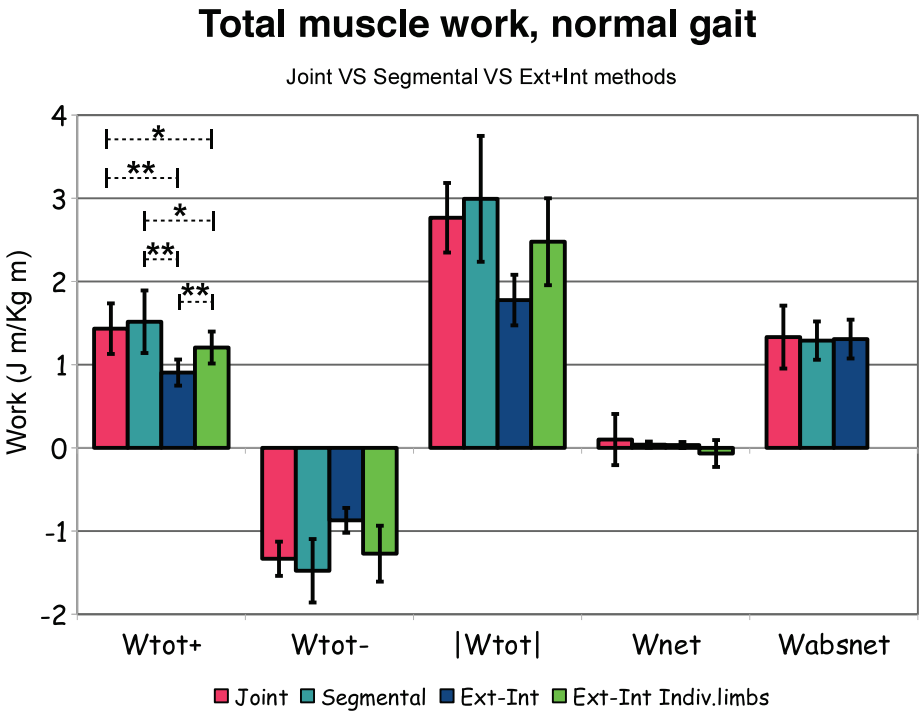

Figure 5.9: Whole-body *positive*, *negative*, *absolute*, *net* and *absnet* muscle mechanical work for healthy children, computed with all the three approaches during normal gait. External/Internal *positive*, *negative*, *absolute* and *net* work values were also computed with the *individual limbs* method. Results are presented as means values $\pm$ 1 SD. $*p < 0.05$, $**$ $p < 0.01$. Further plots and statistical analysis results for *Wtot+* and *Wabsnet* comparisons are shown in appendix.

The difference is reduced, but still significant ($p < 0.05$), if the external work fraction is computed with the individual limbs method, which means that even computing external work with the individual limbs method, there are still other reciprocal cancellations of positive and negative work fractions happening at the level of the trunk and upper limbs. More details on the statistical analysis results are shown in appendix.

Wnet is almost zero, as expected from walking at constant speed. However, net Joint work is slightly positive, and net External/Internal work computed with the individual limbs method is slightly negative. This findings will be further discussed in chapter 6.

Standard deviations are different for the different methods. This is not surprising since data, although collected from the same trials, are processed by using different information and algorithms (Segmental work is based only on kinematics and inertial parameters, while

Joint work makes additional use of force plate data).

By comparing the $|Wtot|$ and $Wabsnet$ values we can have an idea of how large is the amount of work that can be associated to energy transfer processes. Despite authors assertions in (Willems et al., 1995) about the equivalence of the different methods, the traditional External/Internal method, based on the centre of mass as a global point representing the whole body, gives a total body work measure which is mathematically already affected by a certain degree of energy transfers not measurable any more!
Indeed, for the External/Internal work method the difference between $|Wtot|$ and $Wabsnet$ is about 0.5 J*m/Kg*m, while for the Segmental method the difference is about 1.7 J*m/Kg*m, more than its correspondent value of $Wabsnet$.

5.4 Muscle power and work during simulated walker-assisted gait

Similarly to what has been done in the previous section, we can apply the same reasonings to walker locomotion. We have to be aware, however, that results obtained here come from a simulated condition, with healthy children asked to use the walker in order to walk while trying to unload their lower limbs.

Mean loading on both handles, computed on the processed trials, was 29 $\pm$ 10 % of subject's body weight. Mean normalized walking speed was 0.164 $\pm$ 0.045. Data relative to all single trials are presented in appendix, figures A.3 and A.4.

By comparing Fig. 5.10 with Fig. 5.6 (taking into account the different scales of the graphs), we can get useful information on the energetic strategies used during the two different movements: Level walking and walker-assisted gait. In the latter case, amplitude of the power curves is reduced. Of course, also walking speed was reduced with the walker. The shape of the curves related to the different methods looks now more similar, with almost complete reduction of the negative peak of the Joint power curve after foot-off, because weight acceptance is now shared among the contralateral leg and the two upper limbs.

During each step two phases of power production and power absorption are evident,

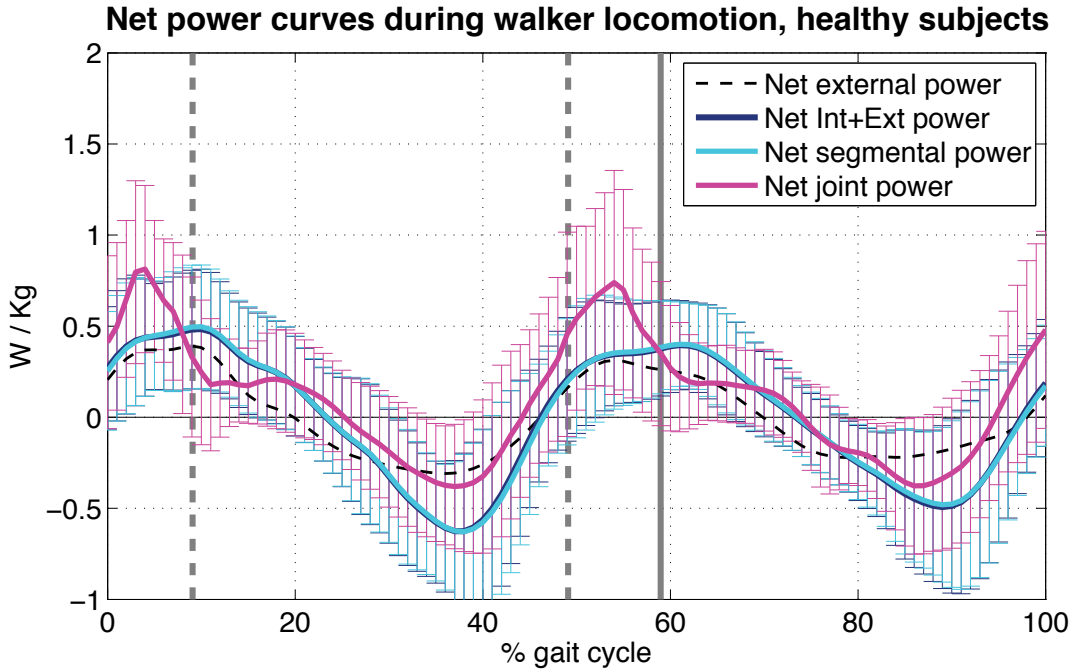

Figure 5.10: Relationship between *net* power curves during a complete gait cycle computed with the three different methods during walker trials, for healthy subjects. *External* power was also added to the plot as mean value only. Results are presented as mean values ± 1 SD. Continuous vertical line represents the ipsilateral foot-off event, dashed lines represent contralateral foot-off and foot-strike events.

with maximum positive power associated to the push-off phase for all methods, even if the curves have different slopes. The two steps look not completely identical, particularly for the Segmental (and its equivalent External/Internal) power curve which shows higher positive power maximum and lower negative power minimum during the first step.

The Joint power curve appears globally unbalanced towards positive values, an observation confirmed by work values computed.

The External power curve, associated to the centre of mass, again highlights the ability to describe the timing of the positive/negative phases of whole-body muscle mechanical work production and absorption.

The estimation of positive and negative muscle mechanical work performed separately by the lower body and the upper body during walker locomotion, shown in Fig. 5.11, gives a comprehensive view of the overall muscle action on joints and segments, under the condition of no energy transfers between segments.

With respect to normal gait, upper body Joint work is increased, while Segmental

work is reduced, because there is not pendular motion of the upper limbs any more, and also the amplitude of trunk power fluctuations is reduced, as evidenced by figures 5.3 and 5.4.

Lower body work is reduced and is about a half of that produced during normal gait for both methods, with a distinction for the positive Joint work component, which remains significatively higher than its negative counterpart.

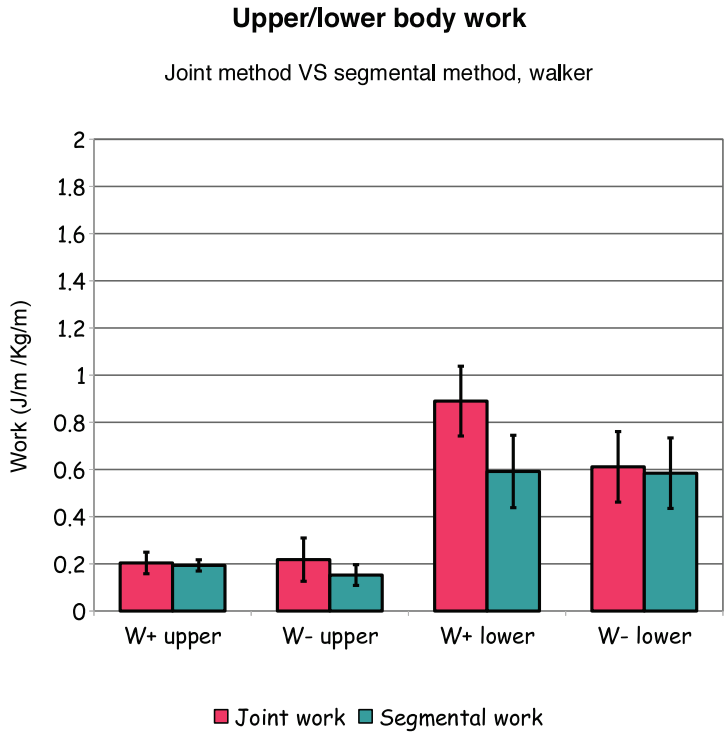

Figure 5.11: Positive and negative components of muscle mechanical work done by the upper and lower body, computed with the Joint and Segmental powers methods, during walker locomotion. Results are presented as mean values ± 1 SD.

Whole body total work obtained by computing the different measures of muscle mechanical work ($Wtot+$, $Wtot$-, $|Wtot|$, $Wnet$, $Wabsnet$) during walker locomotion with the three different methods are shown in figure 5.12.

Results confirm the equivalence of all approaches when muscle mechanical work is computed as $Wabsnet$ ($F(2,18) = 0.068, p = 0.935, \eta^2 = 0.007$). Differently from normal gait, positive work ($Wtot+$) results are significantly different ($p < 0.01$) among all the methods. This confirms that, depending on the movement being investigated, the pre-

vention of energy transfers between segments might lead to possible differences in work values also between the Joint and the Segmental methods.

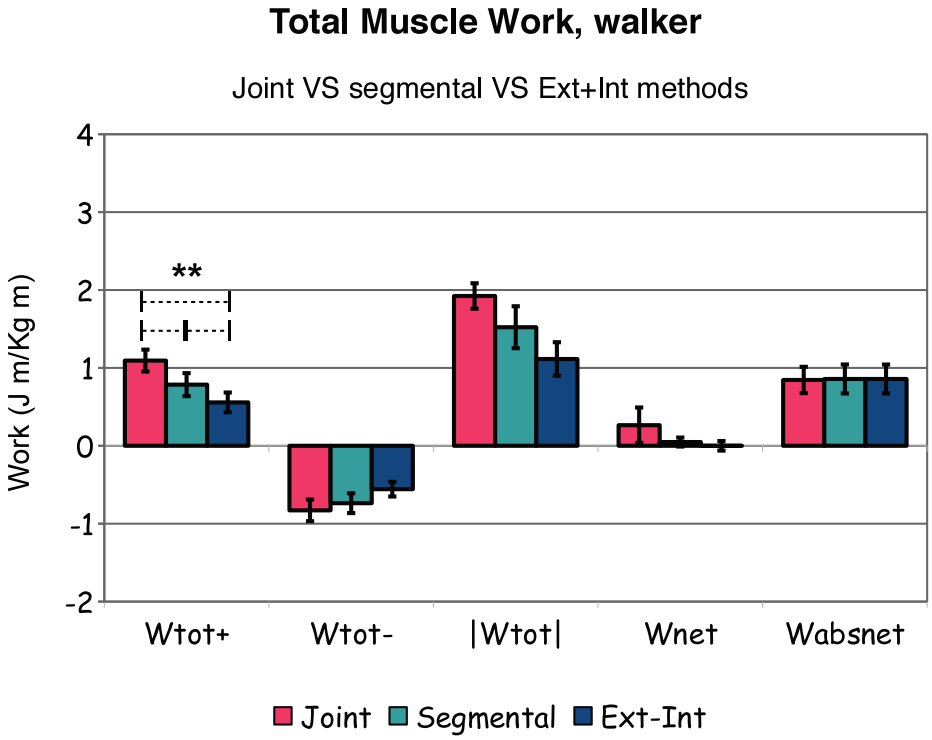

Figure 5.12: Whole-body *positive*, *negative*, *absolute*, *net* and *absnet* muscle mechanical work for healthy children, computed with all the three approaches during walker locomotion. Results are presented as means values $\pm$ 1 SD. ($**$ $p < 0.01$, for reciprocal comparisons among all approaches).

5.5 Muscle work during impaired gait

The full-body model tested and validated on the group of healthy children was applied to a small group of cerebral palsy children to estimate muscle mechanical work during impaired gait.

The different work values ($Wtot+$, $Wtot-$, $|Wtot|$, $Wnet$, $Wabsnet$) were computed with the Joint, Segmental and External/Internal powers methods depending on the available information provided by data acquired. Subjects were evaluated while walking in their ordinary condition in terms of walking aids and orthosis, and it was not possible to collect both kinematics and kinetics data on all the subjects and on all the trials. Details on single trials data are described in appendix, figures A.6 and A.7.

Net power curves during the gait cycle are described in Fig. 5.13. Subject AP was the only subject evaluated during both normal walking and walker locomotion and power curves could be computed with both Joint and Segmental methods during one trial for each condition. For subject AV power curves with the two methods could be computed for one trial during normal walking. Subjects MM, IA and MF were wearing shoes and bilateral ankle foot orthosis (AFO), while subject AP was wearing shoes and subject AV was barefoot.

Amplitude and shape of the power curves is quite different from subject to subject, and is related to walking condition (normal gait or walker) and level of impairement, that influence walking speed and gait asymmetries. Remebering that *net* power curves are obtained under the hypothesis of allowing energy transfers between segments, the amplitude of the curve increases if there has been an increased power production or absorption, but also if there has been a reduced energy recovery which depends on appropriate synchronization of the movement of body segments.

A careful observation of the power curves, compared also with data obtained from healthy children in figures 5.6 and 5.10, can therefore provide useful informations on the overall locomotion function of the subject considered.

The large positive peak of joint power production evident during the double support phase for the healthy subjects has now almost disappeared, reflecting reduced propulsive action performed by the ankle joint.

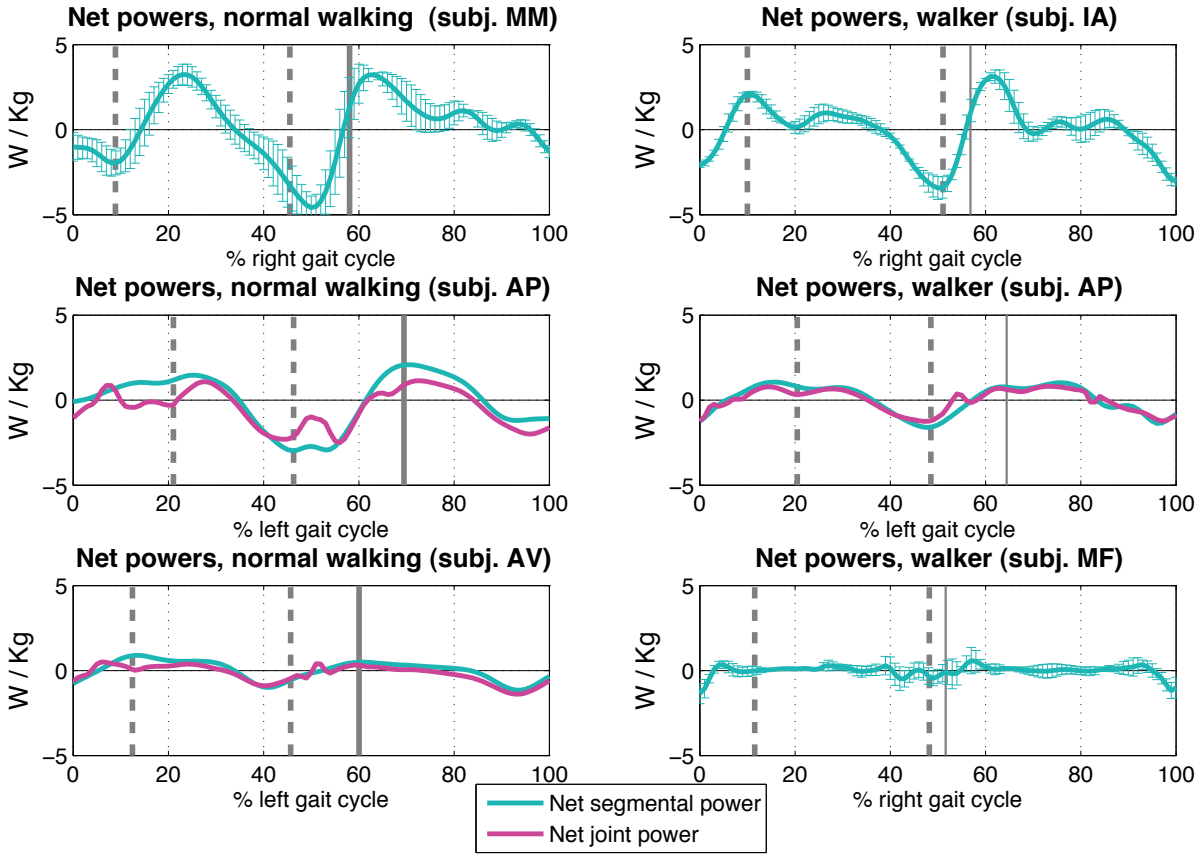

Figure 5.13: Whole body joint and segmental net power curves during a gait cycle in five CP children during gait (left column) or walker locomotion (right column). Lower limbs joint power could be computed only when clean contact with the force plates was obtained from both feet. For subjects AP and AV joint power is compared with segmental power obtained from the same trial only, while plots for subjects MM, IA, MF illustrate segmental power curves as mean values (± 1 SD) of three gait cycles relative to the same side, left or right, depending on the subject. The vertical gray line represents the foot-off event of the ipsilateral foot, while gray dashed lines represent foot-off and foot-strike events of the contralateral foot. Normalized speeds for the left column data were, from the top, 0.24, 0.20, 0.17, while for the right column they were 0.17, 0.06, 0.13.

Differences between the two steps can highlight the weakness of one body side against the other. An augmented negative power observed during a particular phase of the gait cycle may be related to weakness of those muscles that should be active at that time instant, with the consequence of forcing the subject to produce increased positive work during another phase of the cycle (e.g. subjects MM and AP during walking).

In terms of symmetry, the use of the walker seems to be beneficial, as we can see by

observing the power plots for subject AP in the two conditions.

A lower walking speed lowers dramatically the amplitude of power curves (subject MF, normalized walking speed equal to 0.06). However, time normalization is done with respect to the gait cycle, therefore the final energetic cost of locomotion evaluated in terms of muscle mechanical work will be dependent on the real duration of the gait cycles (section 5.6).

Figures 5.14 and 5.15 illustrate the total muscle mechanical work results obtained by computing the different work values (*Wtot+*, *Wtot-*, $|Wtot|$, *Wnet*, *Wabsnet*) with the three approaches: Joint, Segmental and External/Internal (combined limbs method, with COM computed from kinematics) and by subdividing total work in positive and negative muscle work performed separately by the lower body and the upper body during walking and during walker locomotion.

Results show a large inter-subject variability, which suggests that the level of impairement and walking strategy affects considerably the values of muscle mechanical work. Subjects that appeared visually having less capability to maintain balanced equilibrium, compensate with the action of the upper limbs and more pronounced jerky movements, which resulted in increased muscle mechanical work (subjects MM and AP).

Normalized walking speed was reduced for all CP subjects with respect to trials acquired on healthy children, both with and without walker.

A visual inspection of between-methods variability highlights, for CP subjects in both conditions, a closer correspondence between Segmental and External/Internal methods also when energy transfers are not allowed ($|Wtot|$), and a reduced gap between these values and those obtained when allowing for energy transfers (*Wabsnet*). This findings, together with increased values of *Wabsnet*, seem to indicate that CP children have reduced capability to make use of energy recuperation.

Opposite to the closer correspondence, in healthy children data, between the values of *Wabsnet* computed with Segmental and External/Internal methods, larger differences are noticeable between these two methods and the Joint power method, for AP subject during normal walking and walker locomotion.

Additionally, *Wnet* during gait is now, for subjects AP and AV, negative, a result that

looks energetically quite puzzling.

The use of the walker allows subject AP to go slower, with all values of muscle mechanical work slightly reduced and *Wnet* close to zero for all methods.

Half of the total muscle mechanical work done by subject MF is produced by the upper body, and, despite his very slow walking speed, he has Segmental total muscle work values very close to those of subject AP, whose normalized speed is doubled.

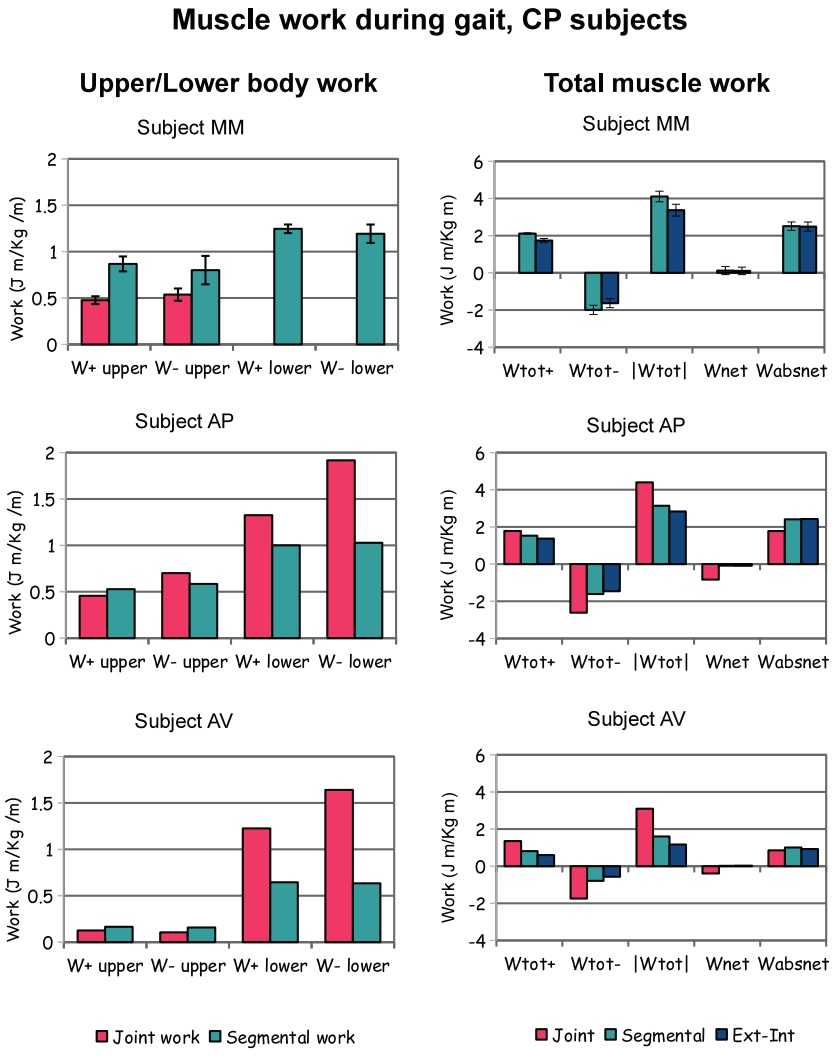

Figure 5.14: Upper body, lower body and whole body muscle mechanical work during impaired gait for 3 subjects computed with the different approaches. No good GRF data were available for MM subject, therefore his data are relative to kinematic measures only. Good bilateral GRF data were available during one trial only for subjects AP and AV, and therefore results from these trials only are shown. Normalized speed for the 3 subjects was, respectively, 0.24, 0.20, 0.17.

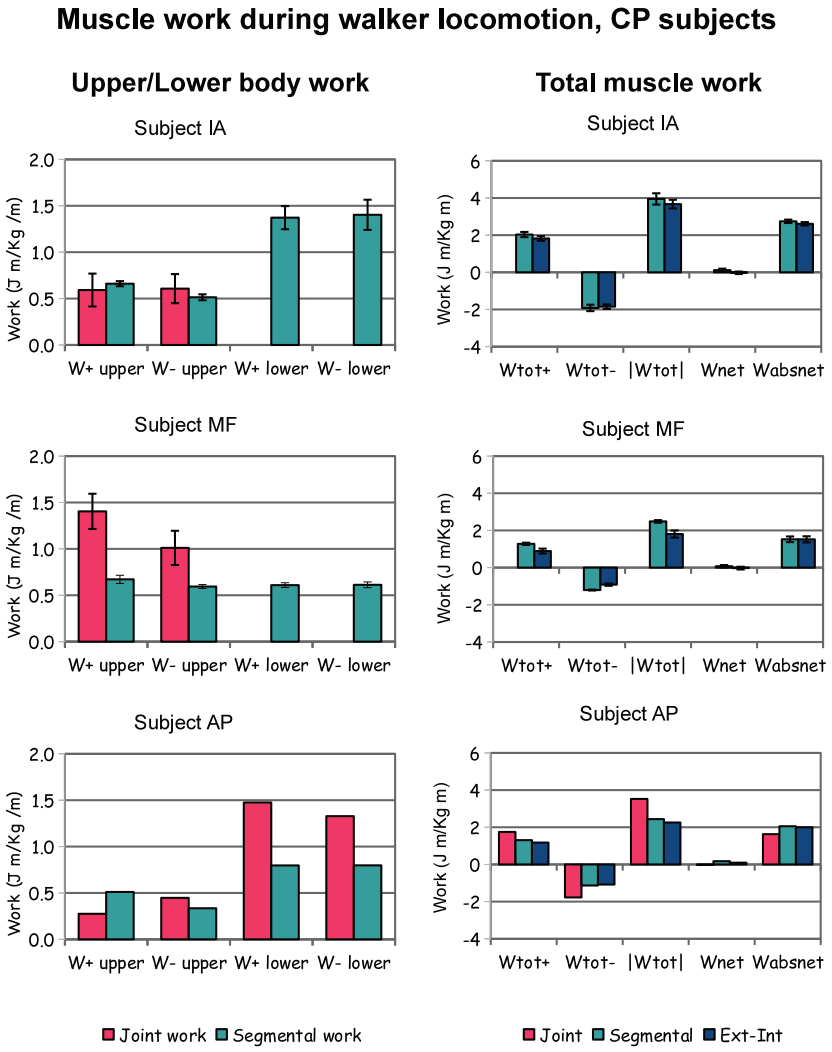

Figure 5.15: Upper body, lower body and whole body muscle mechanical work during impaired gait for 3 subjects computed with the different approaches. No complete GRF data were available for IA and MF subjects, therefore their data are relative to kinematic measures only. Good bilateral GRF data were available during one trial only for subjects AP, and therefore results from this single trial are shown. Normalized speed for the 3 subjects was, respectively, 0.17, 0.06, 0.13.

5.6 Gait/walker, healthy/CP comparisons

Unfortunately, the number of CP subjects is too small and impairements too different to be able to generalize the results obtained. However, the visualization of total muscle mechanical work values as a function of normalized walking speed for both healthy and CP children might help to highlight some useful elements of comparison.

Fig. 5.16 shows the relationship between intra-subject mean values of $|Wtot|$ and *Wabsnet* for the two groups of subjects during normal gait and during walker locomotion. Of course, a fair comparison between the two groups is possibile only during gait.

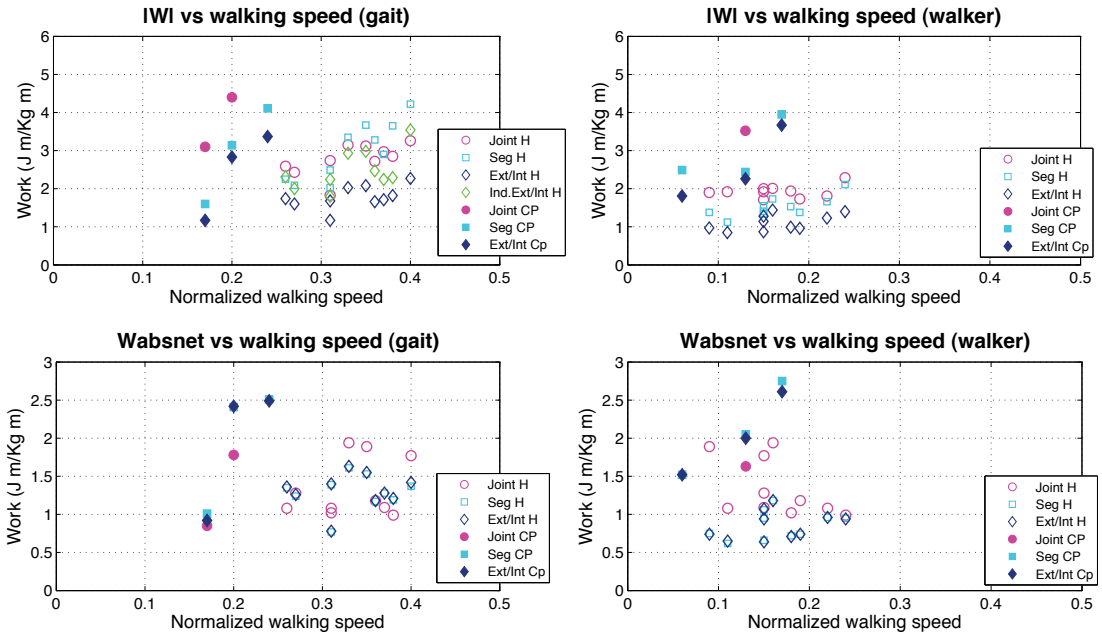

Figure 5.16: Comparison of $|Wtot|$ and *Wabsnet* values for all the subjects means, computed with the three approaches, during normal gait and during walker locomotion, as a function of the normalized walking speed $v*$. Empty markers are relative to the healthy group data (H), filled markers to CP group data (CP).

Looking at healthy children data during normal gait, even if subjects were all walking at their self-selected walking speed, and therefore speed range is quite narrow, it seems that $|Wtot|$, is increasing with walking speed, while *Wabsnet* remains rather constant between 1 and 2 J*m/Kg*m. With the walker, instead, this linear relationship of $|Wtot|$

with walking speed seemsto be very mild.
Although CP children have a lower self selected walking speed, their work values are already equal or higher than those of the healthy subjects, and for both $|Wtot|$ and *Wabsnet* we cannot say anything about a possible relationship of work values with speed, since physical impairements are too different among subjects.

Another parameter which has been often used as a global index of locomotion efficiency is the *recovery index* (Cavagna et al., 2000). Even if it is based on an extreme simplification of subject's gait modelled as an inverted pendulum, and results obtained have to be considered carefully (Zatsiorsky, 2002; Aleshinsky, 1986c) it can provide an approximate measure of the mechanical energy conservation that the subject is able to obtain by converting COM potential energy into kinetic energy and viceversa.

The *recovery index*, ρ, can be expressed as the difference between the summation of the individual positive increments of potential and kinetic energy of the COM and the positive increment of the total mechanical energy associated to the COM (which is equivalent to the positive external work done on the COM):

$$Recovery(\%)\,\rho = \frac{\Delta K_E^+ + \Delta P_E^+ - W_{ext}^+}{\Delta K_E^+ + \Delta P_E^+} 100 \tag{5.1}$$

with ΔK_E^+ e ΔP_E^+ being the positive increments of kinetic and potential energy during the gait cycle, and W_{ext}^+ the positive external muscle mechanical work estimated.

Recovery values in Fig. 5.17 are all in the interval 50..90% for healthy subjects during normal gait, similarly to (Schepens et al., 2004) who reported recovery values around 65% for children walking at about 1.5 m/s, while values are very different among CP subjects and seem to be inversely correlated with total muscle work (lower recovery values, 20..35%, belonging to AP and MM subjects, are associated to larger muscle work values, like *Wabsnet* around 2 J*m/Kg*m).

The use of a walker indeed prevents high values for the recovery index, since the inverted pendulum model used for normal walking is not valid any more. This is confirmed by the numbers, who are all below 50% for both groups.

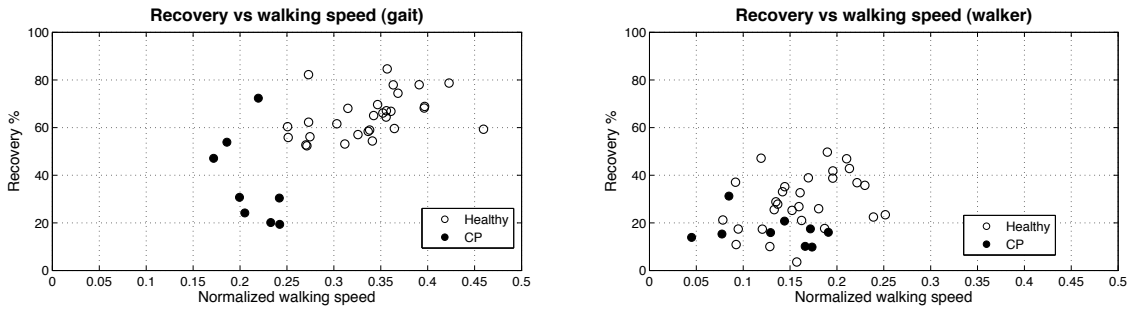

Figure 5.17: Recovery index values during normal gait and during walker locomotion, as a function of the normalized walking speed v^*. Empty markers are relative to the healthy group data from all individual trials (H), filled markers to CP group data from individual trials (CP).

Chapter 6

Discussion

The aims of the present study were to investigate the meaning of muscle mechanical work and its estimation via *indirect* methods, during normal gait and walker-assisted gait in healthy and cerebral palsy (CP) children. Limitations, innovative aspects and results related to our research are discussed together in the following.

Existing approaches used to estimate the muscle mechanical work involved in human movement all start from the fundamental definition of work and energy-balance equations for a rigid body. However, the difficulty of applying these definitions to a complex system as the human body observed from the outer world, in order to find a link between mechanical work and metabolic energy consumption, has compelled researchers to define their own system of hypotheses (chapter 1).

Despite aiming to measure the same physiological quantity, each method was originally based on different assumptions about i) founding equations, ii) between segments energy transfers, iii) interpretation of negative muscle work, iv) different meaning given to common terms as *internal* work, which all together affected the magnitude of final work values and alimented a terminological confusion.

Attempts to theoretically (Aleshinsky, 1986a,b) and experimentally (van de Walle et al., 2010, 2012) compare the different *indirect* approaches among them or against *direct* estimates provided by musculo-skeletal models (Sasaki et al., 2009; Prilutsky et al., 1996) have given indication that the results obtained are fairly different. However, those investigations compared the different approaches exactly as they were originally defined

in the literature and results were therefore biased by the different estabilished hypotheses.

Starting from the founding equations of motion of a rigid frame, we represented the human body through a multi-linked system of rigid segments (chapter 4) and by measuring its movement and its interaction with external forces we could estimate the rate of change of mechanical energy of the segments and the power produced at the level of the different joints (chapter 2).

Lower limbs joint powers are consistent with related literature on healthy children (Schwartz et al., 2008). To the best of our knowledge, there are no validated data on trunk and upper limb joint powers on children. However, despite the results might be affected by the limitations described in chapter 4, our data confirm that magnitude of upper body powers during normal walking are limited to about 10% of ankle and knee maximum power values.

The joint power curves give a representation of the *cause* of the movement as propulsive or braking action on the segments, while the segmental power curves information comes from the consequent kinematic *effect* of those forces on the body segments (section 5.2).

The analysis of the whole-body power functions during the gait cycle demonstrated that the different approaches are able to evidence approximately the same phases of overall positive or negative work production, while differing in the magnitude of positive and negative power values separately considered.

In agreement with the theoretical findings described in chapter 1, our results show that all the approaches are equivalent only if their computations are based on the same energetical hypothesis of allowing for energy transfers between all body segments (*net* power curves and *absnet* muscle work values). Between segments energy transfers were not restricted to particular groups of segments as it has been done by some authors in previous research (e.g. allowing for transfers between segments of the same limb but not between upper arm and trunk). Our assumption is rather extreme, of course, but it appeared more interesting, here, to focus on the conceptual differences between allowing or not allowing for energy transfers, rather than discussing which transfers can be thought as biomechanically reasonable and which not. This last aspect represents indeed an in-

teresting evolution of the discussion, and should be addressed in future investigations.

Differences among the different approaches emerge when it is necessary to make a distinction between positive and negative values of muscle power, thus preventing energy transfers between segments. In this case, the combined limbs External/Internal work method demonstrated to provide the lowest whole-body mechanical work values.

In our analysis, we have considered only the possibility of energy transfers between segments happening at the same time instant, without considering any possible energy recuperation during time, that might however be possible in certain situations, for example in terms of elastic energy recovery.

It is now hard to say which hypotheses are able to better represent the real physiological situation. The solution closer to reality is probably in between the two conditions of all energy transfers allowed and no energy transfers at all. The computation of work values in both cases might therefore provide useful information on the amount of simultaneous positive and negative work performed, and the analysis of the associated whole-body power curves can add further insights by allowing to localize these actions during time.

In any condition, anyway, we have to be aware that we are trying to infer muscles (which are inside the body) work by looking at their *net* output effect from the outside. Therefore, the information we get has to be critically considered. An analysis of muscles electrical activity via surface electromyography (S-EMG) with the quantification of concurrent action of agonist-antagonist muscles around the same joint might provide insights on the efficiency of the movement performed. However, numerical quantification of the level of muscle coactivation suffers the problem of finding a robust method for amplitude normalization of S-EMG data, in order to compare the level of activity of different muscles. The available analysis of EMG data, although functionally useful, can provide qualitative information on the timing of muscles activation only.

To compare our values of estimated muscle mechanical work with previous publications on healthy children during level walking we had to take into account criteria that were used for work normalization, walking speed during the trials and age of the subjects.

In (Schepens et al., 2004) the value of External/Internal muscle work was computed

with the individual limbs method and some particular hypotheses on between segments energy transfers. A rough normalization by mean subjects height gives a value close to our result of 1.21 J*m/Kg*m for a similar mean walking speed (0.9 m/s) and age between 6 and 13 years.

In (van de Walle et al., 2010) authors computed positive and negative Joint work, total absolute Segmental work, positive External/Internal work with the Individual limbs method. At walking speed slightly higher (1.2 m/s), they found values of Joint work (2.80 J*m/Kg*m) similar to ours (2.77) after applying the same normalization, while Segmental work and External/Internal work are higher than ours and previous results of (Schepens et al., 2004) (4.06 and 2.52 against our 2.99 and 1.21). Since the Segmental and External/Internal approaches are critically dependent on the smoothness of kinematic data provided by the filtering process (because numerical differentiation is needed to calculate kinetic energy (Winter, 2005)) we suppose that this is the reason for the discrepancy from (van de Walle et al., 2010) data and (Schepens et al., 2004) and our data. The conjecture cannot be verified, since authors did not describe the filter they used.

A limitation of our study is that we collected data at self-selected speed only. From visual inspection of results shown in Fig. 5.16 it seems that $|Wtot|$ values linearly increase with speed for all methods, while a similar pattern is not evident for the *Wabsnet* values. We might therefore speculate that, during gait, magnitude of positive and negative power curves produced by body muscles increases with walking speed, but that the relative phase between the two curves does not change, resulting in possibility for energy transfers that is also increased, to give approximately the same amount of *net* power output. However, this should be verified testing all subjects over a wider range of walking speeds.

When turning towards studying impaired walking in CP subjects, movements do not follow a criterion of energy optimization any more, and work values are therefore different from case to case.

Unfortunately, we could collect data on a few subjects only, with walking patterns very different from each other, and complete bilateral ground reaction forces not available for all the trials. Available results, however, seem to evidence higher work values for CP

subjects with respect to healthy children when walking at similar or slower speed and, moreover, a correlation between the increase of work values and the gravity of impairement. Results also seem to suggest that the more impaired is gait, the more *Wabsnet* component increases with respect to $|Wtot|$, suggesting a decreased *in-phase* activity of the positive and negative whole-body power curves (which results in reduced possibilities for reciprocal power terms cancellations), a finding that is confirmed also by values of $|Wtot|$ getting closer between Segmental and External/Internal methods.

Besides the muscle mechanical work values, which give an overall information on the amount of energy involved in the walking movements, a detailed analysis of the pattern of the whole-body *positive*, *negative* and *net* power curves during the gait cycle provides useful insights on the overall power production and absorption during the different phases of gait, an information particularly useful to investigate gait asymmetries or to evaluate the effects of orthosis and rehabilitation interventions.

In more severe gait impairements, walking aids are needed for equilibrium and support purposes. To be able to evaluate how whole-body muscle mechanical work is affected by the use of a posterior walker it is necessary to measure force interaction of the subject with the walker frame (chapters 3, 4).

The development of two instrumented handles to be applied to children's walkers allowed to measure upper limbs joint kinematics and kinetics, an extension of traditional lower limbs gait analysis, and to estimate muscle mechanical work also in this walking condition, with all the three approaches. Intrumentation and model testing on healthy children confirmed theoretical expectations, demonstrating that the three approaches are equivalent when energy transfers between segments are allowed, while they are all different when energy transfers are not allowed. A comparison of healthy children muscle mechanical work values while using the posterior walker with those measured on three CP children show that CP subjects have higher work values when walking at similar speeds.

One of the CP children was tested in both walking conditions. His results show that, although walking speed was slightly reduced with the walker, work values remained more or less the same, apart from a reduced total negative Joint work, which led to *net* Joint

work equal to zero. A more symmetrical behaviour of the *net* power curves during the two steps of the gait cycle was noticed when using the walker.

While considering normal subjects data, the analysis of *net* power curves in the two situations, normal gait and walker locomotion, reveals a smoother pattern in the latter condition, especially during push-offs and double support phases. Apart from the difference in amplitude, whole-body power curves highlight a similarity in shape to the *external* power curve computed from the changes in mechanical energy of the centre of mass, thus confirming the validity of the centre of mass as a global indicator of the *net* (energetical) behaviour of the body.

A problem is evident from our data collection: Measuring valid, bilateral, lower limbs kinetic data in pathologic gait is difficult, depending on force plates dimension and positioning, and subject's compliance and fatiguability. Moreover, for correct bilateral kinetic analysis, data should be collected from at least three force plates, otherwise GRF of one of the two legs will be missing during one of the two double support phases. In this work, assuming symmetry between subsequent cycles, we completed missing data by copying, interpolating and pasting necessary lower limb kinetics from the following gait cycle and then visually inspecting the result for consistency.
On the other hand, instrumented handles placed on a walker can always be used, and upper limbs and trunk kinetics can be assessed independently from the lower limbs, giving useful information on bilateral weight bearing, joint loading, walker usage strategies (chapter 4).

For healthy children normal gait we found a *net* Joint work which is different from zero, and positive. The finding is confirmed for walker-assisted gait of healthy subjects. The sign, however, is reversed for CP children during normal gait, and is equal to zero with the walker. Although authors did not comment this aspect in their results, a similar difference in positive and negative Joint work components is present also in (van de Walle et al., 2010).

This discrepancy was found and discussed also by other authors (De Vita et al., 2007; Zelik and Kuo, 2010), and the explanation seems to be related to the limitations of the hypothesis of rigidity of the body segments. Particularly, in (Zelik and Kuo, 2010) it was shown that at lower walking speeds the net Joint work became negative, which might explain the result we found for CP children, who walk slower than their healthy pairs. However, authors compared only lower limbs powers versus COM power, without considering that some positive power produced by the ankle might also have been transferred, and dissipated, more proximally at the trunk. Also, if energy dissipation might explain the result of positive net Joint work during healthy children gait, the explanation of net Joint work being negative for CP children appears more complex.

This topic still leaves, therefore, open issues to be investigated, besides the improvement and validation of 3-dimensional full-body kinetic models.

Chapter 7

Conclusions

The estimation of muscle mechanical work can be a useful parameter to be used to investigate movement efficiency. At variance with the use of musculo-skeletal models, a promising but still complicated and evolving approach, *indirect* methods allow to estimate muscle work by measuring body kinematics and kinetics.

Different methods to indirectly estimate muscle mechanical work during walking have been presented in the literature: the External+Internal work, the Segmental work and the Joint work approaches. Although attempts have been made to investigate differences among them, all methods are still used in research and clinical applications, not only to study walking and running, but also cycling and other movements.

A deeper understanding of theoretical differences and analogies was therefore necessary, to know what is exactly computed by each method and help to make a more appropriate use of this information when studying walking or running, either for improvement of sport performance or rehabilitation of impaired gait.

The aims of this work were therefore the discussion of open issues related to muscle mechanical work estimation and the development and evaluation of models for the clinical application of this measure to study gait and walker-assisted locomotion.

Theoretical differences among the methods have been discussed, and were confirmed by the results obtained.

Differences or equivalence in the muscle mechanical work values obtained depend on

the different assumptions defined for energy transfers allowed between body segments. Since the limitation of energy transfers modifies the funding equations, the methods, originally equivalent in their seminal equations, lead to diverging results.

The separate estimation of positive and negative components of whole-body muscle mechanical work appears particularly crucial to highlight significative differences among the methods. It is important, therefore, to be aware of the limitations and advantages that each method can provide.

The Joint powers approach, based on inverse dynamics computations, is theoretically more precise and correct than the Segmental powers approach for the estimation of total positive and negative muscle mechanical work. However, since it depends on force plates and instrumented handles data, it is also the most complex to realize, especially when studying impaired gait, and the finding of non zero *net* work has to be further investigated.

The External powers approach based on the centre of mass, due to the way it is defined, sistematically underestimates total positive and negative work. Results are partially improved by using the *individual limbs* power computation. The method can be useful when there is the need to represent the whole body via a single point, by computing *external* work during walking or running using force plates only. But if *internal* work, which is based on full-body kinematic data, has to be added to the computations, the complete *External+Internal* measures do not give any practical advantage with respect to the Segmental work approach.

Despite the differences, all methods can provide some useful information to investigate locomotion efficiency. However, they all suffer from either methodological or experimental limitations. Specific instrumented handles had to be developed to measure force interaction between hands and walker frame during walker-assisted locomotion, an information that is used in both the Joint powers and the Segmental powers approaches.

Our results evidenced that, apart from the critical issues described, the analysis of whole-body muscle mechanical power curves (either *positive*, *negative* or *net*), besides work values, can provide valuable information on the overall locomotion function, highlighting propulsive deficits, gait asymmetries, movement inefficiencies with reduced energy recuperation. Unfortunately our data were relative to self-selected speed only. It would

have been interesting to investigate further if speed affects similarly the work values obtained with the different approaches.

Even if we could collect data on a very small number of CP subjects, there seems to be an evident correlation between the seriousness of movement alterations and the magnitude of muscle mechanical work computed. When applying this analysis to impaired walking, it will be necessary to classify carefully movement hability of the subjects in order to allow inter-subject comparisons and to possibly derive generalized information useful for the rehabilitation process.

A detailed and correct definition of anthropometric properties for a precise full-body kinetic model appeared also a challenging task.

Future developments should therefore aim to improve the reliability of the biomechanical models applied in the analysis, while enlarging the number of subjects acquired. On the other hand, further investigation of the physiological and mechanical nature of muscle energy expenditure and work production during locomotion, including information on muscle electrical activity and enhancing the use of musculo-skeletal models is necessary (Neptune et al., 2009b), to better understand the relationships between measured metabolic energy consuption and mechanical output.

Appendix A

Basic and auxiliary results

This appendix contains details on collected data and on statistical analysis.

A.1 All trials data, healthy children

The following tables contain muscle mechanical work values computed for the healthy children with the different approaches. Data are presented from single trials and as intra-subject means. Overall mean and standard deviation (SD) values for all subjects are show at the bottom of the tables. Trial number is relative to all trials acquired for that subject. Normalized walking speed and the mean percentage of body weight put on the handles during the gait cycle are also listed in the table for each trial.

A.1.1 Normal gait

Tables in Fig.A.1 describe *positive* and *negative* work, divided in different components: Upper and lower body components for Joint and Segmental methods (W+ upper, etc.), external component computed with both the combined (Wext(COM)+, WextCOM-) and the individual limbs methods (ExtWposIndiv.limbs, ExtWnegIndiv.limbs), internal component computed with respect to the centre of mass (Wint+ upper segments, etc.).
Tables in Fig.A.2 describe the total work components computed with the three approaches plus External work evaluated with individual limbs method: *Wtot+*, *Wtot-*, $|Wtot|$, *Wnet*, *Wabsnet*.

UPPER BODY AND LOWER BODY WORK COMPONENTS

Subject	Trial	Norm speed	W+ upper joints	W- upper joints	W+ lower joints	W- lower joints	W+ upper segments	W- upper segments	W+ lower segments	W- lower segments	Wext (COM)+	Wext (COM)-	Wint+ upper segments	Wint- upper segments	Wint+ lower segments	Wint- lower segments	Ext Wpos indiv.limbs	Ext Wneg indiv.limbs
EC	6	0.303	0.13	-0.15	0.93	-1.35	0.29	-0.31	0.92	-0.90	0.40	-0.40	0.05	-0.05	0.35	-0.35	0.69	-0.86
	10	0.312	0.07	-0.11	1.16	-1.58	0.35	-0.22	1.04	-0.95	0.51	-0.32	0.04	-0.04	0.42	-0.41	0.74	-0.46
FC	11	0.361	0.05	-0.10	1.26	-0.94	0.28	-0.26	1.35	-1.33	0.30	-0.26	0.04	-0.04	0.53	-0.53	0.58	-0.61
	12	0.363	0.09	-0.15	1.33	-1.55	0.25	-0.29	1.33	-1.32	0.21	-0.24	0.04	-0.04	0.54	-0.54	0.70	-0.59
	15	0.368	0.08	-0.11	1.43	-1.05	0.29	-0.31	1.42	-1.41	0.21	-0.25	0.05	-0.04	0.58	-0.56	0.61	-0.81
FF	2	0.273	0.15	-0.18	1.07	-1.32	0.26	-0.25	0.89	-0.88	0.46	-0.45	0.03	-0.03	0.37	-0.36	0.75	-0.68
	3	0.270	0.17	-0.10	1.10	-1.15	0.27	-0.17	0.93	-0.90	0.55	-0.43	0.02	-0.02	0.39	-0.38	0.83	-0.78
	16	0.251	0.15	-0.16	1.05	-1.17	0.28	-0.23	0.87	-0.83	0.53	-0.46	0.02	-0.02	0.35	-0.34	0.87	-0.68
GV	2	0.326	0.12	-0.19	1.61	-1.09	0.26	-0.21	1.37	-1.32	0.48	-0.39	0.04	-0.04	0.53	-0.52	0.80	-0.94
	4	0.342	0.12	-0.23	1.75	-1.10	0.30	-0.26	1.45	-1.43	0.44	-0.39	0.05	-0.05	0.55	-0.55	0.78	-0.92
	6	0.337	0.13	-0.19	1.72	-1.19	0.29	-0.26	1.46	-1.43	0.44	-0.38	0.06	-0.06	0.56	-0.55	0.71	-1.05
GZ	6	0.271	0.16	-0.13	1.01	-1.08	0.17	-0.17	0.88	-0.85	0.47	-0.44	0.02	-0.02	0.36	-0.35	0.67	-0.56
	7	0.275	0.12	-0.15	1.10	-1.12	0.17	-0.18	0.94	-0.93	0.42	-0.43	0.03	-0.03	0.39	-0.38	0.61	-0.71
	12	0.251	0.13	-0.13	1.01	-1.16	0.15	-0.15	0.83	-0.82	0.38	-0.38	0.02	-0.02	0.33	-0.33	0.56	-0.60
IC	3	0.397	0.16	-0.26	1.65	-1.26	0.47	-0.46	1.73	-1.72	0.47	-0.45	0.10	-0.10	0.66	-0.66	0.66	-0.98
	9	0.423	0.19	-0.20	1.67	-1.15	0.50	-0.46	1.65	-1.61	0.34	-0.25	0.12	-0.12	0.65	-0.65	0.78	-1.46
	11	0.391	0.18	-0.23	1.60	-1.22	0.45	-0.47	1.55	-1.58	0.33	-0.40	0.11	-0.10	0.66	-0.65	0.94	-1.21
LC	4	0.315	0.12	-0.12	0.92	-0.68	0.30	-0.22	0.81	-0.66	0.41	-0.20	0.05	-0.05	0.29	-0.28	0.57	-0.53
	5	0.357	0.14	-0.15	0.89	-0.79	0.27	-0.30	0.87	-1.00	0.16	-0.31	0.04	-0.05	0.35	-0.38	0.65	-0.45
	7	0.273	0.11	-0.09	0.80	-0.70	0.22	-0.23	0.61	-0.63	0.16	-0.19	0.05	-0.05	0.25	-0.25	0.63	-0.48
MS	13	0.338	0.13	-0.13	1.31	-1.23	0.23	-0.24	1.29	-1.27	0.30	-0.32	0.02	-0.02	0.51	-0.49	0.46	-0.49
	17	0.356	0.09	-0.10	1.33	-1.30	0.32	-0.25	1.45	-1.41	0.31	-0.22	0.03	-0.03	0.55	-0.55	0.51	-0.52
	22	0.459	0.09	-0.05	1.53	-1.27	0.44	-0.42	1.83	-1.81	0.35	-0.30	0.04	-0.04	0.68	-0.69	0.41	-0.82
PT	4	0.364	0.13	-0.20	1.31	-1.19	0.39	-0.35	1.12	-1.09	0.45	-0.39	0.04	-0.04	0.43	-0.44	0.65	-0.69
	7	0.341	0.07	-0.22	1.40	-1.50	0.29	-0.28	0.97	-0.97	0.40	-0.43	0.03	-0.02	0.41	-0.40	0.76	-0.43
	8	0.396	0.14	-0.21	1.21	-1.33	0.35	-0.37	1.24	-1.28	0.25	-0.30	0.06	-0.06	0.50	-0.50	0.46	-0.79
VT	10	0.347	0.10	-0.09	1.66	-1.23	0.30	-0.34	1.44	-1.45	0.38	-0.43	0.06	-0.06	0.57	-0.57	0.68	-0.77
	12	0.352	0.07	-0.10	1.76	-1.20	0.29	-0.30	1.50	-1.56	0.39	-0.47	0.06	-0.06	0.59	-0.59	0.77	-0.99
	13	0.356	0.08	-0.08	1.79	-1.19	0.41	-0.32	1.60	-1.50	0.45	-0.28	0.05	-0.05	0.59	-0.59	0.89	-1.02

INTRA-SUBJECT MEANS

EC		0.307	0.101	-0.131	1.045	-1.464	0.319	-0.267	0.980	-0.924	0.455	-0.363	0.044	-0.044	0.387	-0.382	0.717	-0.663
FC		0.364	0.074	-0.123	1.341	-1.179	0.273	-0.288	1.367	-1.351	0.240	-0.249	0.041	-0.042	0.548	-0.543	0.629	-0.670
FF		0.265	0.156	-0.143	1.074	-1.213	0.269	-0.218	0.897	-0.868	0.516	-0.448	0.023	-0.023	0.369	-0.364	0.814	-0.713
GV		0.335	0.124	-0.201	1.695	-1.128	0.284	-0.247	1.426	-1.390	0.454	-0.388	0.053	-0.052	0.547	-0.541	0.764	-0.969
GZ		0.266	0.138	-0.139	1.037	-1.121	0.166	-0.167	0.885	-0.870	0.422	-0.417	0.023	-0.023	0.358	-0.353	0.614	-0.624
IC		0.403	0.176	-0.231	1.638	-1.211	0.473	-0.463	1.645	-1.638	0.382	-0.365	0.108	-0.108	0.657	-0.655	0.797	-1.216
LC		0.315	0.123	-0.117	0.872	-0.723	0.261	-0.251	0.761	-0.760	0.242	-0.234	0.047	-0.046	0.299	-0.303	0.614	-0.488
MS		0.384	0.102	-0.093	1.391	-1.268	0.332	-0.305	1.522	-1.495	0.322	-0.279	0.032	-0.032	0.580	-0.574	0.462	-0.607
PT		0.367	0.114	-0.210	1.308	-1.342	0.345	-0.335	1.110	-1.114	0.367	-0.370	0.042	-0.041	0.448	-0.446	0.622	-0.637
VT		0.352	0.086	-0.091	1.735	-1.206	0.331	-0.320	1.514	-1.502	0.407	-0.392	0.055	-0.055	0.584	-0.582	0.780	-0.925
	MEAN	0.336	0.119	-0.148	1.314	-1.185	0.305	-0.286	1.211	-1.191	0.381	-0.350	0.047	-0.047	0.478	-0.474	0.681	-0.751
	STD	0.047	0.031	0.049	0.305	0.192	0.079	0.080	0.319	0.321	0.091	0.072	0.024	0.024	0.121	0.120	0.112	0.218

Figure A.1: Computed work components during normal gait, healthy subjects. All trials data, intra-subject mean values and overall mean values (see text for details). Work is expressed in (J*m/Kg*m). Empty line corresponds to missing trial for that subject.

TOTAL BODY WORK

			Joint					Segmental					ExtInt					ExtInt Indiv.limbs			
Subject	Trial	Norm speed	Wtot+	Wtot-	|Wtot|	Wnet	Wabsnet	Wtot+	Wtot-	|Wtot|	Wnet	Wabsnet	Wtot+	Wtot-	|Wtot|	Wnet	Wabsnet	Wtot+	Wtot-	|Wtot|	Wnet
EC	6	0.30	1.06	-1.50	2.56	-0.45	1.04	1.21	-1.21	2.43	0.00	1.28	0.80	-0.80	1.61	0.00	1.29	1.10	-1.26	2.36	-0.17
	10	0.31	1.24	-1.69	2.92	-0.45	1.00	1.38	-1.17	2.55	0.22	1.50	0.97	-0.77	1.75	0.20	1.51	1.20	-0.92	2.12	0.29
FC	11	0.36	1.31	-1.04	2.35	0.27	1.13	1.63	-1.59	3.22	0.04	1.24	0.87	-0.83	1.70	0.03	1.26	1.15	-1.18	2.32	-0.03
	12	0.36	1.42	-1.70	3.12	-0.28	1.16	1.58	-1.61	3.19	-0.03	1.11	0.78	-0.82	1.60	-0.04	1.11	1.28	-1.17	2.45	0.11
	15	0.37	1.51	-1.16	2.67	0.35	1.25	1.71	-1.72	3.43	-0.01	1.16	0.84	-0.85	1.69	-0.02	1.18	1.23	-1.42	2.65	-0.19
FF	2	0.27	1.22	-1.50	2.72	-0.28	1.04	1.14	-1.13	2.27	0.02	1.29	0.87	-0.84	1.71	0.02	1.31	1.15	-1.07	2.22	0.08
	3	0.27	1.27	-1.24	2.51	0.02	1.25	1.20	-1.07	2.27	0.13	1.39	0.96	-0.84	1.80	0.12	1.42	1.24	-1.18	2.41	0.06
	16	0.25	1.20	-1.32	2.52	-0.12	0.96	1.16	-1.06	2.22	0.09	1.36	0.90	-0.82	1.72	0.08	1.37	1.23	-1.05	2.28	0.19
GV	2	0.33	1.73	-1.28	3.01	0.45	1.94	1.63	-1.53	3.16	0.10	1.62	1.06	-0.96	2.02	0.10	1.63	1.37	-1.51	2.88	-0.14
	4	0.34	1.87	-1.33	3.20	0.55	1.96	1.75	-1.69	3.44	0.05	1.58	1.05	-0.99	2.04	0.05	1.60	1.39	-1.52	2.91	-0.13
	6	0.34	1.85	-1.38	3.23	0.48	1.90	1.75	-1.69	3.44	0.06	1.62	1.06	-0.99	2.04	0.07	1.65	1.33	-1.66	2.99	-0.33
GZ	6	0.27	1.17	-1.21	2.38	-0.05	1.26	1.06	-1.02	2.08	0.03	1.28	0.84	-0.82	1.66	0.03	1.30	1.05	-0.93	1.98	0.12
	7	0.27	1.22	-1.27	2.49	-0.06	1.45	1.11	-1.11	2.22	0.00	1.29	0.83	-0.83	1.66	0.00	1.30	1.02	-1.12	2.14	-0.09
	12	0.25	1.14	-1.29	2.43	-0.15	1.14	0.98	-0.98	1.96	0.01	1.16	0.74	-0.74	1.47	0.00	1.17	0.91	-0.95	1.86	-0.04
IC	3	0.40	1.81	-1.52	3.32	0.29	1.74	2.20	-2.18	4.39	0.02	1.43	1.23	-1.21	2.43	0.02	1.54	1.42	-1.73	3.16	-0.31
	9	0.42	1.85	-1.36	3.21	0.50	1.72	2.16	-2.07	4.22	0.09	1.18	1.11	-1.02	2.13	0.09	1.21	1.55	-2.23	3.79	-0.68
	11	0.39	1.78	-1.45	3.24	0.33	1.84	2.00	-2.05	4.05	-0.05	1.48	1.10	-1.15	2.26	-0.05	1.52	1.71	-1.96	3.67	-0.25
LC	4	0.31	1.04	-0.80	1.84	0.25	1.11	1.10	-0.88	1.98	0.22	0.96	0.75	-0.53	1.27	0.22	0.95	0.91	-0.86	1.77	0.05
	5	0.36	1.03	-0.94	1.97	0.10	1.07	1.13	-1.30	2.44	-0.17	0.76	0.56	-0.74	1.30	-0.18	0.79	1.05	-0.88	1.93	0.17
	7	0.27	0.91	-0.79	1.70	0.12	1.06	0.83	-0.85	1.68	-0.03	0.58	0.46	-0.48	0.94	-0.02	0.61	0.93	-0.77	1.70	0.16
MS	13	0.34	1.44	-1.36	2.80	0.09	1.24	1.52	-1.51	3.03	0.02	1.21	0.83	-0.83	1.66	0.01	1.24	0.99	-0.99	1.99	0.00
	17	0.36	1.42	-1.40	2.82	0.01	1.00	1.77	-1.66	3.43	0.11	1.18	0.89	-0.80	1.69	0.10	1.19	1.09	-1.10	2.19	-0.01
	22	0.46	1.62	-1.32	2.94	0.30	0.73	2.27	-2.23	4.50	0.04	1.19	1.07	-1.03	2.10	0.04	1.19	1.13	-1.55	2.68	-0.41
PT	4	0.36	1.44	-1.40	2.84	0.04	1.02	1.51	-1.44	2.95	0.06	1.23	0.93	-0.87	1.80	0.06	1.22	1.13	-1.17	2.30	-0.05
	7	0.34	1.47	-1.72	3.19	-0.24	1.22	1.26	-1.26	2.52	0.00	1.38	0.83	-0.85	1.68	-0.01	1.37	1.19	-0.85	2.04	0.34
	8	0.40	1.35	-1.54	2.89	-0.19	1.02	1.60	-1.65	3.25	-0.05	1.24	0.81	-0.85	1.66	-0.05	1.25	1.02	-1.35	2.36	-0.33
VT	10	0.35	1.76	-1.32	3.08	0.43	1.84	1.74	-1.78	3.52	-0.05	1.48	1.00	-1.05	2.06	-0.05	1.50	1.31	-1.39	2.70	-0.09
	12	0.35	1.83	-1.30	3.13	0.53	2.00	1.79	-1.86	3.65	-0.07	1.59	1.05	-1.12	2.17	-0.08	1.61	1.43	-1.64	3.07	-0.21
	13	0.36	1.87	-1.27	3.14	0.61	1.82	2.01	-1.82	3.83	0.19	1.51	1.09	-0.91	2.00	0.18	1.54	1.53	-1.65	3.18	-0.12

INTRA-SUBJECT MEANS

EC		0.31	1.15	-1.59	2.74	-0.45	1.02	1.30	-1.19	2.49	0.11	1.39	0.89	-0.79	1.68	0.10	1.40	1.15	-1.09	2.24	0.06
FC		0.36	1.42	-1.30	2.72	0.11	1.18	1.64	-1.64	3.28	0.00	1.17	0.83	-0.83	1.66	-0.01	1.18	1.22	-1.25	2.47	-0.04
FF		0.26	1.23	-1.36	2.59	-0.13	1.08	1.17	-1.09	2.25	0.08	1.35	0.91	-0.83	1.74	0.07	1.36	1.21	-1.10	2.31	0.11
GV		0.33	1.82	-1.33	3.15	0.49	1.94	1.71	-1.64	3.35	0.07	1.61	1.05	-0.98	2.03	0.07	1.63	1.36	-1.56	2.93	-0.20
GZ		0.27	1.17	-1.26	2.43	-0.09	1.28	1.05	-1.04	2.09	0.01	1.24	0.80	-0.79	1.60	0.01	1.26	1.00	-1.00	2.00	0.00
IC		0.40	1.81	-1.44	3.26	0.37	1.77	2.12	-2.10	4.22	0.02	1.37	1.15	-1.13	2.27	0.02	1.42	1.56	-1.98	3.54	-0.42
LC		0.31	0.99	-0.84	1.83	0.16	1.08	1.02	-1.01	2.03	0.01	0.77	0.59	-0.58	1.17	0.00	0.78	0.96	-0.84	1.80	0.12
MS		0.38	1.49	-1.36	2.85	0.13	0.99	1.85	-1.80	3.65	0.05	1.19	0.93	-0.88	1.82	0.05	1.21	1.07	-1.21	2.29	-0.14
PT		0.37	1.42	-1.55	2.97	-0.13	1.09	1.45	-1.45	2.90	0.01	1.28	0.86	-0.86	1.71	0.00	1.28	1.11	-1.12	2.24	-0.01
VT		0.35	1.82	-1.30	3.12	0.52	1.89	1.85	-1.82	3.67	0.02	1.53	1.05	-1.03	2.08	0.02	1.55	1.42	-1.56	2.98	-0.14
	MEAN	0.336	1.433	-1.333	2.766	0.100	1.332	1.516	-1.477	2.993	0.039	1.289	0.905	-0.871	1.776	0.034	1.308	1.206	-1.272	2.478	-0.066
	STD	0.047	0.304	0.206	0.418	0.307	0.378	0.376	0.382	0.757	0.037	0.230	0.157	0.149	0.304	0.037	0.233	0.192	0.336	0.523	0.163

Figure A.2: Whole body muscle mechanical work during normal gait computed with the different methods (see text for details).

A.1.2 Walker-assisted gait

Tables in Fig.A.3 describe *positive* and *negative* work during walker locomotion, divided in different components: Upper and lower body components for Joint and Segmental methods (W+ upper, etc.), external component computed with the combined limbs method (Wext(COM)+, WextCOM-), internal component computed with respect to the centre of mass (Wint+ upper segments, etc.), positive and negative work done on the two handles (W+ right handle, etc.).

Therefore, the final positive and negative work done by the upper body (W+ upper segments and handles, etc) is obtained by the summation of work associated to upper body segments and work done on the handles.

Tables in Fig.A.4 describe the total work components computed with the three approaches: *Wtot+*, *Wtot-*, $|Wtot|$, *Wnet*, *Wabsnet*.

UPPER BODY AND LOWER BODY WORK COMPONENTS

Subject	Trial	Norm speed	Bodyweight % on handles	W+ upper joints	W- upper joints	W+ lower joints	W- lower joints	W+ upper segments	W- upper segments	W+ lower segments	W- lower segments	Wext (COM)+	Wext (COM)-	Wint+ upper segments	Wint- upper segments	Wint+ lower segments	Wint- lower segments	W+ right handle	W- right handle	W+ left handle	W- left handle
EC	7	0.17	36.00	0.18	-0.12	0.72	-0.85	0.10	-0.12	0.54	-0.65	0.20	-0.32	0.01	-0.01	0.25	-0.25	0.02	0.00	0.01	0.00
	11	0.16	50.00	0.27	-0.26	0.93	-0.84	0.21	-0.20	0.59	-0.65	0.30	-0.34	0.02	-0.01	0.25	-0.24	0.02	0.00	0.01	0.00
	12	0.21	54.00	0.15	-0.11	0.82	-0.58	0.12	-0.09	0.61	-0.61	0.19	-0.16	0.01	-0.01	0.22	-0.21	0.01	0.00	0.02	0.00
FC	9	0.19	30.00	0.13	-0.20	0.64	-0.59	0.12	-0.12	0.50	-0.51	0.21	-0.22	0.01	-0.01	0.19	-0.19	0.02	0.00	0.02	0.00
	10	0.18	23.00	0.13	-0.22	0.95	-0.62	0.17	-0.13	0.54	-0.46	0.36	-0.24	0.01	-0.01	0.18	-0.18	0.03	0.00	0.03	0.00
	11	0.20	21.00	0.14	-0.24	0.71	-0.61	0.16	-0.15	0.57	-0.56	0.31	-0.31	0.01	-0.01	0.23	-0.22	0.02	0.00	0.02	0.00
FF	16	0.22	30.00	0.19	-0.14	0.92	-0.52	0.17	-0.13	0.66	-0.67	0.38	-0.35	0.01	-0.01	0.27	-0.27	0.02	0.00	0.04	0.00
	19	0.21	19.00	0.15	-0.16	0.87	-0.68	0.14	-0.13	0.68	-0.65	0.32	-0.30	0.01	-0.01	0.27	-0.27	0.02	0.00	0.02	0.00
GV	4	0.13	25.00	0.33	-0.33	1.19	-0.59	0.13	-0.16	0.81	-0.78	0.58	-0.57	0.02	-0.02	0.29	-0.29	0.01	0.00	0.03	0.00
	16	0.16	51.00	0.21	-0.24	0.78	-0.33	0.10	-0.10	0.57	-0.53	0.36	-0.33	0.01	-0.01	0.20	-0.20	0.02	0.00	0.04	0.00
	19	0.19	25.00	0.17	-0.17	1.10	-0.61	0.15	-0.14	0.81	-0.77	0.45	-0.40	0.01	-0.01	0.30	-0.30	0.01	0.00	0.02	0.00
GZ	6	0.16	37.00	0.19	-0.14	0.88	-0.52	0.18	-0.16	0.52	-0.51	0.23	-0.19	0.01	-0.01	0.17	-0.17	0.03	0.00	0.02	0.00
	12	0.15	21.00	0.18	-0.12	0.63	-0.60	0.07	-0.10	0.53	-0.55	0.28	-0.33	0.01	-0.01	0.18	-0.18	0.02	0.00	0.01	0.00
	16	0.14	29.00	0.26	-0.13	0.77	-0.73	0.07	-0.07	0.55	-0.57	0.21	-0.23	0.01	-0.01	0.20	-0.20	0.02	0.00	0.02	0.00
IC	9	0.16	20.00	0.30	-0.20	0.68	-0.77	0.19	-0.13	0.64	-0.63	0.49	-0.40	0.01	-0.01	0.25	-0.25	0.00	-0.01	0.04	0.00
	14	0.14	24.00	0.25	-0.20	0.74	-0.73	0.17	-0.17	0.65	-0.65	0.49	-0.48	0.01	-0.01	0.27	-0.27	0.00	0.00	0.03	0.00
	10	0.13	36.00	0.22	-0.27	0.98	-0.44	0.14	-0.13	0.53	-0.46	0.30	-0.22	0.01	-0.01	0.18	-0.18	0.01	0.00	0.04	0.00
LC	7	0.12	30.00	0.11	-0.46	0.75	-0.28	0.11	-0.29	0.28	-0.32	0.11	-0.38	0.01	-0.01	0.10	-0.10	0.03	0.00	0.03	0.00
	13	0.09	24.00	0.41	-0.44	0.94	-0.52	0.17	-0.23	0.30	-0.26	0.23	-0.27	0.01	-0.01	0.08	-0.08	0.03	0.00	0.02	0.00
	16	0.13	21.00	0.20	-0.18	0.91	-0.55	0.16	-0.25	0.39	-0.46	0.35	-0.49	0.01	-0.01	0.16	-0.16	0.03	0.00	0.03	0.00
MS	9	0.25	12.00	0.18	-0.08	0.95	-0.83	0.19	-0.11	0.94	-0.93	0.30	-0.21	0.01	-0.01	0.36	-0.35	0.01	0.00	0.00	-0.01
	12	0.24	13.00	0.11	-0.15	1.20	-1.00	0.12	-0.11	0.94	-0.93	0.39	-0.39	0.01	-0.01	0.38	-0.38	0.02	0.00	0.02	0.00
	13	0.23	10.00	0.10	-0.13	1.22	-0.91	0.14	-0.18	0.82	-0.82	0.37	-0.40	0.01	-0.01	0.31	-0.31	0.03	0.00	0.02	0.00
PT	10	0.12	26.00	0.30	-0.42	0.79	-0.77	0.22	-0.34	0.41	-0.42	0.40	-0.55	0.01	-0.01	0.13	-0.12	0.02	0.00	0.03	0.00
	11	0.14	31.00	0.18	-0.48	0.39	-0.40	0.18	-0.17	0.58	-0.51	0.43	-0.39	0.02	-0.01	0.22	-0.22	0.01	0.00	0.03	0.00
	15	0.20	20.00	0.30	-0.26	0.98	-0.73	0.16	-0.09	0.52	-0.50	0.31	-0.21	0.01	-0.01	0.20	-0.19	0.02	0.00	0.02	0.00
VT	10	0.09	44.00	0.23	-0.21	1.35	-0.41	0.22	-0.21	0.60	-0.56	0.42	-0.39	0.01	-0.01	0.20	-0.20	0.02	0.00	0.06	0.00
	12	0.08	39.00	0.21	-0.18	0.96	-0.32	0.08	-0.08	0.45	-0.42	0.24	-0.21	0.01	-0.01	0.16	-0.17	0.04	0.00	0.04	0.00
	13	0.09	37.00	0.18	-0.16	1.05	-0.43	0.13	-0.13	0.53	-0.51	0.24	-0.23	0.01	-0.01	0.20	-0.20	0.03	0.00	0.04	0.00

INTRA-SUBJECT MEANS

								W+ upper segments and handles	W- upper segments and handles							
EC		0.18	46.67	0.20	-0.16	0.83	-0.76	0.17	-0.14	0.58	-0.64	0.23	-0.27	0.01	-0.01	0.24	-0.24
FC		0.19	24.67	0.13	-0.22	0.77	-0.61	0.20	-0.13	0.54	-0.51	0.29	-0.26	0.01	-0.01	0.20	-0.20
FF		0.22	24.50	0.17	-0.15	0.89	-0.60	0.20	-0.13	0.67	-0.66	0.35	-0.32	0.01	-0.01	0.27	-0.27
GV		0.16	33.67	0.23	-0.25	1.02	-0.51	0.17	-0.13	0.73	-0.69	0.46	-0.43	0.01	-0.01	0.27	-0.26
GZ		0.15	29.00	0.21	-0.13	0.76	-0.62	0.15	-0.11	0.54	-0.54	0.24	-0.25	0.01	-0.01	0.18	-0.18
IC		0.15	26.67	0.25	-0.22	0.80	-0.64	0.21	-0.15	0.61	-0.58	0.43	-0.37	0.01	-0.01	0.24	-0.23
LC		0.11	25.00	0.24	-0.36	0.87	-0.45	0.20	-0.26	0.32	-0.34	0.23	-0.38	0.01	-0.01	0.11	-0.12
MS		0.24	11.67	0.13	-0.12	1.12	-0.91	0.18	-0.13	0.90	-0.90	0.35	-0.33	0.01	-0.01	0.35	-0.35
PT		0.15	25.67	0.26	-0.39	0.72	-0.63	0.23	-0.20	0.50	-0.48	0.38	-0.38	0.01	-0.01	0.18	-0.18
VT		0.09	40.00	0.20	-0.18	1.12	-0.39	0.22	-0.14	0.53	-0.50	0.30	-0.28	0.01	-0.01	0.19	-0.19
	MEAN	0.164	28.750	0.204	-0.218	0.890	-0.611	0.193	-0.153	0.592	-0.584	0.325	-0.327	0.009	-0.009	0.223	-0.221
	STD	0.045	9.582	0.046	0.092	0.148	0.150	0.024	0.044	0.154	0.149	0.081	0.063	0.002	0.002	0.065	0.064

Figure A.3: Computed work components during walker gait, healthy subjects. All trials data, intra-subject mean values and overall mean values (see text for details). Work is expressed in (J m /Kg m). Empty line corresponds to missing trial for that subject.

TOTAL BODY WORK

Subject	Trial	Norm speed	Joint					Segmental and W handles					ExtInt				
			Wtot+	Wtot-	|Wtot|	Wnet	Wabsnet	Wtot+	Wtot-	|Wtot|	Wnet	Wabsnet	Wtot+	Wtot-	|Wtot|	Wnet	Wabsnet
EC	7	0.17	0.90	-0.97	1.87	-0.07	0.73	0.67	-0.78	1.44	-0.11	0.82	0.45	-0.58	1.03	-0.13	0.80
	11	0.16	1.20	-1.10	2.30	0.10	0.80	0.83	-0.85	1.69	-0.02	0.72	0.56	-0.60	1.16	-0.04	0.71
	12	0.21	0.97	-0.69	1.66	0.28	0.58	0.77	-0.70	1.47	0.07	0.62	0.42	-0.38	0.79	0.04	0.62
FC	9	0.19	0.77	-0.79	1.56	-0.03	0.59	0.68	-0.63	1.30	0.05	0.59	0.41	-0.42	0.83	-0.01	0.58
	10	0.18	1.09	-0.84	1.92	0.25	0.78	0.78	-0.60	1.37	0.18	0.74	0.54	-0.43	0.97	0.11	0.74
	11	0.20	0.86	-0.85	1.70	0.01	0.82	0.76	-0.70	1.47	0.06	0.90	0.54	-0.54	1.08	0.01	0.91
FF	16	0.22	1.12	-0.66	1.78	0.46	0.80	0.89	-0.80	1.69	0.08	0.97	0.65	-0.62	1.27	0.03	0.97
	19	0.21	1.01	-0.84	1.85	0.17	0.77	0.86	-0.78	1.64	0.08	0.95	0.60	-0.57	1.18	0.03	0.94
GV	4	0.13	1.52	-0.91	2.43	0.60	1.46	0.98	-0.93	1.91	0.05	1.44	0.88	-0.88	1.76	0.01	1.45
	16	0.16	0.98	-0.57	1.55	0.42	0.74	0.73	-0.64	1.37	0.09	0.90	0.56	-0.54	1.10	0.03	0.91
	19	0.19	1.26	-0.78	2.05	0.48	1.17	1.00	-0.91	1.91	0.09	1.19	0.76	-0.71	1.46	0.05	1.19
GZ	6	0.16	1.06	-0.66	1.72	0.40	0.58	0.75	-0.67	1.42	0.08	0.52	0.41	-0.37	0.78	0.04	0.50
	12	0.15	0.82	-0.72	1.53	0.10	0.65	0.64	-0.65	1.29	-0.01	0.79	0.47	-0.52	0.99	-0.04	0.78
	16	0.14	1.03	-0.87	1.89	0.16	0.55	0.67	-0.65	1.31	0.02	0.66	0.41	-0.43	0.84	-0.02	0.64
IC	9	0.16	0.98	-0.96	1.94	0.02	0.98	0.88	-0.77	1.65	0.10	1.20	0.75	-0.65	1.40	0.09	1.21
	14	0.14	0.98	-0.93	1.91	0.05	1.18	0.85	-0.82	1.68	0.03	1.32	0.77	-0.77	1.54	0.00	1.33
	10	0.13	1.20	-0.70	1.90	0.49	0.82	0.72	-0.59	1.31	0.14	0.66	0.50	-0.41	0.91	0.08	0.66
LC	7	0.12	0.87	-0.74	1.61	0.13	0.70	0.45	-0.60	1.06	-0.15	0.53	0.22	-0.49	0.71	-0.27	0.57
	13	0.09	1.35	-0.96	2.31	0.39	0.93	0.51	-0.49	1.00	0.02	0.47	0.31	-0.36	0.67	-0.04	0.48
	16	0.13	1.11	-0.74	1.85	0.38	0.95	0.61	-0.71	1.32	-0.10	0.86	0.51	-0.67	1.18	-0.16	0.90
MS	9	0.25	1.13	-0.91	2.04	0.21	0.98	1.13	-1.05	2.18	0.08	0.94	0.67	-0.58	1.25	0.09	0.88
	12	0.24	1.31	-1.15	2.46	0.17	0.95	1.10	-1.04	2.14	0.06	1.01	0.78	-0.78	1.56	0.00	1.02
	13	0.23	1.32	-1.04	2.36	0.28	1.04	1.01	-1.00	2.01	0.02	0.88	0.68	-0.72	1.40	-0.04	0.91
PT	10	0.12	1.09	-1.19	2.28	-0.10	0.81	0.68	-0.77	1.45	-0.09	1.07	0.54	-0.68	1.22	-0.14	1.08
	11	0.14	0.57	-0.88	1.45	-0.31	0.53	0.79	-0.68	1.47	0.11	1.02	0.67	-0.63	1.29	0.04	1.02
	15	0.20	1.28	-0.99	2.27	0.29	0.77	0.72	-0.59	1.31	0.13	0.76	0.51	-0.41	0.92	0.10	0.73
VT	10	0.09	1.57	-0.61	2.19	0.96	1.23	0.90	-0.78	1.67	0.12	0.92	0.64	-0.60	1.23	0.04	0.93
	12	0.08	1.17	-0.50	1.67	0.67	0.73	0.60	-0.51	1.11	0.10	0.63	0.41	-0.39	0.80	0.02	0.62
	13	0.09	1.23	-0.59	1.82	0.64	0.97	0.73	-0.64	1.37	0.09	0.69	0.46	-0.44	0.89	0.02	0.67

INTRA-SUBJECT MEANS

EC		0.18	1.02	-0.92	1.94	0.10	0.70	0.75	-0.78	1.53	-0.02	0.72	0.48	-0.52	0.99	-0.04	0.71
FC		0.19	0.90	-0.82	1.73	0.08	0.73	0.74	-0.64	1.38	0.09	0.74	0.50	-0.46	0.96	0.04	0.74
FF		0.22	1.06	-0.75	1.81	0.31	0.78	0.87	-0.79	1.66	0.08	0.96	0.63	-0.60	1.23	0.03	0.96
GV		0.16	1.26	-0.75	2.01	0.50	1.12	0.90	-0.83	1.73	0.07	1.18	0.73	-0.71	1.44	0.03	1.18
GZ		0.15	0.97	-0.75	1.71	0.22	0.60	0.69	-0.65	1.34	0.03	0.66	0.43	-0.44	0.87	-0.01	0.64
IC		0.15	1.05	-0.87	1.92	0.19	0.99	0.82	-0.73	1.55	0.09	1.06	0.67	-0.61	1.28	0.06	1.07
LC		0.11	1.11	-0.81	1.92	0.30	0.86	0.52	-0.60	1.12	-0.08	0.62	0.35	-0.50	0.85	-0.16	0.65
MS		0.24	1.25	-1.03	2.29	0.22	0.99	1.08	-1.03	2.11	0.05	0.95	0.71	-0.69	1.40	0.02	0.94
PT		0.15	0.98	-1.02	2.00	-0.04	0.70	0.73	-0.68	1.41	0.05	0.95	0.57	-0.57	1.14	0.00	0.94
VT		0.09	1.33	-0.57	1.90	0.76	0.97	0.74	-0.64	1.38	0.10	0.75	0.50	-0.47	0.97	0.03	0.74
	MEAN	0.164	1.094	-0.829	1.923	0.265	0.845	0.785	-0.737	1.522	0.048	0.858	0.557	-0.557	1.114	0.000	0.858
	STD	0.045	0.141	0.139	0.163	0.227	0.169	0.148	0.127	0.269	0.057	0.186	0.127	0.094	0.215	0.061	0.186

Figure A.4: Whole body muscle mechanical work during walker gait computed with the different methods (see text for details).

A.2 Details on statistics

Statistical comparison of the results obtained for the healthy children during normal gait and walker with the different methods was performed on the parameters *positive* work (W+) and *absolute-net* work (Wabsnet). Evaluations were made by using analysis of variance for repeated measures. Results are summarized in the following tables. In addiction to the bar plots representing mean values ± SD in chapter 5, data are also illustrated in Fig. A.5 as median and quartile values.

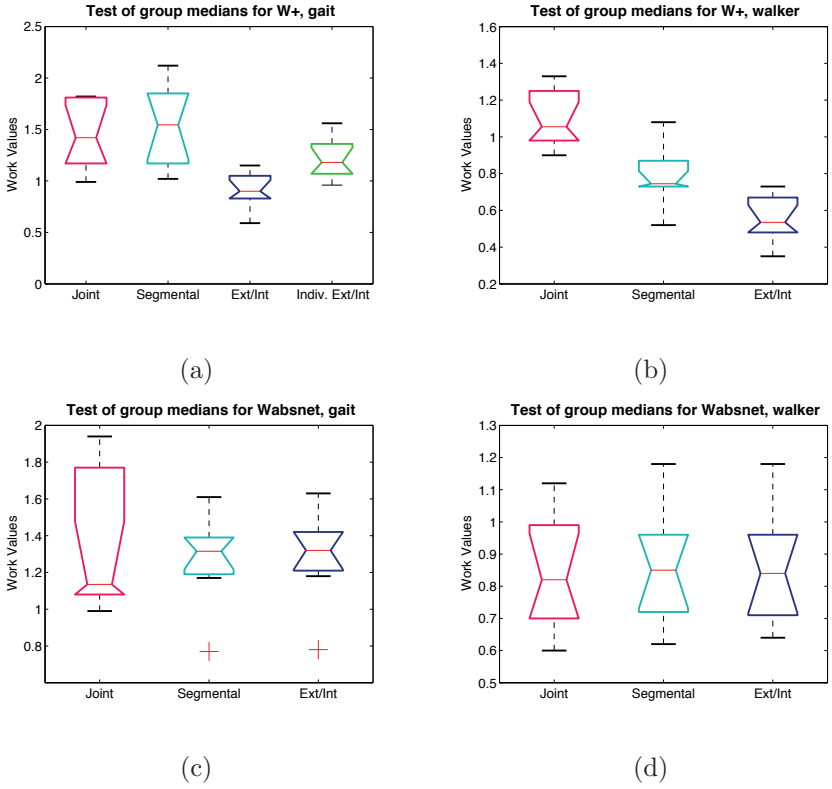

Figure A.5: Box and whisker plots for comparisons between values of mechanical work W+ and Wabsnet computed with the different methods. The box has lines at the lower quartile, median, and upper quartile values. Notches display the variability of the median between samples. Box plots whose notches do not overlap have different medians at the 5% significance level. Whiskers extend from each end of the box to the adjacent values in the data. Length of the whiskers is specified as 1.0 times the interquartile range. Points beyond the whiskers are displayed with the + symbol.

Statistics results. healthy subjects. gait

Data

Subject	Norm. speed	W+ Joint W+	W+ Seg W+	W+ ExtInt W+	W+ Ind W+	Wabsnet Joint Wabsnet	Wabsnet Seg Wabsnet	Wabsnet ExtInt Wabsnet
EC	0.31	1.15	1.30	0.89	1.15	1.02	1.39	1.40
FC	0.36	1.42	1.64	0.83	1.22	1.18	1.17	1.18
FF	0.26	1.23	1.17	0.91	1.21	1.08	1.35	1.36
GV	0.33	1.82	1.71	1.05	1.36	1.94	1.61	1.63
GZ	0.27	1.17	1.05	0.80	1.00	1.28	1.24	1.26
IC	0.40	1.81	2.12	1.15	1.56	1.77	1.37	1.42
LC	0.31	0.99	1.02	0.59	0.96	1.08	0.77	0.78
MS	0.38	1.49	1.85	0.93	1.07	0.99	1.19	1.21
PT	0.37	1.42	1.45	0.86	1.11	1.09	1.28	1.28
VT	0.35	1.82	1.85	1.05	1.42	1.89	1.53	1.55

Normality test (Lilliefors)

test res.	0	0	0	0	0	0	0
p	0.36	>0.5	>0.5	>0.5	0.06	0.30	0.35

RESULTS ON W+. alpha = 0.05

Tests of Within-Subjects Effects

Source		Type III Sum of Squares	df	Mean Square	F	Sig.	Partial Eta Squared
Eval.	Sphericity Assumed	2.241	3	0.747	38.242	0.000	0.809
	Greenhouse-Geisser	2.241	1.583	1.416	38.242	0.000	0.809
	Huynh-Feldt	2.241	1.864	1.202	38.242	0.000	0.809
	Lower-bound	2.241	1	2.241	38.242	0.000	0.809
Error(Eval.)	Sphericity Assumed	0.527	27	0.020			
	Greenhouse-Geisser	0.527	14.246	0.037			
	Huynh-Feldt	0.527	16.78	0.031			
	Lower-bound	0.527	9	0.059			

Pairwise Comparisons

(I) Eval.	(J) Eval.	Mean Difference (I-J)	Std. Error	Sig.a	95% Confidence Interval for Differencea Lower Bound	Upper Bound
Joint	Seg	-0.083	0.054	0.945	-0.265	0.098
	Ext/Int	.528*	0.057	0.000	0.335	0.721
	Ind Ext	.227*	0.054	0.014	0.045	0.408
Seg	Joint	0.083	0.054	0.945	-0.098	0.265
	Ext/Int	.611*	0.084	0.000	0.329	0.892
	Ind Ext	.310*	0.081	0.024	0.039	0.581
Ext/Int	Joint	-.528*	0.057	0.000	-0.721	-0.335
	Seg	-.611*	0.084	0.000	-0.892	-0.329
	Ind Ext	-.301*	0.028	0.000	-0.396	-0.205
Ind Ext	Joint	-.227*	0.054	0.014	-0.408	-0.045
	Seg	-.310*	0.081	0.024	-0.581	-0.039
	Ext/Int	.301*	0.028	0.000	0.205	0.396

Based on estimated marginal means

a. Adjustment for multiple comparisons: Bonferroni.

*. The mean difference is significant at the .05 level.

RESULTS ON Wabsnet. alpha = 0.05

Tests of Within-Subjects Effects

Source		Type III Sum of Squares	df	Mean Square	F	Sig.	Partial Eta Squared
Eval.	Sphericity Assumed	0.009	2	0.005	0.165	0.849	0.018
	Greenhouse-Geisser	0.009	1.003	0.009	0.165	0.695	0.018
	Huynh-Feldt	0.009	1.004	0.009	0.165	0.695	0.018
	Lower-bound	0.009	1.000	0.009	0.165	0.694	0.018
Error(Eval.)	Sphericity Assumed	0.495	18	0.028			
	Greenhouse-Geisser	0.495	9.023	0.055			
	Huynh-Feldt	0.495	9.032	0.055			
	Lower-bound	0.495	9	0.055			

Statistics results. healthy subjects. Walker

Data		W+			Wabsnet		
Subject	Norm. speed	Joint W+	Seg W+	ExtInt W+	Joint Wabsnet	Seg Wabsnet	ExtInt Wabsnet
EC	0.18	1.02	0.75	0.48	0.70	0.72	0.71
FC	0.19	0.90	0.74	0.50	0.73	0.74	0.74
FF	0.22	1.06	0.87	0.63	0.78	0.96	0.96
GV	0.16	1.26	0.90	0.73	1.12	1.18	1.18
GZ	0.15	0.97	0.69	0.43	0.60	0.66	0.64
IC	0.15	1.05	0.82	0.67	0.99	1.06	1.07
LC	0.11	1.11	0.52	0.35	0.86	0.62	0.65
MS	0.24	1.25	1.08	0.71	0.99	0.95	0.94
PT	0.15	0.98	0.73	0.57	0.70	0.95	0.94
VT	0.09	1.33	0.74	0.50	0.97	0.75	0.74

Normality test (Lilliefors)

test res.	0	0	0	0	0	0
p	0.3700	0.3747	>0.5	>0.5	0.1809	0.1208

RESULTS ON W+. alpha = 0.05

Tests of Within-Subjects Effects

Source		Type III Sum of Squares	df	Mean Square	F	Sig.	Partial Eta Squared
Eval.	Sphericity Assumed	1.452	2	0.726	84.356	0.000	0.904
	Greenhouse-Geisser	1.452	1.307	1.111	84.356	0.000	0.904
	Huynh-Feldt	1.452	1.439	1.009	84.356	0.000	0.904
	Lower-bound	1.452	1	1.452	84.356	0.000	0.904
Error(Eval.)	Sphericity Assumed	0.155	18	0.009			
	Greenhouse-Geisser	0.155	11.764	0.013			
	Huynh-Feldt	0.155	12.952	0.012			
	Lower-bound	0.155	9	0.017			

Pairwise Comparisons

(I) Eval.	(J) Eval.	Mean Difference (I-J)	Std. Error	Sig.a	95% Confidence Interval for Difference -a	
					Lower Bound	Upper Bound
Joint	Seg	.309*	0.049	0.000	0.164	0.454
	Ext/Int	.537*	0.047	0.000	0.398	0.676
Seg	Joint	-.309*	0.049	0.000	-0.454	-0.164
	Ext/Int	.228*	0.022	0.000	0.164	0.292
Ext/Int	Joint	-.537*	0.047	0.000	-0.676	-0.398
	Seg	-.228*	0.022	0.000	-0.292	-0.164

Based on estimated marginal means

a. Adjustment for multiple comparisons: Bonferroni.

*. The mean difference is significant at the .05 level.

RESULTS ON Wabsnet. alpha = 0.05

Tests of Within-Subjects Effects

Source		Type III Sum of Squares	df	Mean Square	F	Sig.	Partial Eta Squared
Eval.	Sphericity Assumed	0.001	2	0.001	0.068	0.935	0.007
	Greenhouse-Geisser	0.001	1.009	0.001	0.068	0.803	0.007
	Huynh-Feldt	0.001	1.013	0.001	0.068	0.804	0.007
	Lower-bound	0.001	1	0.001	0.068	0.800	0.007
Error(Eval.)	Sphericity Assumed	0.137	18	0.008			
	Greenhouse-Geisser	0.137	9.085	0.015			
	Huynh-Feldt	0.137	9.117	0.015			
	Lower-bound	0.137	9	0.015			

A.3 All trials data, CP children

The following tables contain muscle mechanical work values computed for the CP children with the different approaches. Data are presented from single trials. Intra-subject means and standard deviation (SD) values were computed only when the same information was available on all the trials. Since good kinetic data were available on a few subjects in one trial only, data from those trials (evidenced in light blue on the tables) were used for further processing and comparisons. Trial number is relative to all trials acquired for that subject. Normalized walking speed is also listed in the table for each trial. For walker locomotion, the mean percentage of body weight put on the handles during the gait cycle is also listed in the table for each trial.

Upper table in Fig.A.6 describes *positive* and *negative* work, divided in different components: Upper and lower body components for Joint and Segmental methods (W+ upper, etc.), external component computed with the combined limbs method (Wext(COM)+, WextCOM-), internal component computed with respect to the centre of mass (Wint+ upper segments, etc.).
The lower table describes the total work components computed with the three approaches: *Wtot+*, *Wtot-*, $|Wtot|$, *Wnet*, *Wabsnet*.

Upper table in Fig.A.7 describes *positive* and *negative* work during walker locomotion, divided in different components: Upper and lower body components for Joint and Segmental methods (W+ upper, etc.), external component computed with the combined limbs method (Wext(COM)+, WextCOM-), internal component computed with respect to the centre of mass (Wint+ upper segments, etc.), positive and negative work done on the two handles (W+ right handle, etc.).
The final positive and negative work done by the upper body (W+ upper segments and handles, etc) is obtained by the summation of work associated to upper body segments and work done on the handles.
The lower table describes the total work components computed with the three approaches: *Wtot+*, *Wtot-*, $|Wtot|$, *Wnet*, *Wabsnet*.

UPPER BODY AND LOWER BODY WORK COMPONENTS

Subject	Trial	Norm speed	W+ upper joints	W- upper joints	W+ lower joints	W- lower joints	W+ upper segments	W- upper segments	W+ lower segments	W- lower segments	Wext (COM)+	Wext (COM)-	Wint+ upper segments	Wint- upper segments	Wint+ lower segments	Wint- lower segments
MM	5	0.24	0.49	-0.47			0.78	-0.63	1.30	-1.08	1.08	-0.78	0.23	-0.20	0.39	-0.38
	6	0.25	0.43	-0.53			0.92	-0.93	1.20	-1.24	0.98	-1.03	0.25	-0.30	0.42	-0.38
	7	0.23	0.51	-0.61			0.91	-0.84	1.24	-1.26	1.20	-1.18	0.31	-0.29	0.36	-0.36
AP	1	0.20	0.46	-0.70	1.32	-1.92	0.53	-0.58	1.00	-1.03	0.88	-0.94	0.12	-0.14	0.37	-0.38
	2	0.21	0.50	-0.70			0.53	-0.56	1.02	-0.99	0.81	-0.80	0.12	-0.14	0.37	-0.36
AV	11	0.17	0.13	-0.11	1.23	-1.64	0.17	-0.16	0.65	-0.63	0.34	-0.31	0.02	-0.02	0.24	-0.24
	15	0.22	0.10	-0.16			0.32	-0.33	0.75	-0.83	0.23	-0.29	0.03	-0.03	0.28	-0.29
	27	0.19	0.07	-0.08			0.20	-0.18	0.65	-0.63	0.33	-0.29	0.01	-0.01	0.27	-0.27
MEAN MM (all trials)		0.24	0.48	0.54			0.87	0.80	1.25	1.19	1.09	1.00	0.26	0.26	0.39	0.38
SD MM		0.01	0.04	0.07			0.08	0.15	0.05	0.10	0.11	0.20	0.04	0.05	0.03	0.01

TOTAL BODY WORK

Subject	Trial	Norm speed	Joint					Segmental					ExtInt				
			Wtot+	Wtot-	|Wtot|	Wnet	Wabsnet	Wtot+	Wtot-	|Wtot|	Wnet	Wabsnet	Wtot+	Wtot-	|Wtot|	Wnet	Wabsnet
MM	5	0.24						2.07	-1.71	3.78	0.36	2.27	1.69	-1.36	3.06	0.33	2.22
	6	0.25						2.12	-2.17	4.29	-0.05	2.55	1.66	-1.71	3.37	-0.06	2.53
	7	0.23						2.15	-2.10	4.25	0.05	2.72	1.87	-1.83	3.69	0.04	2.71
AP	1	0.20	1.78	-2.62	4.40	-0.84	1.78	1.53	-1.61	3.14	-0.08	2.41	1.37	-1.46	2.83	-0.09	2.42
	2	0.21						1.55	-1.54	3.09	0.00	2.12	1.30	-1.30	2.61	0.00	2.06
AV	11	0.17	1.35	-1.75	3.10	-0.39	0.85	0.81	-0.79	1.60	0.02	1.01	0.60	-0.57	1.17	0.03	0.92
	15	0.22						1.07	-1.16	2.23	-0.09	0.78	0.54	-0.61	1.15	-0.08	0.72
	27	0.19						0.85	-0.81	1.66	0.04	0.96	0.61	-0.57	1.18	0.04	0.94
MEAN MM (all trials)		0.24						2.11	-1.99	4.11	0.12	2.51	1.74	-1.63	3.37	0.10	2.49
SD MM		0.01						0.04	0.25	0.28	0.22	0.23	0.11	0.24	0.32	0.20	0.25

Figure A.6: Computed work components and whole body muscle mechanical work during normal gait, CP subjects (see text for details). Work is expressed in (J*m/Kg*m). Empty areas correspond to missing data for that trial.

UPPER BODY AND LOWER BODY WORK COMPONENTS

Subject	Trial	Norm speed	Bodyweight % on handles	W+ upper joints	W- upper joints	W+ lower joints	W- lower joints	W+ upper segments	W- upper segments	W+ lower segments	W- lower segments	Wext (COM)+	Wext (COM)-	Wint+ upper segments	Wint- upper segments	Wint+ lower segments	Wint- lower segments	W+ right handle	W- right handle	W+ left handle	W- left handle
IA	4	0.17	30	0.48	-0.48			0.48	-0.52	1.28	-1.23	1.29	-1.30	0.06	-0.06	0.40	-0.36	0.08	0.00	0.11	0.00
	5	0.17	26	0.50	-0.55			0.45	-0.48	1.33	-1.44	1.22	-1.33	0.07	-0.07	0.46	-0.46	0.09	0.00	0.10	0.00
	9	0.17	28	0.80	-0.78			0.55	-0.54	1.51	-1.55	1.34	-1.34	0.09	-0.08	0.55	-0.54	0.06	0.00	0.07	0.00
MF	5	0.05	28	1.38	-1.17			0.52	-0.57	0.60	-0.65	0.56	-0.66	0.04	-0.04	0.16	-0.16	0.06	0.00	0.05	0.00
	8	0.07	28	1.64	-0.91			0.62	-0.61	0.64	-0.60	0.81	-0.79	0.06	-0.06	0.14	-0.14	0.06	0.00	0.03	0.00
	9	0.07	31	1.19	-0.95			0.58	-0.58	0.59	-0.59	0.74	-0.75	0.05	-0.05	0.11	-0.10	0.06	0.00	0.04	0.00
AP	5	0.13	29	0.28	-0.45	1.48	-1.33	0.43	-0.33	0.80	-0.80	0.88	-0.77	0.03	-0.03	0.27	-0.28	0.05	0.00	0.03	0.00
	10	0.14	27	0.48	-0.47			0.33	-0.34	0.74	-0.84	0.68	-0.70	0.03	-0.03	0.29	-0.32	0.09	0.00	0.07	0.00
	13	0.20	27	0.48	-0.39			0.34	-0.37	1.02	-0.94	0.86	-0.85	0.02	-0.02	0.39	-0.38	0.07	0.00	0.06	0.00

INTRA-SUBJECT MEANS

							W+ upper segments and handles	W- upper segments and handles		
MEAN IA (all trials)	0.17	28	0.59	0.61			0.66	0.51	1.37	1.40
SD IA	0.00	2	0.18	0.16			0.03	0.03	0.12	0.16
MEAN MF (all trials)	0.06	29	1.40	1.01			0.67	0.59	0.61	0.61
SD MF	0.01	2	0.23	0.14			0.04	0.02	0.03	0.03

TOTAL BODY WORK

Subject	Trial	Norm speed	Joint					Segmental and W handles					ExtInt				
			Wtot+	Wtot-	|Wtot|	Wnet	Wabsnet	Wtot+	Wtot-	|Wtot|	Wnet	Wabsnet	Wtot+	Wtot-	|Wtot|	Wnet	Wabsnet
IA	4	0.17						1.95	-1.74	3.69	0.20	2.75	1.74	-1.72	3.47	0.02	2.60
	5	0.17						1.95	-1.92	3.87	0.04	2.69	1.76	-1.86	3.62	-0.10	2.53
	9	0.17						2.20	-2.09	4.29	0.11	2.84	1.97	-1.96	3.93	0.01	2.71
MF	5	0.05						1.23	-1.22	2.45	0.01	1.27	0.75	-0.86	1.62	-0.11	1.34
	8	0.07						1.35	-1.22	2.57	0.13	1.79	1.02	-0.99	2.01	0.03	1.67
	9	0.07						1.27	-1.18	2.44	0.09	1.51	0.90	-0.90	1.80	0.00	1.56
AP	5	0.13	1.75	-1.77	3.52	-0.02	1.63	1.31	-1.13	2.44	0.18	2.05	1.18	-1.08	2.26	0.09	2.00
	10	0.14						1.23	-1.18	2.40	0.05	1.73	1.00	-1.05	2.05	-0.05	1.66
	13	0.20						1.49	-1.31	2.80	0.19	2.31	1.27	-1.25	2.52	0.02	2.23

INTRA-SUBJECT MEANS

MEAN IA (all trials)	0.17						2.03	-1.92	3.95	0.12	2.75	1.82	-1.85	3.67	-0.03	2.61
SD IA	0.00						0.14	0.17	0.30	0.08	0.09	0.13	0.12	0.24	0.07	0.09
MEAN MF (all trials)	0.06						1.28	-1.21	2.49	0.07	1.52	0.89	-0.92	1.81	-0.03	1.52
SD MF	0.01						0.06	0.03	0.07	0.06	0.15	0.13	0.06	0.19	0.07	0.16

Figure A.7: Computed work components and whole body muscle mechanical work walker gait, CP subjects (see text for details). Work is expressed in (J*m/Kg*m). Empty areas correspond to missing data for that trial.

References

S. Y. Aleshinsky. An energy "sources" and "fractions" approach to the mechanical energy expenditure problem, part 1. *J. of Biomechanics*, 19(4): 287–293, 1986a.

S. Y. Aleshinsky. An energy "sources" and "fractions" approach to the mechanical energy expenditure problem, part 2. *J. of Biomechanics*, 19(4): 295–300, 1986b.

S. Y. Aleshinsky. An energy "sources" and "fractions" approach to the mechanical energy expenditure problem, part 3. *J. of Biomechanics*, 19(4): 301–306, 1986c.

S. Y. Aleshinsky. An energy "sources" and "fractions" approach to the mechanical energy expenditure problem, part 4. *J. of Biomechanics*, 19(4): 307–309, 1986d.

S. Y. Aleshinsky. An energy "sources" and "fractions" approach to the mechanical energy expenditure problem, part 5. *J. of Biomechanics*, 19(4): 311–315, 1986e.

M. Alonso and E. J. Finn. *Fundamental University Physics - Mechanics*, volume I. Addison-Wesley, 1969.

A. Audenino, L. Goglio, and M. Rossetto. *Metodi sperimentali per la progettazione.* Levrotto e Bella, 1997. (In Italian).

R. A. Bachschmidt, G. F. Harris, and G. G. Simoneau. Walker-assisted gait in rehabilitation: a study of biomechanics and instrumentation. *IEEE Trans Neural Syst Rehabil Eng*, 9(1): 96–105, 2001.

J. Bates, J. Stebbins, and T. Theologis. Development of a kinematic trunk model for routine clinical use. In *Proceedings of the JEGM*, pages poster n.140, 2010.

B. C. Bennett, M. F. Abel, A. Wolovick, T. Franklin, P. E. Allaire, and C. Kerrigan. Center of mass movement and energy transfer during walking in children with cerebral palsy. *Arch. Phys. Med. Rehabil.*, 86: 2189–2194, 2005.

A. Cappozzo. The forces and couples in the human trunk during level walking. *Journal of Biomechanics*, 16(4): 265–277, 1983.

A. Cappozzo, F. Figura, M. Marchetti, and A. Pedotti. The interplay of muscular and external forces in human ambulation. *Journal of Biomechanics*, 9: 35–43, 1976.

A. Cappozzo, U. Della Croce, A. Leardini, and L. Chiari. Human movement analysis using stereophotogrammetry. part 1: theoretical background. *Gait and Posture*, 21: 186–196, 2005.

G. A. Cavagna. Force platform as ergometers. *J. Appl. Physiol.*, 39: 174–179, 1975.

G. A. Cavagna. *Muscolo e Locomozione*. Raffaello Cortina, 1988. (In Italian).

G. A. Cavagna and M. Kaneko. Mechanical work and efficiency in level walking and running. *J. of Physiology*, 268: 467–481, 1977.

G. A. Cavagna, H. Thys, and A. Zamboni. The sources of external work in level walking and running. *J. of Physiology*, 262: 639–657, 1976.

G. A. Cavagna, N. C. Heglund, and C. R. Taylor. Mechanical work in terrestrial locomotion: Two basic mechanisms for minimizing energy expenditure. *Am. J. Physiol.*, 233 (5): 243–261, 1977.

G. A. Cavagna, P. A. Willems, and N. C. Heglund. The role of gravity in human walking: pendular energy exchange, external work and optimal speed. *J. of Physiology*, 528(3): 657–668, 2000.

L. Chiari, U. Della Croce, A. Leardini, and A. Cappozzo. Human movement analysis using stereophotogrammetry. part 2: Instrumental errors. *Gait and Posture*, 21: 197–211, 2005.

J. W. Dally and W. F. Riley. *Experimental stress analysis*. College House Enterprises, 2005.

D. L. Damiano, T. L. Martellotta, D. J. Sullivan, K. P. Granata, and M. F. Abel. Muscle force production and functional performance in spastic cerebral palsy: Relationship of cocontraction. *Arch. Phys. Med. Rehabil.*, 81: 895–900, 2000.

R. B. Davis, S. Ounpuu, D. Tyburski, and J. R. Gage. A gait analysis data collection and reduction technique. *Human Movement Science*, 10: 575–587, 1991.

P. De Leva. Adjustments to Zatsiorsky-Seluyanov's segment inertia parameters. *Journal of Biomechanics*, 29(9): 1223–1230, 1996.

P. De Vita, J. Helseth, and T. Hortobagyi. Muscles do more positive than negative work in human locomotion. *J. of Experimental Biology*, 210: 3361–3373, 2007.

U. Della Croce, A. Leardini, L. Chiari, and A. Cappozzo. Human movement analysis using stereophotogrammetry. part 4: assessment of anatomical landmark misplacement and its effects on joint kinematics. *Gait and Posture*, 21: 226–237, 2005.

S. L. Delp, F. C. Anderson, A. S. Arnold, P. Loan, A. Habib, C. John, E. Guendelman, and D. G. Thelen. Opensim: Open-source software to create and analyze dynamic simulations of movement. *IEEE Trans on Biomed Eng*, 54(11): 1940–1950, 2007.

C. Detrembleur, A. van den Hecke, and F. Dierick. Motion of the body centre of gravity as a summary indicator of the mechanics of human pathological gait. *Gait and Posture*, 12: 243–250, 2000.

C. Detrembleur, F. Dierick, G. Stoquart, F. Chantraine, and T. Lejeune. Energy cost, mechanical work, and efficiency of hemiparetic walking. *Gait and Posture*, 18: 47–55, 2003.

J. M. Donelan, R. Kram, and A. D. Kuo. Simultaneous positive and negative external mechanical work in human walking. *Journal of Biomechanics*, 35: 117–124, 2002.

R. Dumas, L. Cheze, and J. P. Verriest. Adjustments to mcconville et al. and young et al. body segment inertial parameters. *Journal of Biomechanics*, 40(3): 543–553, 2007.

M. H. A. Eames, A. Cosgrove, and R. Baker. Comparing methods of estimating the total body centre of mass in three dimensions in normal and pathological gaits. *Hum. Mov. Sci.*, 18: 637–646, 1999.

G. Frost, J. Dowling, O. Bar-Or, and K. Dyson. Ability of mechanical power estimations to explain differences in metabolic cost of walking and running among children. *Gait and Posture*, 5: 120–127, 1997.

J. R. Gage, M. H. Schwartz, S. E. Koop, and T. F. Novacheck, editors. *The identification and treatment of gait problems in cerebral palsy.* Mac Keith Press, 2009.

S. A. Gard, S. C. Miff, and A. D. Kuo. Comparison of kinematic and kinetic methods for computing the vertical motion of the body center of mass during walking. *Hum. Mov. Sci.*, 22: 597–610, 2004.

P. Garofalo, A. G. Cutti, M. V. Filippi, S. Cavazza, A. Ferrari, A. Cappello, and A. Davalli. Inter-operator reliability and prediction bands of a novel protocol to measure the coordinated movements of shoulder-girdle and humerus in clinical settings. *Med Biol Eng Comp*, 47: 475–86, 2009.

K. E. Gordon, D. P. Ferris, and A. D. Kuo. Metabolic and mechanical energy costs of reducing vertical center of mass movement during gait. *Arch. Phys. Med. Rehabil.*, 90: 136–144, 2009.

L. L. Haubert, D. D. Gutierrez, C. J. Newsam, J. K. Gronley, S. J. Mulroy, and J. Perry. A comparison of shoulder joint forces during ambulation with crutches versus a walker in persons with incomplete spinal cord injury. *Arch Phys Med Rehabil*, 87: 63–70, 2006.

A. L. Hof. Scaling gait data to body size. *Gait and Posture*, 4: 222?–223, 1996.

B. Hsue, F. Miller, and F. Su. The dynamic balance of the children with cerebral palsy and typical developing during gait. part I: Spatial relationship between COM and COP trajectories. *Gait and Posture*, 29: 465–470, 2009a.

B. Hsue, F. Miller, and F. Su. The dynamic balance of the children with cerebral palsy and typical developing during gait. part II: Instantaneous velocity and acceleration of COM and COP and their relationship. *Gait and Posture*, 29: 471–476, 2009b.

R. K. Jensen. Body segment mass: radius and radius of gyration proportions of children. *J. of Biomechanics*, 19(5): 359–368, 1986.

I. Kingma, M. P. de Looze, H. M. Toussaint, H. G. Klijnsma, and T. B. M. Bruijnen. Validation of a full-body 3-D dynamic linked segment model. *Human Movement Science*, 15: 833–860, 1996.

C. Kirtley. *Clinical Gait Analysis: Theory and Practice*. Churchill Livingstone Elsevier, 2006.

K. A. Konop, K. M. B. Strifling, M. Wang, K. Cao, D. Eastwood, S. Jackson, J. Ackman, H. Altiok, J. Schwab, and G. F. Harris. Upper extremity kinetics and energy expenditure during walker-assisted gait in children with cerebral palsy. *Acta Orthop Traumatol Turc*, 43(2): 156–164, 2009a.

K. A. Konop, K. M. B. Strifling, M. Wang, K. Cao, J. Schwab, D. Eastwood, S. Jackson, J. Ackman, and G. F. Harris. A biomechanical analysis of upper extremity kinetics in children with cerebral palsy using anterior and posterior walkers. *Gait and Posture*, 30: 364–369, 2009b.

A. D. Kuo. The six determinants of gait and the inverted pendulum analogy: A dynamic walking perspective. *Human Movement Science*, 26: 617–656, 2007.

A. Leardini, L. Chiari, U. Della Croce, and A. Cappozzo. Human movement analysis using stereophotogrammetry. part 3: Soft tissue artifacts assessment and compensation. *Gait and Posture*, 21: 212–225, 2005.

A. H. Mackey, S. E. Walt, G. A. Lobb, and N. S. Stott. Reliability of upper and lower limb three-dimensional kinematics in children with hemiplegia. *Gait and Posture*, 22 (1): 1–9, 2005.

V. Marconi, D. Conte, P. Bonetti, A. Cosentino, B. Montagnana, and C. Capelli. Metabolic cost of walking at different speeds in children with cerebral palsy. In *Proceedings of the 18th Annual General Meeting of the European Society of Movement Analysis in Adults and Children*, 2009.

P. Mazzoldi, M. Nigro, and C. Voci. *Elementi di Fisica II, Meccanica e Termodinamica*. Edises, 2006. (In Italian).

J. T. McConville, T. D. Churchill, I. Kaleps, C. E. Clauser, and J. Cuzzi. Anthropometric relationships of body and body segments moments of inertia. *Air Force Aerospace Medical Research Laboratory, Wright-Patterson Air Force base*, OH(AFAMRL-TR): 80–119, 1980.

R. Merletti. *Elementi di elettromiografia di superficie*. C.L.U.T. Torino, 2000. (In Italian).

F. Miller. *Cerebral Palsy*. Springer Science, 2005.

A. E. Minetti, C. Capelli, P. Zamparo, P. E. Di Prampero, and F. Saibene. Effects of stride frequency on mechanical power and energy expenditure of walking. *Medicine and Science in Sports and Exercise*, 27(8): 1194–1202, 1995.

R. R. Neptune, F. E. Zajac, and S. A. Kautz. Muscle force redistributes segmental power for body progression during walking. *Gait and Posture*, 19: 194–205, 2004a.

R. R. Neptune, F. E. Zajac, and S. A. Kautz. Muscle mechanical work requirements during normal walking : the energetic cost of raising the body ' s center-of-mass is significant. *Journal of Biomechanics*, 37: 817–825, 2004b.

R. R. Neptune, K. Sasaki, and S. A. Kautz. The effect of walking speed on muscle function and mechanical energetics. *Gait and Posture*, 28: 135–143, 2008.

R. R. Neptune, C. P. Mc Gowan, and S. A. Kautz. Forward dynamics simulations provide insight into muscle mechanical work during human locomotion. *Exercise and Sport Sciences Reviews*, 2009a.

R. R. Neptune, C. P. Mcgowan, and J. M. Fiandt. The influence of muscle physiology and advanced technology on sports performance. *Annual Review of Biomedical Engineering*, 11, 2009b.

J. Perry. *Analisi del Movimento*. Elsevier, 2005. Ed. italiana a cura di M. G. Benedetti.

M. R. Pierrynowski, D. A. Winter, and R. W. Norman. Transfers of mechanical energy within the total body and mechanical efficiency during treadmill walking. *Ergonomics*, 23(2): 147–156, 1980.

B. I. Prilutsky, L. N. Petrova, and L. M. Raitsin. Comparison of mechanical energy expenditure of joint moments and muscle forces during human locomotion. *Journal of Biomechanics*, 29(4): 405–415, 1996.

S.B.A. Purkiss and D.G.E. Robertson. Methods for calculating internal mechanical work: comparison using elite runners. *Gait and Posture*, 18: 143–149, 2003.

M. Rabuffetti and G. Baroni. Validation protocol of models for centre of mass estimation. *Journal of Biomechanics*, 32: 609–613, 1999.

O. Rettig, L. Fradet, P. Kasten, P. Raiss, and S. I. Wolf. A new kinematic model of the upper extremity based on functional joint parameter determination for shoulder and elbow. *Gait and Posture*, 30: 469–76, 2009.

J. Richards. *Biomechanics in clinic and research*. Churchill Livingstone Elsevier, 2008.

T. Robert, L. Cheze, R. Dumas, and J. P. Verriest. Validation of net joint loads calculated by inverse dynamics in case of complex movements: Application to balance recovery movements. *J. of Biomechanics*, 40: 2450–2456, 2007.

D. G. E. Robertson and D. A. Winter. Mechanical energy generation, absorption and transfer amongst segments during walking. *Journal of Biomechanics*, 1980.

D. G. E. Robertson, G. E. Caldwell, J. Hamill, G. Kamen, and S. N. Whittlesey, editors. *Research methods in Biomechanics*. Human Kinetics, 2004.

K. Sasaki, R. R. Neptune, and S. A. Kautz. The relationships between muscle, external, internal and joint mechanical work during normal walking. *Journal of Experimental Biology*, 212(5): 738–744, 2009.

B. Schepens, P. A. Willems, G. A. Cavagna, and N. C. Heglund. Mechanical power and efficiency in running children. *Eur. J. Physiol.*, 442: 107–116, 2001.

B. Schepens, G. Bastien, N. C. Heglund, and P. A. Willems. Mechanical work and muscular efficiency in walking children. *J. Exp. Biol.*, 207: 587–596, 2004.

M. H. Schwartz, A. Rozumalski, and J. P. Trost. The effect of walking speed on the gait of typically developing children. *Journal of Biomechanics*, 41: 1639–1650, 2008.

A. Seth and M. G. Pandy. A neuromusculoskeletal tracking method for estimating individual muscle forces in human movement. *Journal of Biomechanics*, 40: 356–366, 2007.

B. A. Slavens, P. F. Sturm, and G. F. Harris. Upper extremity inverse dynamics model for crutch-assisted gait assessment. *Journal of Biomechanics*, 43: 2026–2031, 2010.

B. A. Slavens, N. Bhagchandani, M. Wang, P. A. Smith, and G. F. Harris. An upper extremity inverse dynamics model for pediatric lofstrand crutch-assisted gait. *Journal of Biomechanics*, 44(11): 2162–2167, 2011.

B. W. Stansfield, S. J. Hillman, M. E. Hazlewood, A. A. Lawson, A. M. Mann, I. R. Loudon, and J. E. Robb. Normalized speed, not age, characterizes ground reaction force patterns in 5- to 12-year-old children walking at self-selected speeds. *Journal of Pediatric Orthopedics*, 21: 395–402, 2001.

K. M. B. Strifling, N. Lu, M. Wanh, K. Cao, J. D. Ackman, J. P. Klein, J. P. Schwab, and G. F. Harris. Comparison of upper extremity kinematics in children with spastic diplegic cerebral palsy using anterior and posterior walkers. *Gait and Posture*, 28: 412–419, 2008.

H. Thys, P. A. Willems, and P. Saels. Energy cost, mechanical work and muscular efficiency in swing-trough gait with elbow crutches. *Journal of Biomechanics*, 29(11): 1473–1482, 1996.

H. Thys, P. A. Willems, and P. Saels. Authors' response: Energy cost, mechanical work and muscular efficiency in swing-trough gait with elbow crutches. *J. of Biomechanics*, 30(8): 863, 1997.

V. B. Unnithan, J. J. Dowling, G. Frost, and O. Bar-Or. Role of cocontraction in the O_2 cost of walking in children with cerebral palsy. *Med. Sci. Sports Exerc.*, 28: 1498–1504, 1996.

V. B. Unnithan, J. J. Dowling, G. Frost, and O. Bar-Or. Role of mechanical power estimates in the O_2 cost of walking in children with cerebral palsy. *Med. Sci. Sports Exerc.*, 31: 1703–1708, 1999.

P. van de Walle, K. Desloovere, S. Truijen, R. Gosselink, P. Aerts, and A. Hallemans. Age-related changes in mechanical and metabolic energy during typical gait. *Gait and Posture*, 31: 495–501, 2010.

P. van de Walle, A. Hallemans, M. Schwartz, S. Truijen, R. Gosselink, and K. Desloovere. Mechanical energy estimation during walking: Validity and sensitivity in typical gait and in children with cerebral palsy. *Gait and Posture*, 35(2): 231–237, 2012.

A. van den Hecke, C. Malghem, A. Renders, C. Detrembleur, S. Palumbo, and T. Lejeune. Mechanical work, energetic cost, and gait efficiency in children with cerebral palsy. *J. Pediatr. Orthop.*, 27(6): 643–647, 2007.

Vicon. *BodyBuilder for biomechanics, technical manual*. Oxford Metrics Ltd.

P. A. Willems, G. A. Cavagna, and N. C. Heglund. External, internal and total work in human locomotion. *Journal of Experimental Biology*, 198: 379–393, 1995.

K. R. Williams and P. R. Cavanagh. A model for the calculation of mechanical power during distance running. *Journal of Biomechanics*, 16(2): 115–128, 1983.

D. A. Winter. *Biomechanics and Motor Control of Human Movement*. Wiley, 2005.

D. A. Winter. A new definition of mechanical work done in human movement. *J. Appl. Physiol.*, 46(1): 79–83, 1979.

G. Wu, F. C. T. van der Helm, H. E. J. Veeger, M. Makhsous, P. Van Roy, C. Anglin, J. Nagels, A. R. Karduna, K. McQuade, X. Wang, F. W.Werner, and B. Buchholz. ISB recommendation on definitions of joint coordinate systems of various joints for the reporting of human joint motion - part ii: shoulder, elbow, wrist and hand. *J. of Biomechanics*, 38(5): 981–992, 2005.

F. E. Zajac, R. R. Neptune, and S. A. Kautz. Biomechanics and muscle coordination of human walking. part I: introduction to concepts, power transfer, dynamics and simulations. *Gait and Posture*, 16: 215–232, 2002.

F. E. Zajac, R. R. Neptune, and S. A. Kautz. Biomechanics and muscle coordination of human walking. part II: lessons from dynamical simulations and clinical implications. *Gait and Posture*, 17: 1–17, 2003.

V. M. Zatsiorsky. Letter to the editor: Comments on "energy cost, mechanical work and muscular efficiency in swing-trough gait with albow crutches". *Journal of Biomechanics*, 30(8): 861, 1997.

V. M. Zatsiorsky. Letter to the editors: Can total work be computed as a sum of the "external"and "internal "work? *Journal of Biomechanics*, 31: 191–192, 1998.

V. M. Zatsiorsky. *Kinetics of Human Motion*. Human Kinetics, 2002.

K. E. Zelik and A. D. Kuo. Human walking isn't all hard work: evidence of soft tissue contributions to energy dissipation and return. *J. of Experimental Biology*, 213: 4257–4264, 2010.